TIDAL EVOLUTION OF EXTRA-SOLAR PLANETS

by

Brian Kendall Jackson

_____

A Dissertation Submitted to the Faculty of the

DEPARTMENT OF PLANETARY SCIENCES

In Partial Fulfillment of the Requirements
For the Degree of

DOCTOR OF PHILOSOPHY

In the Graduate College

THE UNIVERSITY OF ARIZONA

2009

UMI Number: 3356402

INFORMATION TO USERS

The quality of this reproduction is dependent upon the quality of the copy submitted. Broken or indistinct print, colored or poor quality illustrations and photographs, print bleed-through, substandard margins, and improper alignment can adversely affect reproduction.
In the unlikely event that the author did not send a complete manuscript and there are missing pages, these will be noted. Also, if unauthorized copyright material had to be removed, a note will indicate the deletion.

UMI®

THE UNIVERSITY OF ARIZONA
GRADUATE COLLEGE

As members of the Dissertation Committee, we certify that we have read the dissertation

prepared by   Brian Kendall Jackson

entitled   Tidal Evolution of Extra-Solar Planets

and recommend that it be accepted as fulfilling the dissertation requirement for the

Degree of Doctor of Philosophy

_____ Date: April 10, 2009
Richard J. Greenberg

_____ Date: April 10, 2009
Rory K. Barnes

_____ Date: April 10, 2009
William B. Hubbard

_____ Date: April 10, 2009
Jonathan I. Lunine

_____ Date: April 10, 2009
Adam P. Showman

_____ Date: April 10, 2009
Roger V. Yelle

Final approval and acceptance of this dissertation is contingent upon the candidate's
submission of the final copies of the dissertation to the Graduate College.

I hereby certify that I have read this dissertation prepared under my direction and
recommend that it be accepted as fulfilling the dissertation requirement.

_____ Date: April 10, 2009
Dissertation Director: Richard J. Greenberg

Statement by Author

This dissertation has been submitted in partial fulfillment of requirements for an advanced degree at the University of Arizona and is deposited in the University Library to be made available to borrowers under rules of the Library.

Brief quotations from this dissertation are allowable without special permission, provided that accurate acknowledgment of source is made. Requests for permission for extended quotation from or reproduction of this manuscript in whole or in part may be granted by the head of the major department or the Dean of the Graduate College when in his or her judgment the proposed use of the material is in the interests of scholarship. In all other instances, however, permission must be obtained from the author.

SIGNED: Brian Kendall Jackson

Acknowledgments

Given the number of years of training and education required for me to get to this point, it is impossible for me to sufficiently acknowledge everyone who contributed in someway to this dissertation. Instead, I will simply thank the people who had the most direct or recent impact on my life and work.

Foremost, I must thank my father, whose interest in science when I was a child was really the original impetus for my pursuit of science. I still remember watching Carl Sagan's "Cosmos" for the first time and the delight of learning about sulfuric acid rain on Venus and of Percival Lowell's Martian canals.

I should thank also my brother Josh and sister Ashley, my mother and grandparents, who instilled in me a sense of responsibility and diplomacy that has tempered my passion for science with courtesy.

The many teachers I have had over the years also deserve a lot of credit for this dissertation. The guidance of my most recent teachers, my advisers Richard Greenberg and Rory Barnes, was absolutely invaluable to the completion of this work. Epic ballads should be written to honor their tremendous patience in working with me.

I would also like to thank the many LPL alumni whom I have had the pleasure to meet over the years. I am honored to call many of them colleagues and friends. They have shown me that the tradition of LPL involves more than just outstanding scientific research.

The many friends I have made amongst current grad students have contributed in many ways as well, particularly my own incoming class (Doug Archer, Nicole Baugh, David Choi, Eileen Chollet, Colin Dundas, Kelly Kolb, Eric Palmer, and Catherine Neish). You've all made my years at LPL the happiest time of my life.

I also must thank the Order of the Corn for helping me to stay sane. Going beserk and killing dragons every week really did a lot for keeping me balanced.

And in the last, most cherished place, I must thank my fiancée Maki Hattori for helping me to keep my feet on the ground as I chased after the stars in the sky. **大好き**. The chords that bind me to her are profound beyond my understanding. Maybe that just illustrates my ignorance, but I don't think so.

Dedication

To Kepler (1571-1630),

whose deep insight and indomitable courage continue to light our way

Table of Contents

List of Figures

List of Tables

Abstract

In both our solar system and extra-solar planetary systems, tides may have a variety of effects, driving complex orbital evolution and geophysical processes. For extra-solar planets with orbits that pass very close to their host stars, tides have reduced orbital eccentricities and semi-major axes, and the rates of tidal evolution may change dramatically as orbits evolve. Understanding how the orbits have evolved and, ultimately, discerning the origins of close-in extra-solar planets require accounting for all the complexity of tidal evolution. The accompanying dissipation of tidal energy within the planets has probably also affected their internal structures. In some cases, tidal dissipation may account the apparent discrepancy between predictions and observations of the radii of extra-solar planets that transit their host stars. Evolutionary models for these planets that allow determinations of their internal structures and composition must include highly variable tidal heating rates. The same tidal evolution and heating probably also affects the orbital and geophysical properties of rocky extra-solar planets and may play a key role in determining whether such a planet can harbor life. As tides reduce a planet's semi-major axis, the planet may eventually pass so close to its host star that the star's gravity completely disrupts the planet, leading to the destruction of many planets. Tidal destruction has left a discernible signature on the distribution of extra-solar planetary orbits, and so interpretations of the distribution in terms of the origins of planets must include consideration of the effects of tidal destruction.

Chapter 1
Introduction

1.1.   Historical Perspective

Scientific studies of tides extend back at least to the early 1600s, with Johannes Kepler's work on celestial motion (Kaspar 1959). In working out his laws of planetary motion, Kepler suggested that the same invisible force that kept the Moon in orbit about the Earth was also responsible for tides in the Earth's oceans. As a contemporary, Galieo Galilei ridiculed Kepler's idea of invisible forces between widely separated bodies as medieval mysticism and proposed his own explanation for tides, involving accelerations of the ocean as a result of the rotation of the Earth (Koppel 2007). The cause of ocean tides remained unclear until Newton published his Principia in 1687, in which he explained the laws of gravity and motion and correctly attributed ocean tides to the gravitational attraction of the Moon.

In his model for ocean tides, Newton imagined the Earth without continents, completely covered by the ocean. The variation in the strength of the Moon's gravity from one side of the Earth to the other induces a bulge in the ocean's surface on both sides of the Earth, each nearly symmetric about the line connecting the center of the Earth to the center of the Moon. Newton also explained the neap and spring tides, the seasonal variation in high and low tides. He pointed out that the Sun's gravity raises a significant tide in the ocean, which adds to or detracts from the tide raised by the Moon, depending on the alignment of the Sun, Earth and Moon. As successful as it is, however, Newton's model cannot explain all the details of tidal flow. By neglecting interactions between the

tide and land masses, Newton's model does not account for the wide range in tidal amplitude between different tidal bays. For example, the difference in water level between high and low tide in Britain's Bristol Channel can be 15 m, while in the Mediterranean Sea, the difference is measured in centimeters (Koppel 2007).

By the nineteenth century, great scientists like Pierre-Simon Marquis de Laplace, Lord Kelvin and G. H. Darwin (the son of Charles Darwin) began to apply the new technique of harmonic analysis to the problem of ocean tides, and their full complexity began to be grasped. Since the gravitational fields of the Sun and Moon oscillate in time in a complex but periodic way over the surface of the Earth, they can be expressed as a Fourier series, the sum of many oscillating gravitational fields, each with a single period and amplitude. The response of the Earth's tides (either in the oceans or the solid body) can then be expressed as a similar sum of many, oscillating components. The amplitude of the tide at any point on the Earth at any time can be determined by adding up the contributions from all the tidal components.

However, the harmonic tidal model has a significant short-coming: The amplitudes of the various components (the Fourier coefficients) cannot be determined beforehand because each can depend in complex ways on local conditions (such as bay depth, width, orientation, etc.). As a result, several weeks of careful measurement of the tidal are required in order to determine the contribution from each tidal component. Once the contributions from each component are known, the tidal amplitude can be predicted for any time. In fact, Lord Kelvin invented a machine that calculated the tidal amplitude

at a given bay by mechanically summing the leading terms in the Fourier series for the tide, provided with the amplitudes of the various components (the Fourier coefficients).

Although the harmonic tidal model has been successfully applied to the Earth, applying it to other planets (or stars) has proven difficult because the detailed observations required to determine the various tidal components are not possible. In spite of decades of theoretical and observational work, the uncertainties in the tidal response, particularly its dependence on frequency, continue to plague modern studies of tides (**Error! Reference source not found.**).

1.2.   Extra-Solar Systems

From ancient to modern times, the scope of astrophysics has broadened considerably. In Kepler's time, there were six planets and five satellites (our Moon and the four Galilean satellites) to study. Since that time, we've added many planets and satellites to the retinue of our Sun and even discovered hundreds of planets orbiting other stars. Although these extra-solar planetary systems are like our solar system in many ways, there are also many exciting differences, and the variety of orbital and physical properties of extra-solar planets provides important tests of our theories of planet formation. In recent years, much progress has been made in explaining the properties of extra-solar planets, but many fundamental questions remain.

To date, scientists have discovered 300+ planets in other solar systems, with new planets added to the catalog of extra-solar planets almost daily. Owing to biases in the way extra-solar planets are detected, the first extra-solar planets discovered around Sun-

like stars have masses comparable to or in excess of Jupiter, with orbital periods of only a few days. With increasingly long observational baselines, many extra-solar planets with orbital periods of several years have been found. As the development of increasingly sensitive instruments proceeds, extra-solar planets with masses comparable to or even significantly less than Neptune's have been found, and as algorithms for processing observational data become more sophisticated, more and more multiple planetary systems are discovered.

Extra-solar planets span a wide range of orbital properties, and the architectures of multiplanet extra-solar systems may be very different from the architecture of our own solar system. For example, most extra-solar planets have substantial orbital eccentricities, with an average eccentricity around 0.2 (compared to our solar system, where the average orbital eccentricity for planets is about 0.07). Orbital semi-major axes of extra-solar planets span the range from 0.017 AU (for CoRoT-7 b with an orbital period of 0.85 days [exoplanet.eu]) to 115 AU (for Fomalhaut b with a period longer than 800 years [Kalas *et al.* 2009]).

These orbital properties suggest a violent and vigorous formation history, involving gravitational scattering between planets, turbulent interactions between planets and a protoplanetary gas disk, etc. For example, studies of gravitational scattering can reproduce the broad distribution of orbital eccentricities (Chatterjee *et al.* 2008), while studies of interactions between a planet and a gas disk may explain the presence of planets with orbital semi-major axes of only a few hundredths of an AU – the so-called close-in planets (Lin *et al.* 1996).

Many planets in multiplanetary systems have also been found in orbital mean motion resonances (Marcy *et al.* 2001), and many of the planets not in mean motion resonances are involved in subtle secular interactions that seem to require very specific initial configurations (Malhotra 2002; Barnes & Greenberg 2006a). Some studies of the early history of extra-solar planetary systems have considered the formation of mean motion resonances through gas drag and orbital migration (*e.g.* Peale & Lee 2002), while others have shown they may form through gravitational scattering of planets (Raymond *et al.* 2008b).

Observations of extra-solar planets close to their host stars also provide us with information about planetary compositions, internal structures, and atmospheric dynamics. The proximity of close-in planets to their host stars allows their passage across the faces of their host stars, called the primary transit, to be visible from Earth (Charbonneau *et al.* 2007a). These observations allow determinations of the planets' masses and radii, and such observations made in several wavelengths provide transmission spectra of the planets' atmospheres, which can be used to determine atmospheric composition.

By comparing theoretical models of planetary radii that are tailored to each transiting planet, scientists can estimate each planet's internal composition and structure (*e.g.* Fortney *et al.* 2007). For example, HD 149026 b's radius suggests enrichment in heavy elements and the presence of a large rocky core (Sato *et al.* 2005). Comparison of model to observed radii has begun to suggest important trends that may allow us to distinguish between different models for planet formation (Burrows *et al.* 2007).

The passage of planet behind its host star, the secondary transit, is also observable for many close-in planets (*e.g.* Deming *et al.* 2005). By measuring variations in the light from the system as the planet passes behind the star and is occulted, observers can determine the amount of radiation emitted by the planet and make temperature maps of the planet's surface (Knutson *et al.* 2007). These temperature maps are helpful for constraining the dynamics of a transiting planet's atmosphere. For example, a strong hemispheric asymmetry in the temperature between a planet's day and night sides might indicate that dynamical transport of heat is inefficient, while a more uniform distribution suggests heat is readily transported between hemispheres (Showman *et al.* 2008). The efficiency of heat transport depends in complex ways on the atmospheric composition, stellar insolation, among other things, and the atmospheres of close-in planets may behave in ways unseen in our solar system. Thus studying secondary transit observations will elucidate ongoing processes in the atmospheres of close-in planets and fundamental atmospheric physics.

In addition to improving our understanding of planet formation and evolution, the discovery of extra-solar planets has also opened up the possibility of finding life outside our own solar system. Since the discovery of 51 Peg b (Mayor & Queloz 1995), the race has been on to discover an extra-solar planet that could support life, a habitable planet. However, the qualities that make a planet habitable are not well-understood and probably involve a complex interplay between a planet's stellar environment, atmospheric composition, geophysical activity and the availability of biologically useful materials such as water and organic compounds (Lunine 2005). Even if we find a planet that we

consider habitable, it's not clear what will be the signatures of alien life. Much astrobiological research involves studying the signs of life for the Earth that are observable from space and interpreting signals from hypothetical, inhabited planets in order to improve our ability to recognize such planets (*e.g.* Kaltenegger *et al.* 2007).

Understanding the formation histories of planets and determining whether a planet may support life involve piecing together incomplete, confusing and sometimes contradictory data. Given the complexities involved in solving these puzzles, Occam's razor provides an important guide to discerning between the various explanations for the observations: all other things being equal, the simplest explanations are probably correct. In this context, tides play an important and unifying role. The effects of tides help to explain many of the observed orbital and physical properties, where many previous explanations involve unnecessary complication or invoke unique conditions. However, tidal effects may both simplify and complicate our picture of planetary habitability. In many cases, tidal effects may dominate the physical conditions of a potentially habitable planet, and other processes may play secondary roles.

1.3.   Tides and Extra-Solar Systems

The relevance of tides to extra-solar systems was immediately apparent with the discovery of 51 Peg b. With an orbital semi-major axis *a* of only 0.05 AU, 51 Peg b is close enough to its host star that tides undoubtedly played a role in its evolution (Rasio *et al.* 1996). As for planets and satellites in our own solar system, the dissipation of energy through tides plays a major role in shaping the orbital and physical properties of close-in

extra-solar planets, so to determine the original properties of close-in planets and thus constrain their origins, we must consider the effects of tides. Many previous studies have modeled these effects, but made important assumptions that led to erroneous or inaccurate conclusions, often requiring convoluted explanations to bring theoretical expectations into agreement with observations.

For example, the influence of tides is clear in the distribution of orbital eccentricities. The distribution of eccentricities e of planets with semi-major axes $a > 0.2$ AU is very uniform (Chapter 3), with values for e and broadly distributed between 0 and up to near 1. However, for planets with $a < 0.2$ AU, close enough to the host star that tides are important, eccentricities are much smaller (most $e < 0.2$). This dichotomy has been widely attributed to damping of eccentricities by tides after the planets formed and the protoplanetary gas disk dissipated (Rasio *et al.* 1996; Trilling *et al.* 1998; Bodenheimer *et al.* 2001, 2003). Presumably, the initial eccentricities for close-in planets were broadly distributed, like those for planets far enough from their host stars to be unaffected by tides, and, over billions of years, dissipation of energy through tides reduced the eccentricities to give the dichotomy we see today.

Dissipation of tidal energy within the close-in planets certainly plays an important role in this orbital evolution. Many previous models considered only the effects of tides raised on the close-in planets, ignoring the effect of the tides raised on the host stars, under the presumption that the larger mass of the star means the planetary companion raises only a negligible tidal bulge. However, the contribution from the tide on the host star can be non-negligible. In fact, the range of uncertainty in the relevant physical

parameters even allows the tide raised on the host star to dominate the orbital evolution in some cases.

Tidal evolution is also complicated by the reduction of the orbital semi-major axis that necessarily accompanies the eccentricity evolution. As a result of the strong coupling between evolution of e and a, the rates of evolution of e and a may change dramatically over time. In many cases, the rates of tidal damping of e were much smaller in the past. However, motivated by a desire to simplify the problem, many previous studies ignored the coupled evolution of e and a, which resulting overestimates of the rate of tidal circularization. These overestimates have induced many tidal studies to invoke a variety of complex and unnecessary processes to explain the non-zero eccentricities determined for many close-in planets, when the eccentricities can more easily be explained by simply incorporating the coupling between evolution of e and a.

In this dissertation (as in Jackson *et al.* 2008a), we model this coupled evolution for many close-in planets and show that the distribution of initial e values of close-in planets can match that of the general population, without adopting ad hoc assumptions. The accompanying evolution of a values naturally accounts for the non-zero eccentricities of many close-in planets and also suggests most close-in planets had significantly larger a at the start of tidal migration.

Processes to explain the origins of close-in planets, such as gas disk migration (Lin *et al.* 1996) or planet-planet scattering (Nagasawa *et al.* 2008), did not bring all planets to their current orbits. Rather the current values of a were only reached gradually

due to tides. These results may have important implications for planet formation models and evolutionary models of close-in planets.

Just as the distribution of orbits provides important constraints on formation and evolutionary processes, so too do determinations of the physical structure and compositions of extra-solar planets. The information provided by transit observations thus plays a critical role in our understanding of planets. Here, too, tides seem to play a role in our interpretation of observations. In many cases, the observed and theoretical radii of transiting planets show significant disagreement: the radii of many transiting planets are much bigger than expected (*e.g.* Burrows *et al.* 2007).

Initially, studies suggested that tidal heating might explain this discrepency (Bodenheimer *et al.* 2001, 2003). The dissipation of energy within transiting planets warms their interiors, potentially inflating the planets. As thermal models have improved and continued observations have revised orbital eccentricities down, the current tidal heating rates for many planets appears to be too small to account for the degree of inflation observed. However, these thermal models ignored the fact that past tidal heating was probably much larger. As a close-in planet's orbit evolved, the rate of tidal dissipation or heating also evolved, changing by many orders of magnitude in some cases. The heating history of each planet probably contributed significantly to the thermal budget that governed the planet's physical properties, including its radius.

Interpretations of the observed radii in terms of the internal structures and compositions of transiting planets require consideration of this highly variable tidal heating. In this dissertation (as in Jackson *et al.* 2008b), we model the plausible heating

histories for several planets with measured radii. We discuss several planets are discussed, including for example HD 209458 b, which may have undergone substantial tidal heating during the past billion years, perhaps enough to explain its large measured radius.

The same tidal evolution of gaseous close-in planets may also play an important role in the evolution of rocky planets. The tidal heating of hypothetical rocky (or terrestrial) extra-solar planets may span a wide range of values, depending on stellar and planetary properties and orbital properties. Tidal heating may be sufficiently large, possibly exceeding radiogenic heating, and long-lived to drive plate tectonics, similar to the Earth's, which may enhance the planet's habitability. In other cases, excessive tidal heating may result in Io-like planets with violent volcanism, probably rendering them unsuitable for life. On water-rich planets, tidal heating may generate sub-surface oceans analogous to Europa's with similar prospects for habitability. Tidal heating may enhance the outgassing of volatiles, contributing to the formation and replenishment of a planet's atmosphere. Determining whether a planet is habitable or whether observations show signs of life requires consideration of tidal effects.

In this dissertation (as in Jackson *et al.* 2008c), we also model the tidal heating and evolution of hypothetical extra-solar terrestrial planets. We discuss the possible effects on planetary habitability and geophysical processes. In many cases, the conditions on the surface of a rocky extra-solar planet will probably be dominated by the processes of tidal heating taking places in the planet's interior.

The shaping of the orbital distribution by tides is an ongoing process and did not cease once the planets were brought to their current orbits. In this context, the tide raised

on the host star, so often ignored in previous studies, plays a dominant role. Once orbital eccentricities are very small, the tide raised on the planet ceases to affect the orbit, and the tide raised on the star continues to reduce *a* values, eventually pulling a close-in planet so close to its host star that the star's tidal gravity can rip the planet apart or the star can consume the planet. The distribution of orbits shows evidence for ongoing removal of planets, indicating that tidal destruction of close-in extra-solar planets is common.

In this dissertation (as in Jackson *et al.* 2009), we compare predictions of tidal theory to observations to show how they provide evidence for tidal destruction. We discuss the implications for origins of close-in planets and future observations that may corroborate our prediction that tides are destroying close-in planets. Interpretations of the observed orbital distribution in terms the origins of close-in planets must include considerations of this tidal destruction. The process can explain the observed cut-off in small *a* values, the clustering of orbital periods near three days, and the youth of transiting planets relative to non-transiting planets. Contrary to previous interpretations, a mechanism to stop the inward migration of close-in planets at their current orbits is not necessarily required. Planets nearing tidal destruction may be found with extremely small *a*, possibly already stripped of any gaseous envelope. Where one or more planets have already been accreted, a star may exhibit an unusual composition and/or spin rate.

Tides play many different roles and may explain a wide variety of observations, and consideration of all tidal effects is important in interpreting observations. Where, in previous studies, many different trends were attributed to unique processes or conditions,

our work shows they can be attributed to the simple process of tidal evolution. In this way, our work simplifies interpretations, illustrating the importance and efficacy of Occam's razor.

Chapter 2
Tidal Theory

In this chapter, we review details of tidal theory. Rather than deriving the equations from first principles, we discuss limitations and uncertainties of tidal theory and some approximations and assumptions relevant for extra-solar systems.

2.1. Effects of Tides

Whenever two gravitating bodies are close enough to one another, the gravitational potential of one body (the tidally-perturbing body) may be significantly different from one side of the tidally-perturbed body to the other. This variation in the potential may result in deformation of both bodies. (Deformation of one body is illustrated in Figure 2.1.) The size and shape of the tidal bulge depend in a simple way on the proximity of the two bodies and in a complex way on the deformed body's own gravitational field and internal structure. In some cases, the size and shape of the tidal deformation can be used to infer internal properties of the deformed body, such as for Venus (Konopliv & Yoder 1996) or Europa (Hurford 2005).

If the bodies are in a bound orbit around one another, the tidal potential over the surface of each body varies periodically as the bodies revolve and each body rotates on its axis. Pioneering work by Darwin (1879) and others introduced the approach of formulating the tidal potential as a Fourier series with frequencies related to the orbital mean motion and a body's rotation rate. If both the orbital eccentricity e or inclination i

are zero, the resulting Fourier series involves only one frequency, $2(\Omega - n)$, where the factor of two accounts for the symmetry of the tidal bulge (Figure 2.1). If either e or i are non-zero, the tidal potential will involve several components, each proportional to some power of e and i. Each component will also involve a frequency of the form $v_{l,m} = l\Omega - mn$ where Ω is the rotational frequency of the deformed body, n is the orbital mean motion, and l and m are integers. Formally the expansion of the tidal potential can include many terms, but, to low order in e and i, only a few terms and frequencies appear. Although orbital eccentricities of extra-solar planets have been observed to span a wide range (Butler *et al.* 2006; Jackson *et al.* 2008a), where they can be determined, orbital inclinations relative to the host star's equator tend to be small or zero so from here on, we assume $i = 0$.

In determining a body's response to the tidal potential, it is commonly assumed that the body's shape conforms closely to the shape of the tidal potential (Jeffreys 1961; Goldreich 1963; Kaula 1968; Hut 1981). Each component of the tidal potential is imagined to raise its own tidal bulge, with a fixed amplitude, which runs along the tidally deformed body's surface at the corresponding frequency. The total response of the body is determined by adding the response to each component. As the tidally deformed body rotates and the tidally disturbing body revolves in its orbit, the shape of the tidally deformed body continually changes to conform to the tidal potential.
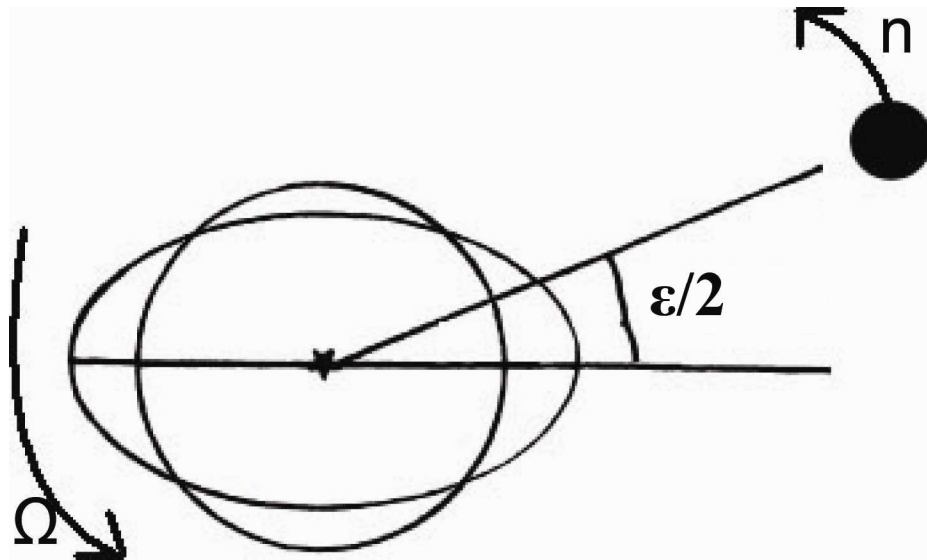
Figure 2.1: Simplified diagram of the tidal bulge, with only one phase lag (ε) shown. The tidal-raising body is shown as the dark circle, and the empty ellipse depicts shape of the tidally-deformed body (grossly exaggerated relative to its undeformed spherical shape). In this figure, the rotation rate is slower than the orbital mean motion, resulting a tidal bulge that points behind the tide-raiser. The angle by which the tidal bulge lags the tide-raiser in space is half the phase lag angle, giving rise to the factor ½. (*c.f.* Ferraz-Mello et al. 2008).

The amplitude of the total tidal deformation depends on the proximity of the tide-raising body to the deformed body: the closer the bodies are to one another, the larger the tidal bulge. If the orbit is eccentric, the size of the deformation will vary periodically. This variation in the amplitude of the total tidal deformation is captured in the superposition of the various tidal components: Near pericenter, the components line up and all contribute constructively, resulting in a larger total tidal bulge. At other points in the orbit, they lie at angles to one another and interfere with one another, resulting in a smaller total tidal bulge.

The amplitude of the total tidal bulge can also depend in complex ways on the internal structure of the tidally deformed body. Dynamical processes within the body may also lead to a complex dependence on frequency for the various tidal components. However, our understanding of the internal structures and processes for most celestial bodies is very limited. Consequently, in classical models (*e.g.* Darwin 1879), the amplitudes A_i of all tidal components are assumed to be proportional to the ratio of the tidal gravity and the deformed body's surface gravity.

If the deformed body were completely elastic, it would respond instantaneously to changes in the tidal potential, and the tidal bulge corresponding to each component would align perfectly with the shape of the corresponding component of the tidal potential. However, no real body is perfectly elastic, and some internal dissipative processes cause the shape of the tidal response to lag the tidal potential in phase. The phase lag corresponding to each frequency $\nu_{l,m}$ is given by $\varepsilon_{l,m}$, and is usually assumed to be small. The phase lag gives rise to a misalignment between the tidal bulge for that component

and the shape of the corresponding component of the tidal potential. The tidal bulge for that component will point either behind or in front of the tide-raiser, depending on the sign of the corresponding frequency (Figure 2.1). For components of the tidal response that point ahead of the tide-raising body (positive frequency), the corresponding phase lag is positive. For components that point behind the tide-raiser (negative frequency), the phase is negative. Components whose corresponding frequencies are zero (*i.e.* they are synchronous with the tide-raising body) have zero phase lag. The misalignment results in a torque that exchanges energy and angular momentum between the orbit and the tidally perturbed body.

The exchange of angular momentum can affect the rotation rate of the tidally perturbed body. If the frequency for a particular tidal component is negative, the tidal torque resulting from that component will spin up the body. If the frequency is positive, the torque will spin down the body. When the orbital eccentricity is zero, the angular velocity of the tide-raiser will be constant over the entire orbit, equal to the orbital mean motion n. If the orbital eccentricity is non-zero, the angular velocity would not be constant: It would be fastest as the tide-raiser passes through pericenter and slowest as it passes through apocenter.

After some time, the tidal torque may drive the rotation to an equilibrium rate in which the net exchange of angular momentum over an orbit is zero. For $e = 0$, this equilibrium rate would be n. If $e \neq 0$, the equilibrium rate will be larger than n and closer to the angular velocity of the tide-raiser as it passes through pericenter because the tidal torque at that point is much larger than at any other point in the orbit. The time to reach

equilibrium and the exact value for the equilibrium rotation rate depend on the system's orbital and physical parameters and details of the tidal response (*e.g.* Peale 1977).

For a rigid body, the presence of a mass asymmetry (such as a large land mass) not associated with the tidal bulge may complicate the evolution and equilibrium rate of rotation. In our own solar system, complex spin-orbit resonances may arise as a result of the interplay between tidal torques and torques from the mass asymmetry, as for Mercury (Goldreich & Peale 1966). Also, for a fluid planet, where the orbital and equatorial planes are not the same, complicated rotation states, such as Cassini states, are possible in certain circumstances (Winn & Holman 2005). However, there are no clear indications of any such complex rotation states among extra-solar planets, so we do not consider them here.

Tidal torques and forces can also affect the orbit as well as the spin. For a tidally deformed body whose rotation rate is faster than the equilibrium rate, the total tidal torque tends to transfer angular momentum from the rotation to the orbit. For such a body whose rotation rate is slower than equilibrium, the tidal torque transfers angular momentum from the orbit to the rotation. In the former case, energy is transferred from the rotation to the orbit, and in the latter case, energy is transferred from the orbit to the rotation. However, in both cases, dissipation within the deformed body reduces the total mechanical energy of the system, while increasing the thermal energy within the body. The variation in orbital elements e and a can be determined by considering conservation of total angular momentum and the work done by the tidal torque (*c.f.* Ferraz-Mello *et al.*

2008). In terms of the phase lags, whose values we've not yet specified, the rates of change for *e* and *a* are (to second order in *e*):

$$\frac{1}{a}\frac{da}{dt} = -\frac{3nk_2Mr^5}{4ma^5}\left[4\varepsilon_{2,2} - e^2(20\varepsilon_{2,2} - \tfrac{147}{2}\varepsilon_{2,3} - \tfrac{1}{2}\varepsilon_{2,1} + 3\varepsilon_{0,-1})\right]$$

(2.1)

$$\frac{1}{e}\frac{de}{dt} = -\frac{3nk_2Mr^5}{8ma^5}\left[2\varepsilon_{2,2} - \tfrac{49}{2}\varepsilon_{2,3} + \tfrac{1}{2}\varepsilon_{2,1} - 3\varepsilon_{0,-1}\right]$$

(2.2)

where *M* is the mass of the tide-raising body, and *m* and *r* are the mass and radius of the tidally deformed body, respectively. The parameter k_2 is the second order Love number (Love 1911) and parameterizes the departure of the gravitational field of the tidally deformed body from spherical, which depends on the internal structure of the body. The rate of dissipation of energy within the tidally deformed body *H* is given by:

$$H = -\frac{3k_2GM^2r^5}{8a^6}\Big\{\left[4\varepsilon_{2,2} + e^2\left(-20\varepsilon_{2,2} + \tfrac{147}{2}\varepsilon_{2,3} + \tfrac{1}{2}\varepsilon_{2,1} - 3\varepsilon_{0,-1}\right)\right]n$$
$$- \left[4\varepsilon_{2,2} + e^2\left(-20\varepsilon_{2,2} + 49\varepsilon_{2,3} + \varepsilon_{2,1}\right)\right]\Omega\Big\}$$

(2.3)

In addition to all assumptions already discussed, these equations neglect interactions between the tidally evolving pair of bodies and other bodies. Such interactions would modify the orbital evolution described here. The majority of the close-in extra-solar planets are not known to be members of a multi-planet system. Models that couple tidal evolution to planet-planet interactions have been developed (Mardling & Lin 2002), but these models usually involve many specific assumptions about the tidal response of bodies, thereby introducing considerable uncertainty as we show in the next section. The effects of planet-planet interactions will become increasingly relevant as

more multiplanetary systems are discovered, though, and future work should include these effects. They were not included here.

With the discovery of extra-solar planets with substantial eccentricities, many authors have considered corrections to these equations for terms larger order in e (and i) (*e.g.* Mardling & Lin 2002; Levrard *et al.* 2009; Wisdom 2009). For these higher order formulations, the range of frequencies that contribute to tidal evolution broadens considerably. However the tidal response of planets and stars is not well understood, even for the narrow range of frequencies considered here. Introduction of many new frequencies also introducing considerable uncertainty, and although they contain more terms, it's not clear these higher order formulations are more accurate than the model used here. Consequently, we didn't use those models.

2.2.   Previous Work on Tidal Phase Lags

So far, the forms of the phase lags have been left unspecified. The rates of orbital evolution depend critically on these values. Unfortunately, even after more than a century of work, the processes that lead to tidal dissipation and evolution for most planetary and stellar bodies remain poorly understood. As a result, the values of the phase lags and their dependence on frequency are mostly unknown. In his original analysis, Darwin assumed the rate of tidal dissipation was proportional to the frequency of forcing. Since that time, studies have considered a variety of dissipative mechanisms, determined their dependence on frequency and the internal structure of the tidally deformed body. However, for all bodies but the Earth, we lack the experimental and observational data

required to determine which of these models best describes the processes of tidal dissipation. Even when such data are available, the inferred rates of tidal evolution are often at odds with theoretical estimates.

The modes of tidal dissipation relevant for a particular celestial body depend on the composition of the body. For example, on Earth tidal dissipation in the oceans dominates, in part, because the tidal amplitudes for the oceans are much larger than for the solid body of the Earth (Macdonald 1964; Dickey *et al.* 1994). For rocky bodies without oceans, dissipation mostly occurs in the viscous mantles, as for Io (Segatz *et al.* 1988). For gaseous bodies, turbulence associated with convection or radiative damping of gravitational waves may provide the dissipation (Goldreich & Nicholson 1977; Ogilvie & Lin 2004).

Studies of these processes have suggested the associated tidal phase lags may span a wide range of values, and each process may involve a complicated dependence on the tidal forcing frequencies. For example, studies of the tidal evolution of binary star systems commonly assert that tidal phase lags are proportional to the forcing frequency, resulting in a constant lag in time between the tidal forcing and response (Zahn 1977). By considering convective turbulence, many such studies have shown that the lag time is probably related to the convective overturn time (Zahn 1989). However, the predicted time lags seem to give tidal evolution rates that are too slow compared to observations of the orbits of binary star systems (Mathieu 1994).

Studies of planets and satellites commonly assert that tidal phase lags are constant in magnitude, independent of frequency, with signs given by the signs of their associated

frequencies (Goldreich 1963; Macdonald 1964; Lambeck 1977). The constant phase lag model has been applied to studies of the Earth-Moon system (Macdonald 1964; Peale & Cassen 1978) and the satellite systems of the giant planets (Yoder & Peale 1981) and is based on observations that dissipation within the Earth is largely insensitive to frequency (Goldreich 1963). However, direct measurements of the retreat of the Moon's orbit and estimates of the dissipation in the Earth suggest the current dissipation rates are probably too large to be consistent with the observed orbital configuration and age of the Moon, suggesting that the rate must have been smaller in the past (Macdonald 1964; Lambeck 1977; Murray & Dermott 1999). For the giant planets in our solar system, theoretical estimates of tidal dissipation based on models of turbulent dissipation (Goldreich & Nicholson 1977) may be inconsistent with observational and dynamical studies of the planets' satellites (Greenberg 1982, 1989; Aksnes & Franklin 2001).

Tidal dissipation is often parameterized in terms of the tidal Q-value (Goldreich 1963). By analogy with the damped harmonic oscillator, Q is defined as the ratio maximum gravitational and elastic energy stored in the tidal deformation during one orbital period to the energy dissipated over one period. For the damped harmonic oscillator driven at a single frequency, there corresponds a single phase lag angle ε. This situation corresponds to the tidal response for $e = 0$, where there is a single driving frequency. However, for a damped harmonic oscillator driven at multiple frequencies, there correspond multiple phase lags. This situation corresponds to the tidal response for a non-zero value of e, in which case there are multiple phase lags $\varepsilon_{l,m}$.

For a phase lag proportional to frequency, $\varepsilon_{l,m} = \tau \nu_{l,m}$, where τ is the tidal time lag (Zahn 1989; Eggleton *et al.* 1998). In the constant Q model, $|\varepsilon_{l,m}|$ = const. for all indices l and m and the magnitudes of all $|\varepsilon_{l,m}|$ are set equal to 1/Q, the tidal dissipation parameter (Goldreich & Soter 1966). As opposed to the constant time lag model, the constant Q model is equivalent to assuming that each $\varepsilon_{l,m}$ has its own lag time, given by $Q/\nu_{l,m}$. (An interesting consequence of this relationship is that a tidal model cannot assume that all phase lags are the same constant in time and the same constant in phase, as is sometimes assumed [Levrard *et al.* 2009].)

Other recent studies have suggested more complex dependences of the tidal phase lags on frequency. For example, recent work suggests a non-linear dependence of tidal phase lags on frequency for gaseous planets and stars under which, in some cases, a resonance between the tidal forcing and the body's response can occur, resulting in rapid dissipation rates for certain frequencies (Ogilvie & Lin 2004; Ogilvie 2009). For rocky planets, recent work suggests tidal phase lags may depend on frequency to some fractional power, based on measurements of the dissipation of seismic energy within the Earth (Efroimsky & Lainey 2007). However the lack of available data makes it difficult to determine which of these various models is the best description of the tidal response of planets and stars. For the sake of simplicity and in the absence of additional constraints, we focus here on the application of the constant Q model.

2.3.   Idiosyncrasies of the Constant Q Tidal Model

Although its conceptual simplicity is appealing, the constant Q model introduces peculiar discontinuities that complicate the tidal evolution equations. As the rotation rate of the deformed body and the orbital mean motion change, some of the tidal frequencies $v_{l,m}$ may approach zero, but the magnitudes of the corresponding phase lags $\varepsilon_{l,m}$ remain constant (by assumption) until the corresponding frequency drops to zero, where the phase lag drops to zero discontinuously. Whether this behavior accurately describes the tidal response of real planets and stars is unclear. However, as long as tidal frequencies do not cross these discontinuities, the constant Q model probably gives at least a qualitatively correct description of tidal evolution. In any case, uncertainties associated with the frequency dependence of the tidal response may be folded into the already considerable uncertainties in the appropriate values of Q for planets and stars (Jackson *et al.* 2008a).

Applying the assumptions of the constant Q model, Equations (2.1), (2.2) and (2.3) become

$$\frac{1}{a}\frac{da}{dt}=\frac{3nk_2Mr^5}{4Qma^5}\left[4sign(v_{2,2})-e^2\left(20sign(v_{2,2})-\tfrac{147}{2}sign(v_{2,3})-\tfrac{1}{2}sign(v_{2,1})+3sign(v_{0,-1})\right)\right] \quad (2.4)$$

$$\frac{1}{e}\frac{de}{dt}=-\frac{3nk_2Mr^5}{8Qma^5}\left[2sign(v_{2,2})-\tfrac{49}{2}sign(v_{2,3})+\tfrac{1}{2}sign(v_{2,1})-3sign(v_{0,-1})\right] \quad (2.5)$$

$$H=-\frac{3k_2GM^2r^5}{8Qma^6}\left\{\left[4sign(v_{2,2})+e^2\left(-20sign(v_{2,2})+\tfrac{147}{2}sign(v_{2,3})+\tfrac{1}{2}sign(v_{2,1})-3sign(v_{0,-1})\right)\right]n\right.$$

$$\left.\left[-4sign(v_{2,2})+e^2\left(-20sign(v_{2,2})+49sign(v_{2,3})+sign(v_{2,1})\right)\right]\Omega\right\} \quad (2.6)$$

where the magnitudes of all the $\varepsilon_{l,m}$ are assumed to be $1/Q$, with signs given by $v_{l,m}$.

Under these assumptions, the equilibrium rotation rate Ω_{equil} to second order in e is given by:

$$\Omega_{equil}=n(1+\tfrac{19}{2}e^2) \quad (2.7)$$

where the factor of 19/2 comes from the particular assumption of frequency dependence of the tidal response. Alternative assumptions would give slightly different factors (Ferraz-Mello *et al.* 2008).

If the $v_{l,m}$ pass from positive to zero to negative values, the contributions of the corresponding $\varepsilon_{l,m}$ to the tidal evolution will change. Because each phase lag carries a different sign and coefficient, changes in each lag can have different effects on the sign and magnitude of the equation. As a result, the behavior of the tidal evolution equations can be complicated.

For example, consider Equation (2.4) for $2\,\Omega < n$. In this case, all $\varepsilon_{l,m}$ except $\varepsilon_{0,-1}$ are negative, and the term in the square brackets of Equation (2.4) is given by

$[-4-e^2(-20 + 147/2 + \frac{1}{2} + 3)] = -4 - 57\ e^2$. However, if $2\,\Omega = n$, $\varepsilon_{2,2}$ and $\varepsilon_{2,3}$ are negative,

$\varepsilon_{0,-1}$ is positive and $\varepsilon_{2,1}$ is zero, and the term in the square bracket transitions

discontinuously to $-4-(113/2)\ e^2$. The same sort of discontinuous transitions occur in each

of the equations. Figure 2.2 shows the discontinuous behavior of Equations (2.4), (2.5),

and (2.6) for a range of Ω and values of e.
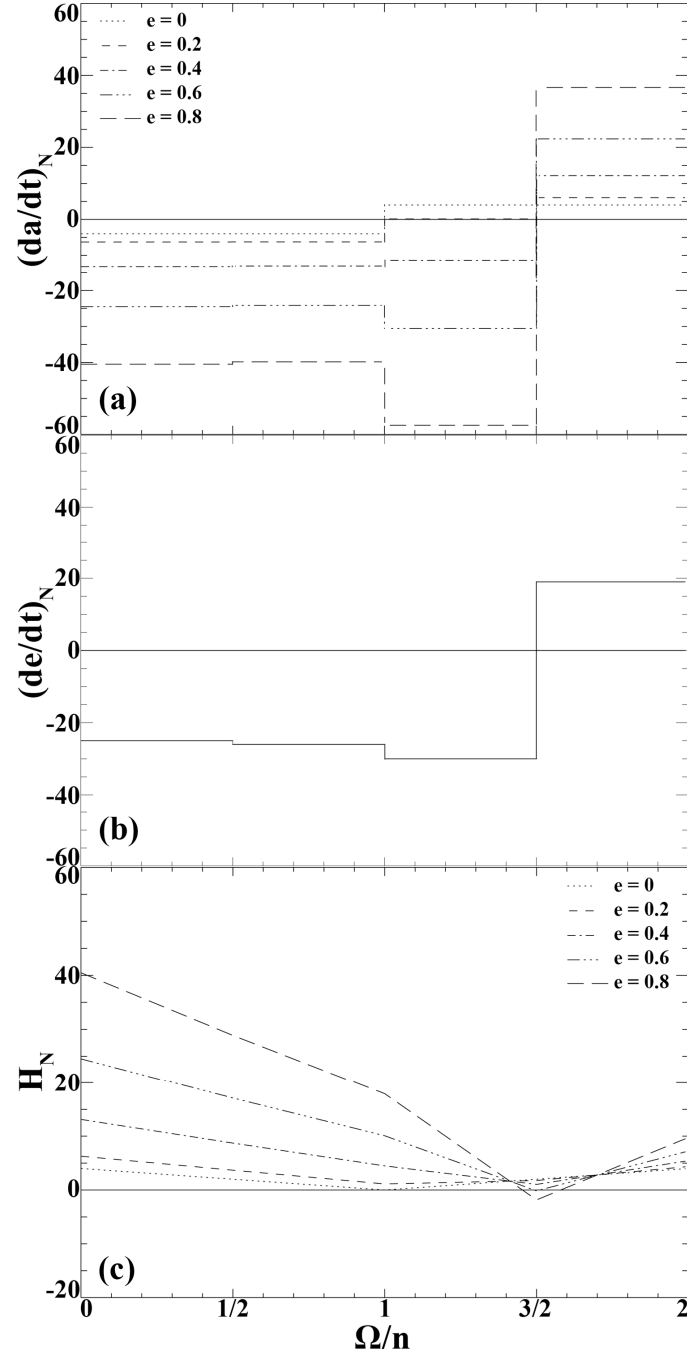
Figure 2.2: Tidal evolution and heating rates as functions of the ratio of the rotation rate Ω to the orbital mean motion n. In each panel, the y-axis represents the term in square brackets for the corresponding equation, the derivative with the physical constants normalized out. For example, $(da/dt)_N \equiv (da/dt)/\left(\dfrac{3nk_2 Mr^5}{4Qma^5}\right)$, with similar definitions for $(de/dt)_N$ and H_N.

For satellite systems in our solar system, the possible discontinuous behavior of the equations does not come into play because the frequencies associated with these systems do not cross the critical values. The rotation rates of most satellites are synchronous with their orbital mean motions (*i.e.* $\Omega \sim n$), and the rotation rates of planets are much faster than the satellites' mean motions (*i.e.* $\Omega \gg n$), and the discontinuous behavior of the constant Q model has gone largely unremarked. It's possible that these discontinuities are important in other tidally evolving systems, such as extra-solar systems.

The transition of *da/dt* from negative to positive values is important in many astrophysical problems. Usually, it is thought that *da/dt* will pass from positive to negative values at the co-rotation radius, *i.e.* at the value of *a* for which $\Omega/n = 1$. Tides will tend to increase *a* when the semi-major axis is larger than the co-rotation radius, and tend to decrease it when the semi-major axis is smaller than the co-rotation radius. However, Figure 2.2 (a) shows that, even for moderate eccentricities ($e \sim 0.4$), the value of Ω/n at which *da/dt* passes from negative to positive values is 3/2. This result implies that, for moderate eccentricities, bodies with mean motions between one and 3/2 times the rotational frequency of the tidally deformed body will experience a tidal torque that reduces the orbital semi-major axis. For $e = 0$, bodies with mean motions in that same range would experience a torque increasing the semi-major axis. In essence, for moderate eccentricities the effective co-rotation radius is larger than for small eccentricities. If true, this result may have important implications for the long-term tidal evolution of many systems.

However, the behavior of *H* shown in Figure 2.2 (c) suggests that terms of higher-order in *e* may be required to accurately model tidal heating rates, which may bear on the behavior of *da/dt*. For *e* = 0, the tidal heating rate drops as Ω/n approaches one, consistent with our expectations: For a planet in a circular orbit, tides only do work and result in tidal heating when the planet's rotation rate is not synchronous with its orbital mean motion. However, for larger values of *e* (> 0.6) in Figure 2.2 (c), *H* drops below zero for $\Omega/n = 3/2$, which is unphysical. This behavior would be equivalent to converting thermal energy within a tidally deformed body back into mechanical energy in the system. This result suggests higher order corrections are required to make the model realistic when *e* is large. The negative but small value of *H* at $\Omega/n = 3/2$ suggests that the required corrections may be small, though.

These results highlight an important potential problem for models that consider very high order corrections to the tidal evolution equations discussed earlier. For higher order formulations that assume constant *Q* (e.g. Mardling & Lin 2002; Wisdom 2009), the broad range of tidal frequencies that contributes many phase lags. The phase lag associated with each of these frequencies will pass through zero at a different ratio of Ω and *n*, with a new critical ratio added for each new frequency. Each new term will therefore add another discontinuous jump to the equations, and these discontinuities are blatantly unphysical. For the arbitrarily large number of terms introduced by these higher order formulations, there exist an arbitrarily large number of discontinuities. As a result, it may be impossible to determine the magnitudes or even the signs of the resulting

equations. In order to develop believable higher order formulations of the equations, we must first improve our understanding of the frequency dependence of the tidal response.

2.4.   Future Work

The discussion here highlights many of the uncertainties and limitations of the current tidal evolution theories. Progress in tidal theory requires that we improve our understanding of the dissipative processes within planets and stars, although much recent work has considered the effects and responses of various mechanisms. However, before we begin studying the complex processes that lead to tidal dissipation, we need to understand the underpinnings of tidal theory. By working out the consequences of many standard assumptions about tidal response of planets and stars, we've shown in this discussion that we still have work to do.

Even with the limitations and uncertainties in tidal modeling, much progress has been made in understanding the effects of tides, particularly in extra-solar systems as presented in the next several chapters. The discoveries of hundreds of extra-solar planets in recent years may help us to significantly improve our understanding of tides. The wide range of orbital and physical properties of extra-solar systems may provide us with important constraints on tidal effects not previously available in our solar system, where eccentricities tend to be small and tidal effects are less pronounced. Future studies should compare the predictions of the various tidal models with the properties of extra-solar systems, perhaps allowing us to discriminate between the various models.

Chapter 3
Tidal Evolution of the Orbits of Extra-Solar Planets

3.1.   Introduction

As discussed in the previous chapter, tides have affected the orbital and physical properties of many extra-solar planets. Evidence for the orbital effects of tides comes from the distribution of orbits. In this chapter, we present the results from a study of the orbital evolution of extra-solar planets close enough to their host stars to be affected by tides. Much of the material in this chapter is drawn from Jackson *et al.* (2008a), and the analysis presented here includes corrections to the tidal evolution equations that were left out in that original analysis. However, these corrections do not qualitatively affect the results of that work.

Figure 3.1 shows the semi-major axes *a* and eccentricities *e* of all observed extra-solar planets. Eccentricities of extra-solar planets with $a > 0.2$ AU are relatively large, averaging 0.2 and broadly distributed up to near 1. The large values seem to run contrary to the prevailing belief that planets form embedded in a protoplanetary gas disk, which would tend to damp out eccentricities through gas and particle drag (*e.g.,* Lissauer 1993; Ida & Lin 2004). The distribution of eccentricities for planets is fairly uniform over *a*, for $a > 0.2$ AU. A Kolmolgorov-Smirnov (K-S) test (Press *et al.* 1996) shows that the *e* distribution for *a* between 0.2 and 1.0 AU matches that for *a* between 1.0 and 5.0 AU at the 96% confidence level. For close-in extra-solar planets (by which we mean $a < 0.2$ AU), *e* tends to be less, although even there the average *e*, 0.09, is larger than is typical

for our solar system. For this very different *e* distribution, the K-S test shows agreement at only the 0.1% level compared with planets further out.

Rasio *et al.* (1996) first suggested that tides raised between close-in planets and their host stars might help explain their relatively low *e* values. Because the magnitude of tidal effects falls off very rapidly with increasing *a*, the action of tides could plausibly have reduced *e* for close-in planets and not for those farther out. Even with that explanation, there remains the question of why extra-solar planetary systems formed with such large eccentricities. It is possible that whatever process generated such large eccentricities was less effective for close-in extra-solar planets. However, here we consider the conventional idea that close-in planets began with a distribution of *e* similar to that of planets farther out. We use that distribution to constrain tidal parameters and evolution rates.

Bear in mind, however, that the *e* value for any extra-solar planet can vary by orders of magnitude over secular timescales (~10,000 yr) due to the dynamical interactions between multiple planets in the system (Barnes & Greenberg 2006). Therefore any conclusions drawn based on the current *e* distribution are subject to uncertainties associated with these interactions. We assume that the statistical sample is adequate enough that these variations average out.
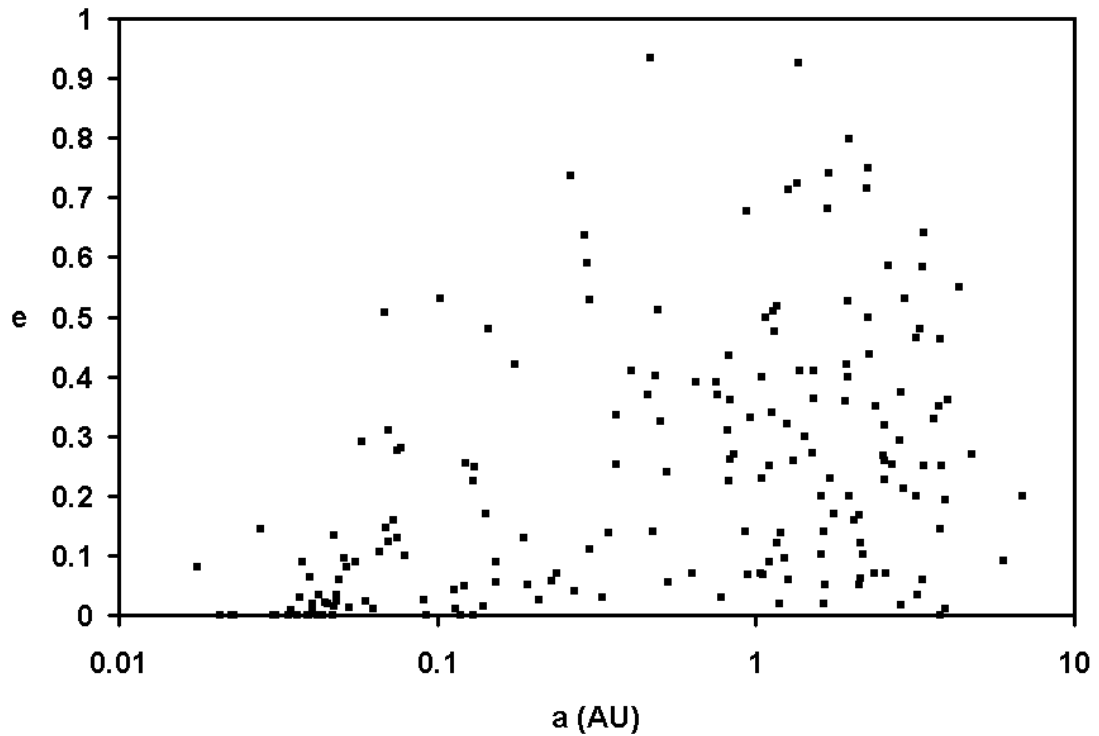
Figure 3.1: Distribution of extra-solar planetary eccentricities *e* and semi-major axes *a*. Most of the data for Figure 3.1 are taken from Butler et al 2006, with supplemental data from Udry *et al.* (2002), MacArthur *et al.* (2004), Mayor *et al.* 2004, Zucker *et al.* (2004), Laughlin *et al.* (2005b), Rivera *et al.* (2005), Vogt *et al.* (2005), Da Silva *et al.* (2006), Johnson *et al.* (2006), Lovis *et al.* (2006), Wright *et al.* (2007), and Bakos *et al.* (2007).

Because the rates of change of e and a depend on the physical properties of the planet and its host star, we can compare computations of tidal evolution (based upon various assumptions about the physical properties) with the observed e distribution (for a > 0.2 AU), using estimates of a system's age, to constrain those properties. Previous work has employed tidal considerations in attempts to constrain extra-solar planetary masses M_p and radii R_p and has investigated tidal heating rates.

Trilling (2000) considered what limits might be placed on a close-in planet's mass if its e is observed to be non-zero. That study used the fact that the smaller the value of M_p, the more quickly the tide raised on a planet by its star can circularize the orbit. Lower limits were derived on the masses of some planets based on the observation that they still have substantial eccentricities. Bodenheimer *et al.* (2003) applied a similar argument to constrain planetary radii. The rate of circularization due to tides raised on a planet increases with a planet's radius, so in principle upper limits could be found for the radius if e has not damped down. Bodenheimer *et al.* (2003) also modeled the effect of tidal heating for HD 209458 b to try to explain the surprisingly large observed radius of 1.27 Jupiter radii (Charbonneau *et al.* 2000). They found that, unless HD 209458 b has no core, tidal heating at the current e is insufficient to explain the large radius.

The constraints provided by those two investigations are questionable for several reasons. First, they depend on assumed values of the tidal dissipation parameter Q_p for the planet. Estimates of Q_p are usually taken from highly uncertain estimates based on models of the tidal evolution the Galilean satellite system (Yoder & Peale 1982; Greenberg 1982, 1989) or on models of dissipation within the planet (Goldreich &

Nicholson 1977; Ogilvie & Lin 2004). Second, they neglected the orbit-circularizing effects of tides raised on the host star by the close-in extra-solar planet. Third, they ignored the strong coupling of the tidal evolution of e with that of a. In our study, rather than assuming values for stellar and planetary Q, we use tidal evolution rates, along with conservative assumptions about M_p and R_p, to test the tidal circularization hypothesis and, in the process, constrain Q_p and Q_*.

To test the hypothesis that tides have been responsible for reducing e, we numerically integrate the canonical tidal evolution equations (Goldreich & Soter 1966) backwards in time for all planets closer than 0.2 AU for which we have adequate information. This range of a values includes all planets for which tidal evolution could conceivably be significant. For each planet, we begin the integrations at the current best estimates of eccentricity and semi-major axis, $e_{current}$ and $a_{current}$, and integrate backwards to the orbital elements, $e_{initial}$ and $a_{initial}$, at the time tides began to dominate the orbital evolution. We assume tidal evolution began when the protoplanetary disk had dissipated and collisional effects became negligible.

We include the effects of the tide raised on the star as well as on the planet since the effects of both can be important (as shown below). We assume that a typical value of Q_p applies to all planets and a typical value of Q_* applies to all stars. *A priori* estimates of these parameters are uncertain, so we repeated the full set of calculations for various pairs of values of Q_p and Q_*. Specific stars and planets may have different values depending their individual internal structure and dynamics, but we assume that the evolution of the population as a whole is not affected by such individual variations.

For each pair of Q_p and Q_*, our integrations yield a distribution of values of $e_{initial}$. We then compare the *computed* distribution of $e_{initial}$ for the close-in planets to the *observed* distribution of e for farther-out extra-solar planets. We determine which pair of tidal dissipation parameters gives the best fit of the computed distribution to the observed one. As we shall show, the Q values obtained in this way are quite reasonable and consistent with previous evidence. The fact that such plausible parameters lead to a match between the computed initial e distributions for close-in planets and the observed e distribution for farther-out planets corroborates the tidal circularization hypothesis. Moreover, our results demonstrate that, for several close-in extra-solar planets, stellar and planetary tides have significantly reduced semi-major axes (as well as eccentricities) *after* the planets formed and gas disk migration ceased (Terquem, Papaloizou & Lin 1999).

In Section 3.2, we present the tidal evolution equations as they apply to close-in extra-solar planets, and we discuss previous studies of tidal evolution. In Section 3.3, we discuss the details of our methodology and the assumptions involved. In Section 3.4, we present the results of our tidal modeling, and in Section 3.5, we discuss their implications and significance. In Section 3.6, we summarize our results and discuss caveats of our study.

3.2.   Tidal Modeling

3.2.1. Tidal Theory as Applied to Extra-Solar Planets

In **Error! Reference source not found.**, we presented a general discussion of tidal theory, with some assumptions and approximations relevant to extra-solar systems (*e.g.* the assumption that orbital inclinations are zero). Here we further simplify the tidal evolution equations, employing more, useful approximations and a notation tailored to extra-solar systems. Recasting Equations (2.4) and (2.5) in a form appropriate for close-in extra-solar planets yields:

$$\frac{1}{a}\frac{da}{dt} = -\left(\frac{63}{2}(GM_*^3)^{1/2}\frac{R_p^5}{Q_p'M_p}e^2 + \frac{9}{2}(G/M_*)^{1/2}\frac{R_*^5 M_p}{Q_*'}\left(1 + \tfrac{57}{2}e^2\right)\right)a^{-13/2} \tag{3.1}$$

$$\frac{1}{e}\frac{de}{dt} = -\left(\frac{63}{4}(GM_*^3)^{1/2}\frac{R_p^5}{Q_p'M_p} + \frac{225}{16}(G/M_*)^{1/2}\frac{R_*^5 M_p}{Q_*'}\right)a^{-13/2} \tag{3.2}$$

Here G is the gravitational constant, R is a body's radius, M its mass and Q' its modified tidal dissipation parameter, and subscripts p and $*$ refer to the planet and star, respectively.

Equations (3.1) and (3.2) differ from Equations (2.4) and (2.5) for several reasons. The numerical coefficients in these equations include a factor representing the tidal Love number k of each distorted body. As written above, the numerical coefficients are what they would be if $k = 3/2$. However, the actual values of the Love numbers for extra-solar planets are unknown and depend on the tidal-effective rigidity of the body, the radial density distribution, etc. Hence, we incorporate into our definition of Q any correction

factor for k_2, defining the modified tidal dissipation parameter $Q' = \dfrac{2}{3k_2}Q$, similar to the

Q' of Goldreich & Soter (1966) but different from the Q discussed in **Error! Reference source not found.**.

Equations (2.4) and (2.5) only considered the effects of tides raised on one body. However, for extra-solar systems, the tides raised on both the planet and the host star may contribute, so Equations (3.1) and (3.2) contain terms to account for the effects of both tides. The effects of the tide raised on the star by the planet are reflected in the terms involving Q'_* (which we call the stellar tide), while the terms involving Q'_p reflect the effect of the tide raised on the planet by the star (which we call the planetary tide).

Using Kepler's law, we've also replaced the orbital mean motion n in Equations (2.4) and (2.5) with $\left(GM_*/a^3\right)^{1/2}$, assuming $M_* \gg M_p$, which is generally valid for close-in extra-solar planets.

Note that Equations (3.1) and (3.2) include corrections to those presented by Jackson *et al.* (2008a). The equations given here include an additional term of order e^2 in Equation (3.1) due to tides raised on the star (*e.g.* Ferraz-Mello *et al.* 2008) and a corrected numerical coefficient in the last term of Equation (3.2). Neither of these corrections is great enough to affect the results in Jackson *et al.* [2008a, b, c], but their effects have been included in this analysis.

As discussed in **Error! Reference source not found.**, Equations (3.1) and (3.2) only include terms up to 2nd order in e. Since, for close-in extra-solar planets, e was much larger in the past, higher-order corrections may be important, but the effects of the

higher-order corrections depend sensitively on the details of the tidal response, which are very uncertain. Future work should investigate the effects of alternative assumptions on tidal circularization and consider higher order corrections to the tidal equations, but our approach is a reasonable first-cut at testing the tidal circularization hypothesis for the population of close-in extra-solar planets, with coupled equations for changes in *a* and *e*.

Equations (3.1) and (3.2) also assume that the planet's orbital period P_p is short compared with the star's rotation period P_*. As discussed in **Error! Reference source not found.**, the relative values of the rotation rate and mean motion have a strong effect on the magnitude and sign of the tidal evolution equations. If the assumption of slow stellar rotation were violated, the terms in tidal evolution equations corresponding to the stellar tide would change magnitude and/or sign.

Is the assumption of sufficiently large P_* reasonable? The rotation of young, rapidly rotating stars is slowed initially due to loss of angular momentum to the circumstellar disk through magnetic coupling between the star and the disk (Tinker *et al.* 2002). This effect can slow a young star's rotation to a period > 10 days in a few Myr. After dissipation of the circumstellar disk, the stellar rotation continues to slow due to shedding of angular momentum through the stellar wind (Skumanich 1972; Verbunt & Zwaan 1981; Ogilvie & Lin 2007), which also helps to keep the star's rotation longer than the revolution period of close-in planets. Trilling (2000) and Barnes (2001) list some stellar rotation periods, corroborating our assumption, with two possible exceptions. In our models, the longest-period planet that experiences any significant tidal evolution is HD 38529 b, with a period of 14 days. The rotation period for its star is unknown, but

many extra-solar host stars have rotation periods > 14 days, corroborating our choice of Equations (3.1) and (3.2). The other exception is τ Boo b, with one reported value for P_* = 3.2 (Henry *et al.* 2000) and P_p = 3.31 days (Butler *et al.* 2006). However, in light of the uncertainties in this determination of P_*, we include τ Boo b here anyway.

As the orbit of a planet evolves and tidal torques transfer angular momentum, it is possible that the stellar rotation rate will reach the equilibrium rate, perhaps even crossing some of the critical ratios discussed in **Error! Reference source not found.**. However, Levrard *et al.* (2009) and Jackson *et al.* (2009), as tidal evolution proceeds, showed that the stellar rotation rate will probably remain much slower than the equilibrium rotation rate for all but one close-in planet (HAT-P-2 b). Future work should consider the complications that may arise from significant changes in the stellar rotation rate.

Equations (3.1) and (3.2) also assume that the rotation rate of the planet is equal to the equilibrium rotation rate (given by Equation (2.7)). This assumption is reasonable because any close-in planet should have spun down to near synchronous rotation in ~ 1 Myr (Peale 1977; Rasio *et al.* 1996), too early to affect tidal orbital evolution, which takes place over billions of years. (There is a small probability that some planets can become trapped in a non-synchronous spin-orbit resonance [Winn & Holman 2005], but for our purposes we assume the probability is negligibly small.)

For many short-period extra-solar planets, tides raised on the planet by the star dominate the tidal evolution of the planet (*i.e.* in Equations (3.1) and (3.2), Q'_p terms dominate). However, given uncertainties in the values of the various relevant parameters, the effects of the tide raised on the star cannot be neglected *a priori*, and indeed our

results show they can be very important. Equations (3.1) and (3.2) also show the strong non-linear coupling between e and a. As a general rule, the equations cannot legitimately be treated separately. When properly considered together, Equations (3.1) and (3.2) cannot be solved in a closed, analytic form for e and a as functions of time. (Adams & Laughlin (2006) considered approximate solutions that may apply in some circumstances.) To find the changes in e and a with time, numerical integration is required, and that is our method.

3.2.2. Previous Studies of Tides in Extra-Solar Systems

Most previous work has employed only selected terms from Equations (3.1) and (3.2) in the effort to explain the low eccentricities among close-in extra-solar planets. Rasio *et al.* (1996), Trilling (2000), and Bodenheimer *et al.* (2003) all took a to be constant in Equation (3.2), neglecting the variation given by Equation (3.1), and neglected the circularizing effect of the stellar tide (the second term in Equation (3.2)). With these approximations, Equation (3.2) becomes

$$\frac{1}{e}\frac{de}{dt}=-\left(\frac{63}{4}\left(GM_*^3\right)^{1/2}\frac{R_p^5}{Q_P'M_p}\right)a^{-13/2}\equiv-\frac{1}{\tau_{circ}} \tag{3.3}$$

The solution of Equation (3.3) is an exponential damping of e on the timescale τ_{circ}.

Trilling (2000) proposed that, if an extra-solar planet's orbit currently has a significant eccentricity (Trilling (2000) chose $e > 0.1$), then τ_{circ} must be longer than the age of the system (τ_{age}), because otherwise e would have damped down by now. Trilling (2000) assumed $R_p = 1.27$ Jupiter radii, independent of M_p, which is reasonable for gas

giants with $0.3\ M_J < M_p < 10\ M_J$ (where M_J is Jupiter's mass) because the polytropic equation of state for hydrogen implies that the planet's radius is insensitive to its mass (Hubbard 1984). Trilling (2000) also adopted the value $Q'_p = 10^5$ and the best available determinations of M_*, a, and e. Then, using Equation (3.3), Trilling (2000) calculated the minimum M_p for several planets, based on the assumption that $\tau_{circ} > \tau_{age}$.

Figure 3.2 illustrates that approach for the extra-solar planet HD 217107 b (e is currently 0.14), showing the relationship between τ_{circ} and M_p. The estimated age of HD 217107 b is ~ 6 Gyr (Takeda *et al.* 2007), which led Trilling (2000) to infer that M_p must be greater than 4 M_J in order to satisfy $\tau_{circ} > \tau_{age}$ (Figure 3.2). However, the picture changes significantly if we include the effect of the tide raised on the star, setting $Q'_* = 10^5$ and $R_* = 1.1$ solar radii (Valenti & Fischer 2005), but still retaining the assumption of constant a and therefore that e damps exponentially with time (but with a different timescale). Since the effect of the stellar tide increases as M_p increases, the circularization timescale now drops for $M_p > 3\ M_{Jup}$. In this case, Figure 3.2 shows that τ_{circ} is smaller than τ_{age} for any value of the planet's mass. Thus, if we were to make inferences simply on the basis of a comparison of τ_{circ} with τ_{age}, the implication would be that e should have damped to zero long ago.
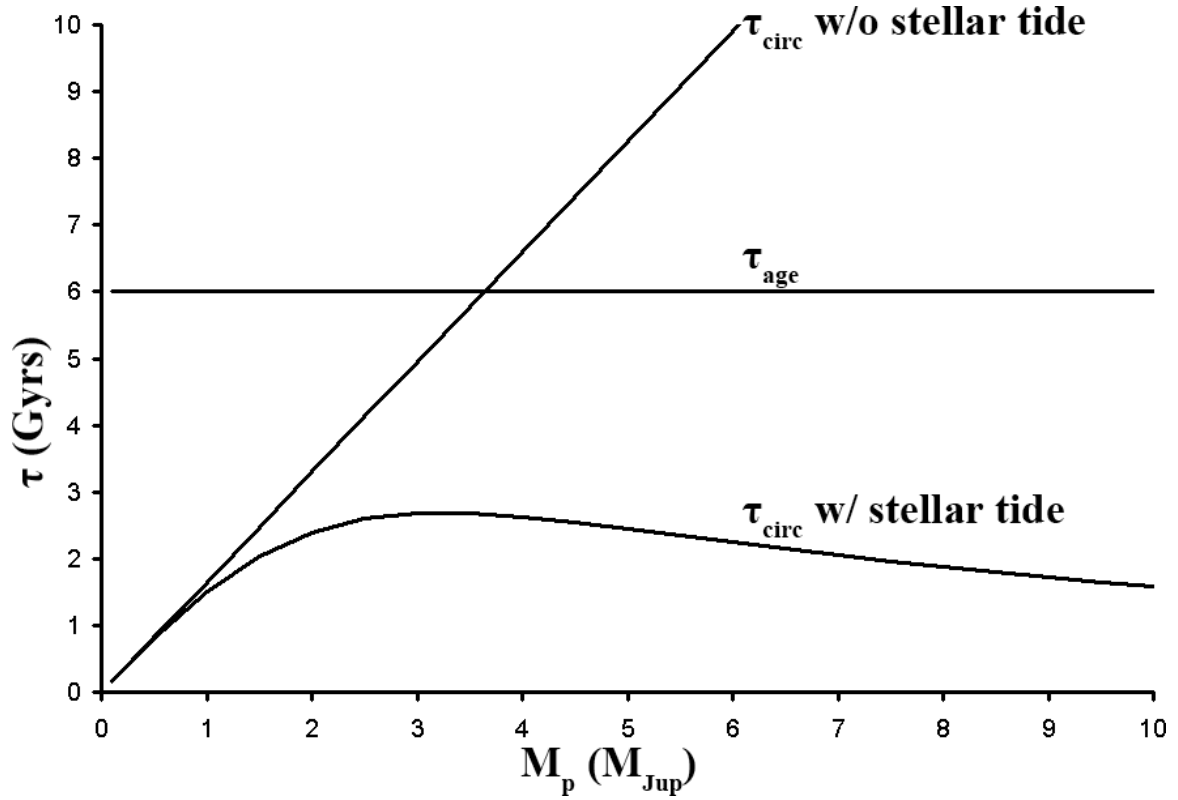
Figure 3.2: Circularization timescale τ_{circ} as a function of planetary mass M_p for HD 217107 b, estimated to have an age ~ 6 Gyr. The line labeled "τ_{circ} w/o stellar tide" is the original eccentricity circularization timescale. If this timescale represented the timescale for exponential decay of e, M_p must be > 4 M_J for the large e to be preserved ($\tau_{circ} > \tau_{age}$). The line labeled "τ_{circ} w/ stellar tide" includes the effect of the tide raised on the star (but still assuming constant a), which causes τ_{circ} to drop for $M_p > 3$ M_{Jup}, such that there is no value of M_p for which $\tau_{circ} > \tau_{age}$.

Bodenheimer *et al.* (2003) applied logic similar to Trilling's in order to constrain R_p, assuming the radial-velocity estimated minimum mass for M_p. Those results suffer from the same approximation used in Trilling (2000): the neglect of tides raised on the star. And both studies assumed a is constant on the right side of Equation (3.2). In addition, both studies assumed a value *a priori* for the poorly constrained Q_P' (Trilling (2000) assumed $Q_P' \sim 10^5$, Bodenheimer *et al.* (2003) $Q_P' \sim 10^6$), which introduced further uncertainty.

Previous considerations of Q' values have shown that constraints are fairly weak, and the mechanisms of tidal friction remain only partially understood, although some progress has been made. For constraints on planetary Q_P', it is reasonable to refer, as Bodenheimer *et al.* (2003) and Trilling (2000) did, to studies of Jupiter. Yoder & Peale (1981) proposed that Q' for Jupiter lay in the range 6×10^4 to 2×10^6. The range comes from consideration of the role of tides on Jupiter in the evolution of its satellite Io. If Jupiter's Q' were smaller than this range (remember small Q' means strong dissipation), Io could not be as close to Jupiter as it is, even taking into account the exchange of orbital energy and angular momentum with the other satellites in the Laplace resonance. However, the upper limit is much more model dependent. It assumes that the Laplace resonance is in a steady-state that involves a balance between effects of tides raised on Io by Jupiter and those raised on Jupiter by Io. We have a reasonable idea of the very small value of Q' for Io, based on its observed volcanism and strong thermal emission. Thus,

dissipation must be high enough in Jupiter ($Q' < 2 \times 10^6$) to maintain the steady-state assumed by Yoder & Peale (1981).

However, it is equally plausible that the Jupiter system is not in that steady-state (Greenberg 1982, 1989), but that tides on Io are currently dominant. In fact, a model of the formation of the Jovian system by Peale & Lee (2002) also suggests that the resonance has evolved over the long term in the way expected if tides on Io dominate. Perhaps more significantly, observations of the evolution of Io's orbital mean motion also show a rate consistent with dominance of tides on Io and negligible tidal dissipation in Jupiter (Aksnes & Franklin 2001).

More recently, Ogilvie & Lin (2004) modeled the hydrodynamic problem of a tidally perturbed gaseous planet. Their results suggested a complex dependence of Q'_P on the tidal forcing frequency and the planet's internal stratification. They conclude that a constant Q'_P does not adequately capture the full tidal dissipation behavior of gas giant planets, but that the effective Q'_P values for close-in extra-solar planets are of order 5×10^6.

Turning next to stars, we find that constraints on Q'_* have been derived from observations of tidally evolved binary stars and from theoretical modeling of stellar tidal dissipation. Mathieu (1994) observed that many main sequence binary stars with orbital periods of 10 days or less have small or zero e. Lin *et al.* (1996) drew on this observation and inferred a value for $Q'_* \sim 10^5$. In considering tidal evolution of its companion planet's orbit, Carone & Patzöld (2007) derived a value $3 \times 10^7 < Q'_* < 2.25 \times 10^9$ for OGLE-TR-56. Ogilvie & Lin (2007) modeled stellar tidal dissipation numerically and found (as they

did for tides on a planet) a complex dependence of Q'_* on tidal forcing frequency and on the mode of dissipation. Taken altogether, these studies illustrate the uncertainty inherent in assuming any values of Q'_*, as well as Q'_P.

It would be inappropriate, except in special cases, to ignore the effect of the stellar tide, which is equivalent to letting $1/Q'_* = 0$. Some previous studies (*e.g.*, Ford & Rasio 2006) assumed that, as a general rule, during tidal evolution of extra-solar planets, orbital angular momentum is conserved. However, that is only true if the tide on the star is negligible. Tides raised on a star transfer angular momentum between the star's rotation and the planet's orbit. Thus interpretations of the orbital distribution among close-in planets that involve conservation of orbital angular momentum during tidal evolution should be regarded with caution.

Next we consider the common assumption that tidal variation of *e* can be estimated by holding *a* constant, which leads to Equation (3.3). To illustrate the effect of allowing *a* to evolve, we numerically integrated Equations (3.1) and (3.2) backward in time for the planet τ Boo b for various Q' values. For comparison, we show the corresponding exponential solutions of Equation (3.3), with *a* held constant at its current value. The results shown in Figure 3.3 reveal that ignoring changes in *a* does not give a good approximation to the actual solution.

In Figure 3.3, for $Q'_* = 10^5$, we see that the behavior of *e* based on Equations (3.1) and (3.2) (solid curve) follows closely the exponential solution of Equation (3.2) with constant *a* (dashed line) for the first few Myr back in time. This close agreement is

reasonable because the actual change in a is small during this time. But further back in time, we see that a begins to change significantly. Consequently, the assumption of constant a is no longer accurate, and the behavior of e begins to deviate from the exponential solution. For smaller values of Q'_* (that is, more dissipation), a varies even more quickly, so the approximation of constant a is inaccurate. Consequently the time variation of e diverges even more from the exponential solution. The commonly made assumption that variation of a can be ignored in Equation (3.2) is not accurate and can lead to incorrect conclusions. For example, the short circularization timescales for close-in planets have led many observers to assume eccentricities are zero when fitting orbital models to data. The calculations here show that eccentricities damp much more slowly than implied by the circularization timescale suggests, so observers should not disregard indications of a non-zero eccentricity for close-in planets.

The complex behavior of e (relative to the exponential solution) leads to a surprising relationship between Q'_* and the change in the value of e over time. In Figure 3.3 we see that the total change in e over 15 Gyr decreases as Q'_* increases from 10^4 to 10^6. That result seems reasonable because tidal effects generally decrease with increasing Q'_*. However, for the larger Q'_* value (*e.g.*, 10^7), the change in e is much greater than any of the cases with smaller Q'_*. The reason is that a changes less, spending more time at low values, which means tidal effects are stronger. Clearly the behavior of e is very different from what would have been predicted by assuming a to be constant in Equation (3.2).

We plot e_{intial} for τ Boo b as a function of both Q'_p and Q'_* in Figure 3.4. Once Q'_* is greater than about 10^7, e_{intial} is independent of tides raised on the star, and for $Q'_p > 10^6$, it is independent of tides raised on the planet. In general, increasing either Q' (decreasing tidal dissipation) tends to decrease the change in e, as one might expect. However, the "heel" of the curves (from the bottom left of the figure $Q'_p \sim 10^2$ and $Q'_* \sim 10^5$ up to $Q'_p = Q'_* = 10^{5.5}$) shows the reversal of this trend that we saw in Figure 3.3. For this region, as Q'_* increases from 10^2, the change in e first decreases (as expected intuitively), but then increases. As shown in Figure 3.3, this phenomenon is explained by the concurrent change in a, which affects the total change in e.

This discussion demonstrates the importance of retaining all the terms in Equations (3.1) and (3.2) and of considering the coupled evolution of a and e given by those equations. Specific terms can only be ignored under special circumstances. Incorporating the effect of the tide on the star and the tidal variation of a significantly improves the accuracy of tidal calculations and, in many cases, leads to qualitatively different behavior.
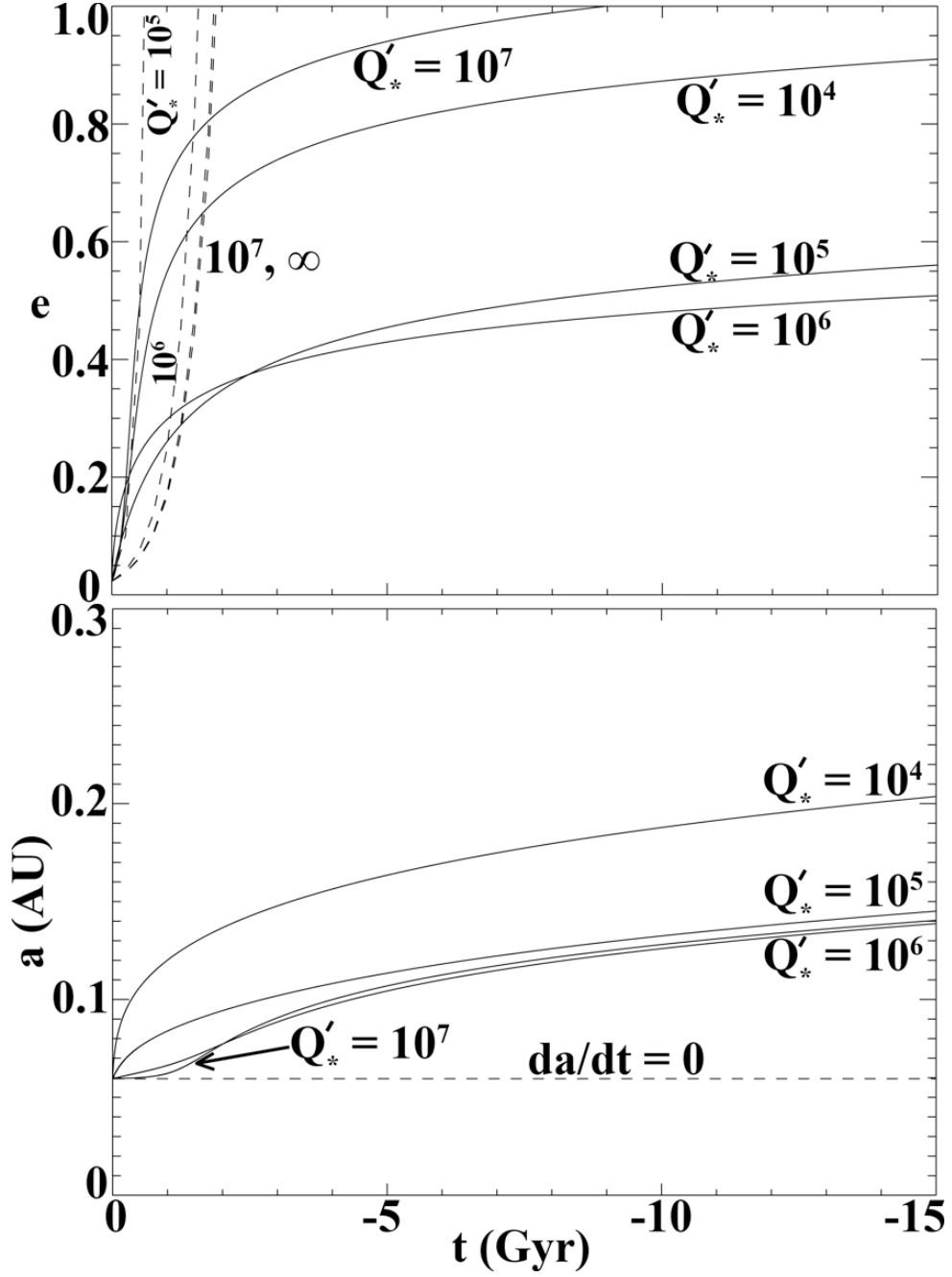
Figure 3.3: Tidal evolution of e and a for τ Boo b backwards in time from their current values ($e_{current} = 0.023$, $a_{current} = 0.0595$ AU). Here Q'_p is fixed at 10^5, and results are shown for various Q'_* values. Solid lines are numerical integration of Equation (3.1) and (3.2). The dashed lines show the exponential solutions to Equation (3.2) with a assumed constant, a common but inappropriate assumption. In the bottom panel, note that the lines labeled $Q'_* = 10^4$ and $Q'_* = 10^6$ are, in fact, correctly labeled. See text for details.
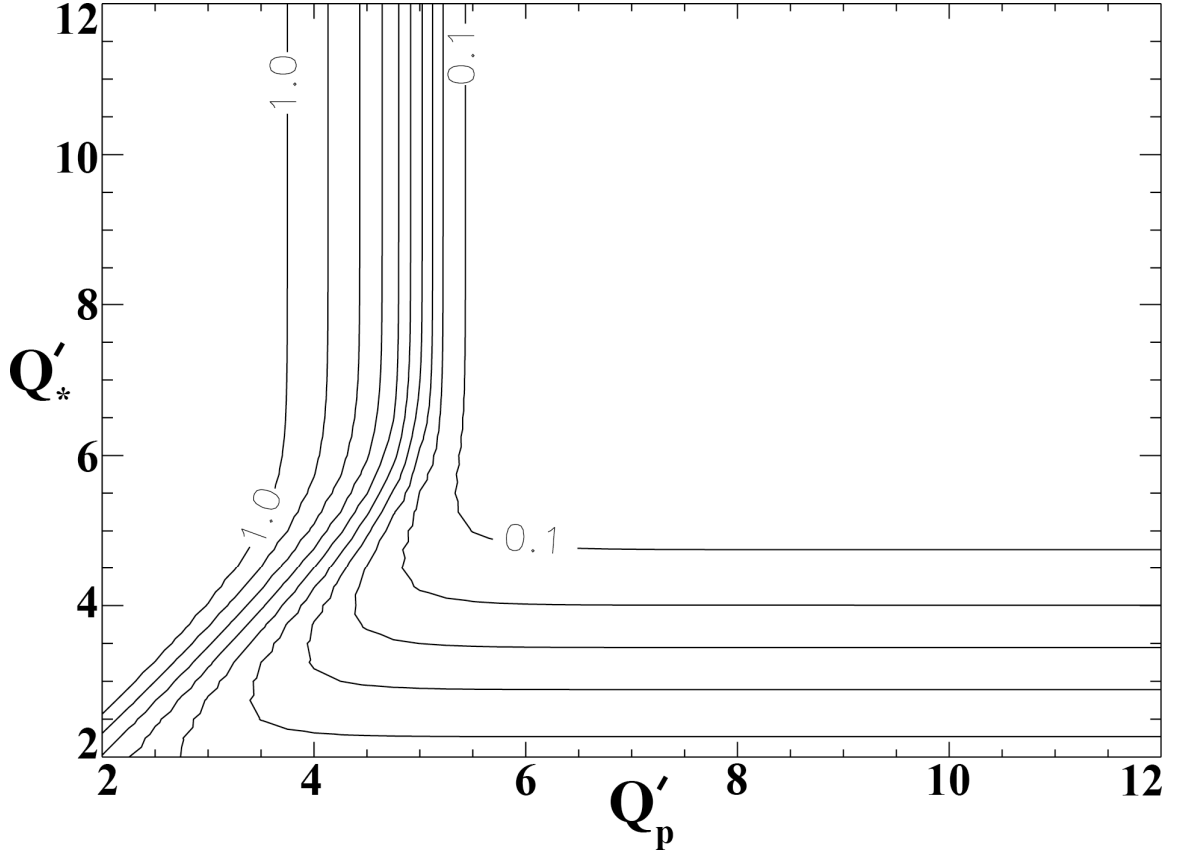
Figure 3.4: A contour plot of the dependence of $e_{initial}$ for τ Boo b on Q'_* and Q'_p. The current value of e is 0.023. The "heel" in the contour lines for $10^2 < Q'_* < 10^6$ illustrates the counter-intuitive relationship of the change in e with Q'_*: Enhancing stellar tidal dissipation (*i.e.* smaller Q'_*) can result in a decreasing amount of change of e. This behavior is not unique to τ Boo b.

3.3.   Method

We numerically integrated Equations (3.1) and (3.2) for all planets with semi-major axes less than 0.2 AU for which we have adequate data (Table 3.1). Tidal evolution is negligible (less than a few percent change in *e* or *a*) for any plausible Q' values if *a* is greater than 0.2 AU. For each planet we ran the integration backward in time from the present to 15 Gyr ago. Also for each planet, we repeated the integration for 289 combinations of Q'_p and Q'_*, evenly distributed over 17 values of each Q' from 10^4 to 10^8 in increments of $10^{0.25}$.

Our sample of planets, listed in Table 3.1, excludes those for which *e* is unknown, although often such planets have *e* tabulated as zero. As discussed previously, short circularization timescales have often induced scientists determining planetary orbits to assume that eccentricities are probably zero for close-in planets. Due to inherent biases, Keplerian fits to radial velocity data tend to overestimate orbital eccentricities (Lucy & Sweeny 1971). Primary and secondary transits provide much tighter constraints on eccentricities (Knutson *et al.* 2007) but cannot be observed for all close-in planets due to the restrictive viewing geometries required (J. Barnes 2007). In any case, many of the eccentricities we use here will be revised in the future as observational constraints improve, and the ranges of *e* allowed by uncertainties for each planet are given in Table 3.2.

We also restricted our study to planets for which there is some estimate available for the age of the system. Otherwise we have no way to determine the time of the initial *e* and *a* values. Age estimates for solar-type stars are difficult and often uncertain (see, *e.g.*,

Saffe *et al.* 2006), but we use the estimates currently available (Table 3.1). For many

systems, only a minimum or maximum age is available. If we could find only a minimum

or maximum age, we used that value; if we found both, we took the average.

In choosing the age of the star as the age of the planetary system, we are assuming

that tides began to dominate orbital evolution of close-in planets shortly after their host

stars formed. Gas disk migration is thought to bring newly-forming planets inward for ~

1 Myr (Chambers 2006), until the gas disk dissipates (Hillenbrand *et al.* 1998). Thus that

migration process is completed on a timescale that is very short compared with tidal

evolution becomes important, and we may assume that the age of the system is equal to

the age of the star.

The values for M_p and R_p come from various sources (see Table 3.1). Where a

minimum mass (*M sin i*) is available from radial-velocity measurements, we set M_p equal

to that value. This assumption should only contribute a small error (~30%, typically) due

to uncertainty regarding the orbital inclination *i* relative to the observer. Three of the

planets we considered have been observed by stellar transit: GJ 436 b (Deming *et al.*

2007), HD 209458 b (Laughlin *et al.* 2005a), and HAT-2-P b (Bakos *et al.* 2007), so for

these planets, we have used the directly measured values of R_p and M_p. For other planets,

we assume a value for R_p based on M_p. For $M_p > 0.3\ M_J$, we fix $R_p = 1.2$ Jupiter radii,

independent of mass. This radius represents the average radius of almost all of the close-

in planets which have been observed by stellar transit (including those with nominal $e = 0$,

which we have not included in this study), and this value is within 10% of nearly all their

radii. (We exclude HD 149026 b from this average because its internal structure may be

anomalous [Burrows *et al.* 2007]). Based on internal modeling, it is reasonable for R_p to be independent of mass for $M_p > 0.3$ M$_{\text{Jup}}$ over this mass range. For planets with a minimum mass less than 0.3 Jupiter masses, we assume the planet has the same density as Jupiter and scale the radius accordingly. This assumption roughly agrees with the known R_p for Uranus, Neptune, and GJ 436 b (Gillon *et al.* 2007b; Deming *et al.* 2007).

Planetary radius is a sensitive function of many factors, including internal structure, thermal history, and atmospheric opacity. Moreover, radiative cooling would tend to reduce R_p (Burrows *et al.* 2007), while tidal heating may counteract that effect to some degree. Our assumptions for R_p can be revised as improved information becomes available but are sufficiently accurate for the current study.

Values for R_* and M_* also come from various sources, as referenced in Table 3.1. In five cases, radii are not given explicitly, but we have computed them from published values of surface gravity. For two stars for which we have no estimates of surface gravity, we computed R_* using the empirical relation between M_* and R_* reported by Gorda & Svechnikov (1996).

3.4.   Results

The 289 combinations of Q'_p and Q'_* that we tested (evenly spanning the range of 10^4 to 10^8 for each Q') gave a wide variety of distributions $e_{initial}$ and $a_{initial}$ values. Figure 3.5 shows these initial distributions, as well as the current distribution, for four pairs of Q' values. One pair, with $Q'_p = 10^6$ and $Q'_* = 10^5$, (bottom right) represents Q' values

that have often been adopted in previous studies of extra-solar tidal evolution. The other three examples represent the best fits of the initial *e* distribution of close-in planets to the distribution farther out.

In Figure 3.5, the white squares represent the current orbital elements of close-in planets, while the black triangles show the "initial" orbital elements based on the solution to the tidal-evolution equations. In cases where a black triangle is co-located with a white square, the equations of tidal evolution simply gave negligible changes in *a* or *e*. Solid black squares represent orbits outside 0.2 AU where we were confident that no tidal evolution could occur.

A qualitative inspection of these examples demonstrates the varying degree of agreement with the *e* distribution farther out. The commonly assumed set of Q'_p and Q'_* exponents (6 and 5, respectively) does not appear to be a good fit. In that case, among the backwards-evolved close-in planets (black triangles), there is an excess of moderate initial *e* values (*e.g.*, > 0.6) compared with planets farther out (the black squares). Of these four examples, the combination of $Q'_p = 10^{6.5}$ and $Q'_*=10^{5.5}$ and $Q'_p = 10^{6.5}$ and $Q'_*=10^{5.25}$ appear to give a good qualitative fits to the population outside $a = 0.2$ AU.
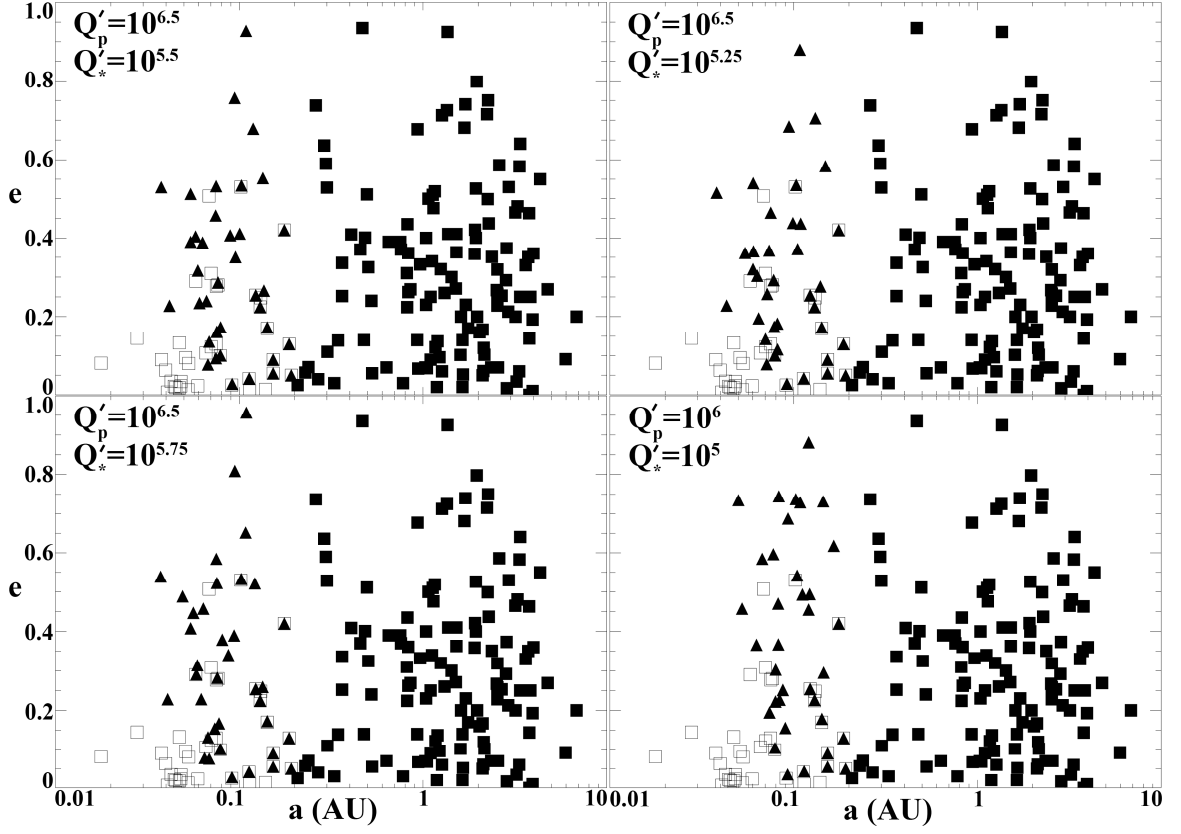
Figure 3.5: Distributions of orbital elements for four examples of pairs of Q'_p and Q'_* values out of the 289 we tested. Squares (filled and open) represent the currently observed orbital elements, with the open squares (with $a < 0.2$ AU) being candidates for significant tidal evolution. Triangles show the initial orbital elements ($e_{initial}$ and $a_{initial}$) determined by integrating the equations of tidal evolution backward in time to the formation of the planet.

A quantitative measure of the degree of agreement between, on one hand, the distribution of the computed initial values of e for the close-in planets and, on the other hand, the e-distribution observed for farther-out (greater a) planets confirms this qualitative impression. Recall that the K-S test showed the e-distribution to be quite consistent over a broad range of a values; the distribution of e for orbits with a from 0.2 to 1 AU is consistent with those from 1 to 5 AU at the 96% level of confidence. So now we can compare our computed initial e distribution for the close-in planets with the standard e distribution observed for $a > 0.2$ AU. Figure 3.6 shows the K-S scores as a function of the two Q values. Here we see reasonably good fits are possible only if $Q'_p \approx 10^{6.5}$, and there is reasonable agreement for a broad range of Q'_*. However, peaks in the K-S score are found with values ~99% for $Q'_* = 10^{5.5}$ or $10^{5.25}$. The fit for $Q'_* = 10^{5.75}$ is only a little worse, with a K-S score of about 97%. For $Q'_p = 10^6$ and $Q'_* = 10^5$, the K-S score is 19%.

Figure 3.7 shows the tidal evolution of a and e over time for each of the planets, for the case of $Q'_p = 10^{6.5}$ and $Q'_* = 10^{5.5}$. (The evolutionary tracks for $Q'_p = 10^{6.5}$ and Q'_* = $10^{5.25}$ are very similar.) The current observed values are at the lower left end of each trajectory in (a, e) space. These points correspond to white squares in Figure 3.5. The tick marks show the position at intervals of 500 Myr, going back in time from the present toward the upper right. Black dots have been placed at a point representing the best age estimate for the planetary system. These are the same points shown as the triangles in Figure 3.5 (top left panel). We have indicated the evolution going back further in time for

use if a more reliable age becomes available, or to indicate the evolutionary path if the Q' values were different (but still with the same ratio assumed here).

The curvature of these trajectories is indicative of the relative importance of the terms in Equations (3.1) and (3.2). A trajectory that is concave to the upper left usually indicates that tides raised on the star are most important, while concavity to the lower right indicates that tides on the planet are the most important.

As e grows, a trajectory initially dominated by the stellar tide can become dominated by the planetary tide. The evolutionary track of 51 Peg b (currently at $a = 0.0527$ AU and $e = 0.013$) illustrates this behavior, reversing concavity around $e = 0.35$ and $a = 0.06$ AU. The dominance reversal is due to the first term in Equation (3.1), which depends only on e^2: for large e, this term dominates da/dt because the planetary tide usually contributes more than the stellar tide. This effect underlines the importance of incorporating all the terms in Equations (3.1) and (3.2) when modeling tidal evolution.
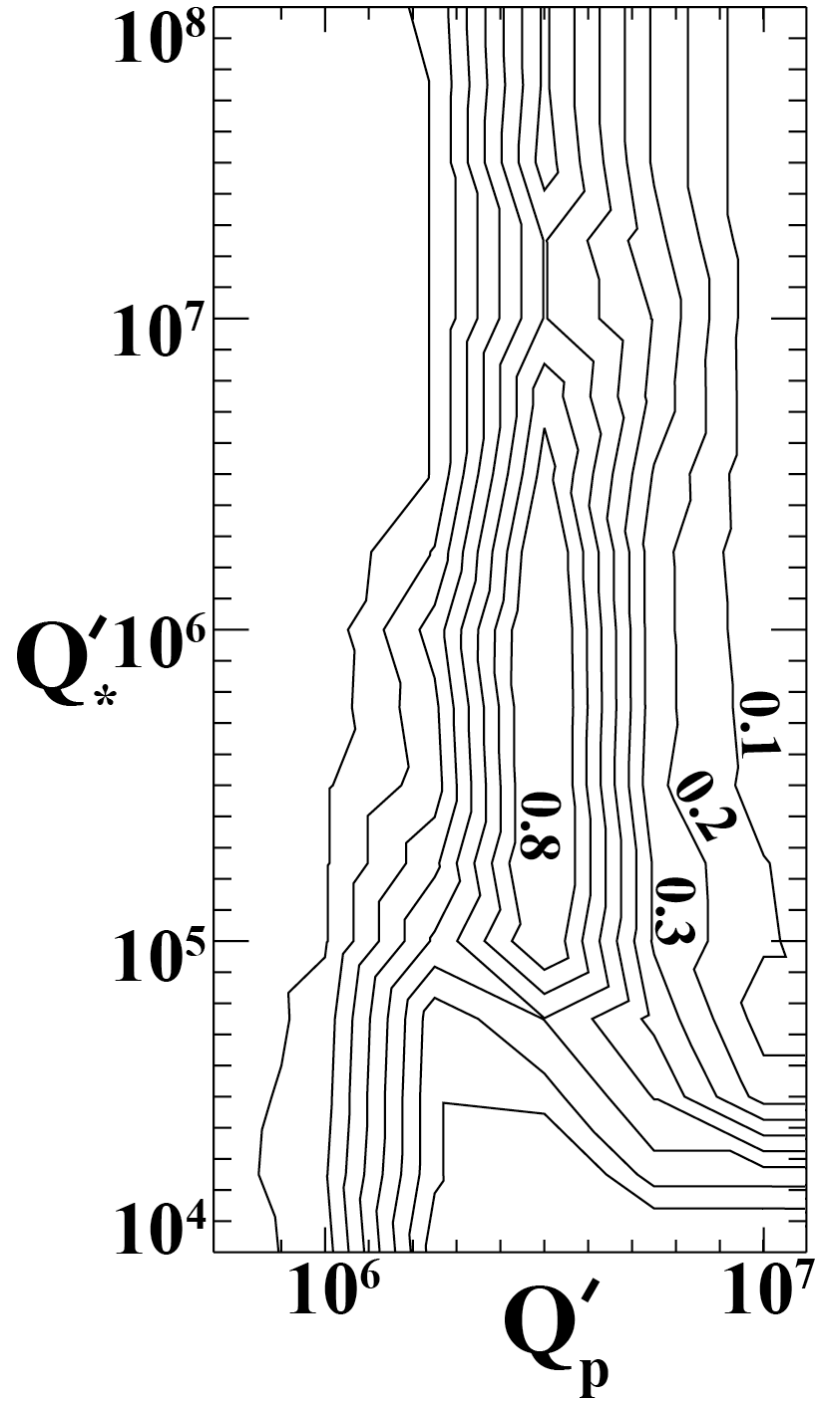
Figure 3.6: A contour plot of K-S test score as a function of Q'_* and Q'_p for comparison of the computed initial e distribution (after integrating tidal evolution back in time) of close-in planets ($a < 0.2$ AU) with the current e distribution for planets with $a < 0.2$ AU. Contours are spaced in 0.1 intervals.

Another important effect evident in Figure 3.7 is the acceleration or deceleration of tidal evolution as e and a decreases. The rate of tidal evolution is reflected in the spacing of tick marks along each trajectory. Moving forward in time from large values of e and a in the past, tidal evolution for many planets accelerates and then decelerates. For example, for 51 Peg b, the tick marks are closely spaced near the top of the trajectory, widely spaced in the middle, and closely spaced again near the bottom (near the present time). To understand this effect, consider tidal evolution moving forward in time. For larger values of a (far in the past), tidal evolution proceeds slowly, since both $(1/e)$ de/dt and $(1/a)$ $da/dt \propto a^{-13/2}$. However, as a decreases, the rate of tidal evolution increases. Later, as e becomes small enough, the rate of evolution can decrease. As a continues to drop, however, tidal evolution can again accelerate (Chapter 6).

Although, currently, tidal evolution for some planets is slower than in the past, some bodies are still undergoing very rapid tidal evolution, such as HD 41004B b. However, with $M_p = 18$ M_J, HD 41004B b is probably not a planet at all, but rather a brown dwarf. In this case, its history and evolution may be different from planets and may also have been affected by perturbations from other bodies in the system (Zhang & Hamilton 2007).

The evolutionary histories derived here include substantial changes in semi-major axis coupled with the changes in eccentricity. Figure 3.8 compares the initial value of a with the current value. Presumably the initial value is the value of a just after other orbit changing effects, such as gas drag or other effects of the planet-formation process, became less important so that tides began to dominate the evolution. For many close-in

planets, Figure 3.8 shows that initial a values were significantly higher than the currently observed values. These initial values of a may represent their locations at the termination of gas disk migration in each early planetary system.

Figure 3.9 indicates where that gas disk migration may have halted for different choices of Q' values. In that figure, we plot, as a function of Q'_* and Q'_p, the inner edge of the initial a distribution, defined here as second smallest $a_{initial}$ for our group of modeled planets as a function of Q'_* and Q'_p. (We use the *second* smallest $a_{initial}$ because, in looking for a trend for $a_{initial}$, we might expect at least one outlier to skew the trend.) The inner edge of $a_{initial}$ values might represent the distance at which gas disk migration halted for the planets. For our best-fit Q' values, the edge is at $a_{initial} = 0.036$ AU (GJ 436 b), about twice as far out as the smallest current a values (Figure 3.1).
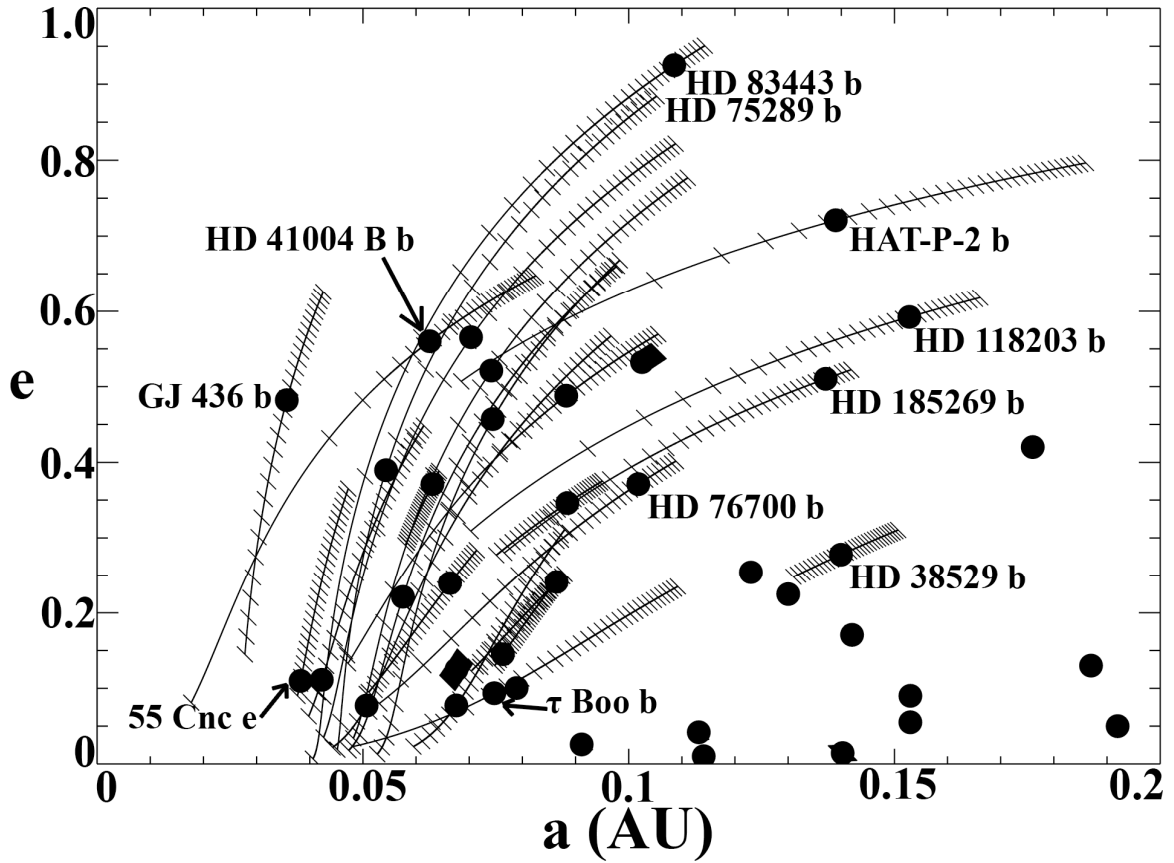
Figure 3.7: Tidal evolution of *e* and *a* for the sample of known close-in extra-solar planets using values $Q'_* = 10^{5.5}$ and $Q'_p = 10^{6.5}$. Solid curves represent the trajectories of orbital evolution from current orbits (lower left end of each curve) backward in time (toward the upper right). On the trajectories, tick marks are spaced every 500 Myr to indicate the rate of tidal evolution. Tidal integrations were performed for 15 Gyr for all planets, but the filled circles indicate the initial values of orbital elements at the beginning of each planet's life. Due to space restrictions, most planets are not labeled. However they can be identified by the (*a*, *e*) values at the lower left end of each trajectory, using Table 3.1. For example, 51 Peg b starts at (*a*, *e*) = (0.0527 AU, 0.013).
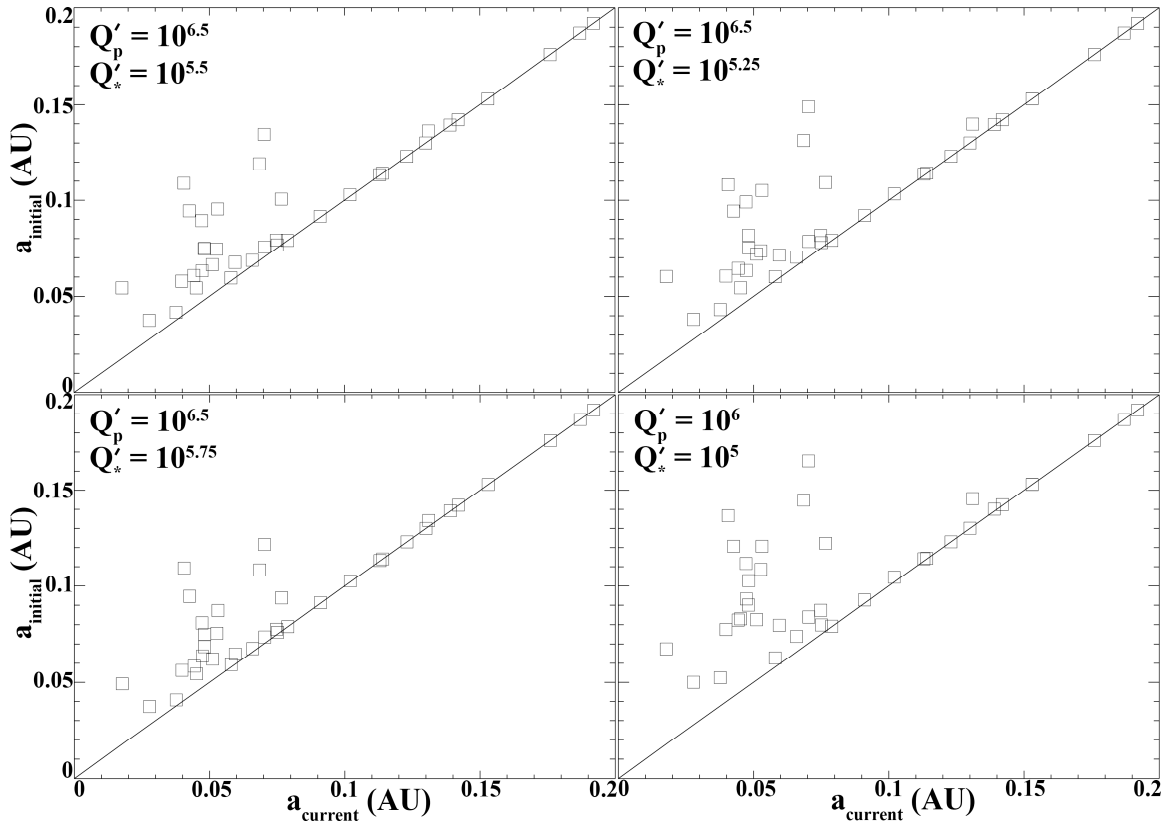
Figure 3.8: Change in a for each close-in planet due to tidal evolution from the initial value to the current value. Results are shown for the same four pairs of Q' values as in Figure 3.5. The distance above the diagonal line ($a_{current} = a_{initial}$) represents the distance a planet has migrated inward (in a) since the nebula dissipated and tides became the dominant effect.
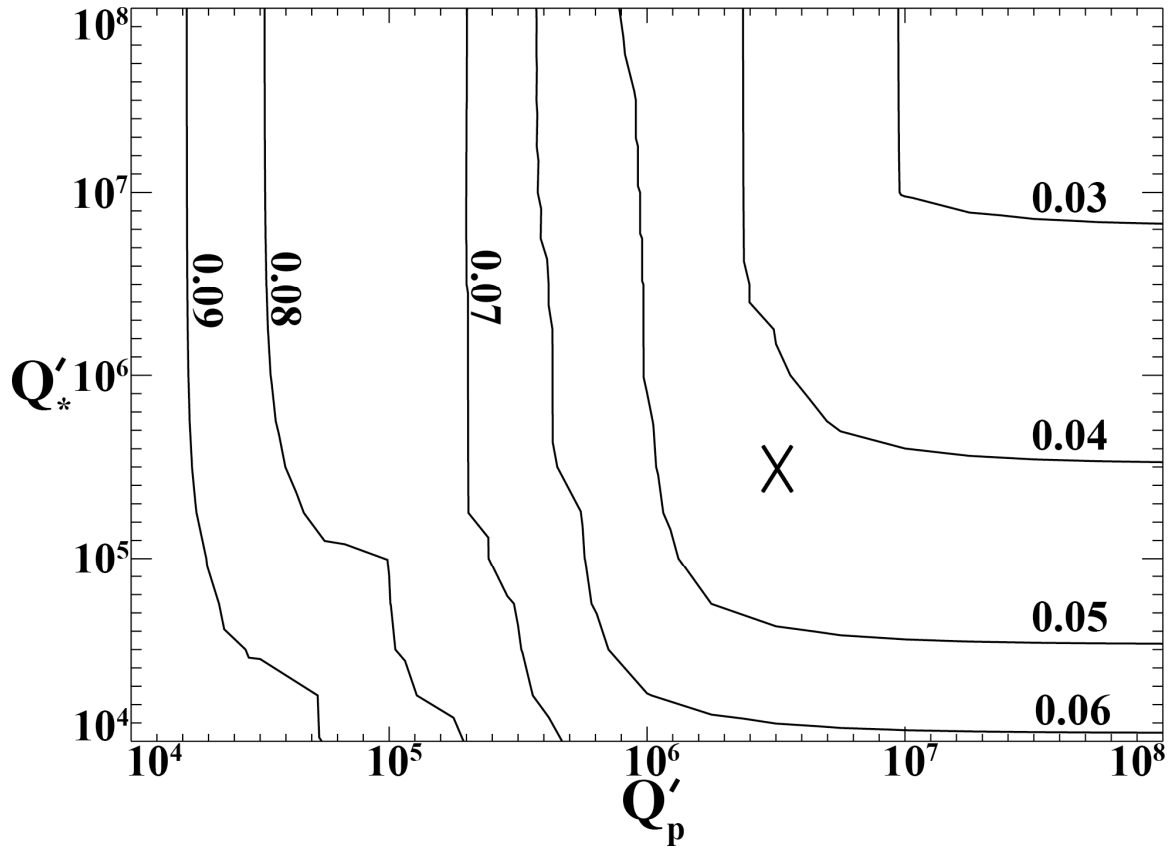
Figure 3.9: The inner edge of the *a* distribution for inferred initial conditions ($a_{initial}$ in AU), as a function of the assumed values of Q'_* and Q'_p. The "inner edge" is the second smallest value of $a_{initial}$. (The smallest value is assumed to be a less significant outlier.) The current edge by this definition is $a_{current} = 0.0278$ AU. For our best-fit Q' values (shown by the X), the inner edge was about twice as far from the star as the current position.

3.5.   Discussion

This investigation supports the hypothesis that tidal interactions between a star and a planet are responsible for the relatively small e values of close-in planets (as proposed by Rasio *et al.* 1996), although our calculations incorporate important corrections to previous studies. We have used a more complete set of tidal evolution equations, including tides raised on both planet and star, considering the strong coupling between eccentricity and semi-major axis evolution, and avoiding inappropriate assumptions such as conservation of angular momentum. Going back in time, the eccentricity distribution is restored to match that of farther-out planets.

Even with the relatively small eccentricities of the close-in planets explained, there remains the unresolved question of the origin of the initial eccentricity distribution of both close-in and farther-out planets. Rasio & Ford (1996) and Weidenschilling & Marzari (1996) originally proposed that planet-planet scattering early in the life of an extra-solar system could naturally lead to the large eccentricities observed. Subsequent work seems to support this initial hypothesis (Rasio & Ford 1996; Ford, Havlikova, & Rasio 2001; Marzari & Weidenschilling 2002; Ford & Rasio 2005; Chatterjee *et al.* 2008). An alternative model to explain the eccentricity distribution is that the eccentricities were set during the formation of planets in a gaseous disk. In this scenario planets excite spiral density waves in the disk, and the subsequent gravitational interactions between the planet and these waves can increase eccentricity. However, models of disk migration appear unable to pump up eccentricities to large (> 0.3) values (*i.e.*, Boss 2000; D'Angelo *et al.* 2006). Since our work has shown even close-in planets formed with much larger e,

the most plausible mechanism for producing the initial e values is the planet-planet scattering model, although some modification to the original views of that model are needed (see, *e.g.*, Barnes & Greenberg 2007). Thus the origin of the large and widely distributed eccentricities among extra-solar planets remains uncertain.

Significant reductions in semi-major axes have accompanied the changes in eccentricity, with important implications. First, models of protoplanetary migration in the primordial gas disk need not carry "hot Jupiters" in as far as their current positions. Lin *et al.* (1996) proposed that migration in the gas disk halted near the inner edge of the disk, a boundary determined by clearing due to the host star's magnetosphere. Our results show that the inner edge for many systems may have been farther out than indicated by the current semi-major axes of the planets, which were only reached during tidal migration long after the nebula had dissipated. In order to evaluate where migration due to the gas disk halted, (and thus where the inner edge of the nebula was) models should account for the subsequent tidal evolution.

In fact, more recent work (Jackson *et al.* 2009; Levrard *et al.* 2009) has shown that tides may have caused many close-in extra-solar planets to migrate all the way into their host stars and be completely destroyed. These recent studies indicate that the orbits of currently observed close-in planets are unstable to tides, contrary to previous studies (*e.g.* Rasio *et al.* 1996). Jackson *et al.* (2009) point out that the inner cut-off in a-values observed for close-in planets probably does not represent an inner edge to a gas disk for all systems or the point at which inward migration of planets stopped. These results are discussed more in Chapter 6.

The tidal changes in orbital semi-major axes also have implications for observations of planetary transits, such as surveys of young open galactic clusters (Bramich *et al.* 2005; Burke *et al.* 2006). The probability to observe a planetary transit increases for smaller semi-major axes, but decreases as orbits become more circular (Borucki et al. 1984; Charbonneau *et al.* 2007a; J. Barnes 2007). Tidal evolution means that the probability of an observable transit depends on a star's age, but the exact relation depends on the particular evolutionary path through (*a*,*e*) space. As our understanding of the statistics of tidal evolution paths improves, the observed frequency of transits in the field and in open clusters may eventually help to constrain planetary formation scenarios, distinguishing, for example, between the relative roles of embedded migration and of gravitational scattering, which set up the initial conditions for tidal evolution. However, transit statistics may not yet be refined enough to be sensitive to detect this effect (Pepper & Gaudi 2005).

The inward evolution of semi-major axes of close-in planets also has implications for their thermal history because the stellar energy received by the planets over their lifetimes may have been less than assumed. For example, Hubbard *et al.* (2007) studied the effects of evaporative mass loss from the close-in extra-solar planets. They calculated that the smaller planets should lose mass more quickly than larger ones. However, the mass-frequency distribution of observed planets is fairly independent of *a*. Thus they concluded that mass loss by evaporation has been negligible, and that any migration in *a* has been independent of mass. However, our results suggest that during tidal evolution, more massive planets may have experienced significantly more migration than less

massive ones, although, balanced against mass loss effects, it's not clear how this process would affect the mass distribution for close-in planets.

The tidally driven changes in semi-major axes also may affect modeling of interior processes in the planets and the implications for their radii. Burrows *et al.* (2007) modeled the effects of radiative cooling and stellar insolation in an attempt to understand the observed radii of transiting planets and their implications for internal structure and atmospheric opacity. Since tides have probably induced migration for many close-in planets from initially more distant orbits, Burrows *et al.* overestimated the total insolation experienced by these planets. Revision of these models taking into account a variable insolation history may give somewhat smaller planetary radii, which may exacerbate disagreement between the theory and radii inferred from transit observations.

On the other hand, tidal heating that accompanied the orbital evolution would have added to the heat budget considered by Burrows *et al.* and might have significant effects on planetary radii, as suggested by Bodenheimer *et al.* (2003). Especially in the past, when *e* was much larger, tidal heating may have contributed significantly to planetary thermal budgets. Jackson *et al.* (2008b) showed that this source of heat is probably important for evaporative mass loss, as well as interior structure. Tidal heating rates have changed dramatically as the orbits evolved, and past heating may be responsible for the inflated radii of many transiting extra-solar planets, as discussed in the next chapter.

3.6.   Conclusions

The results presented here confirm that tidal evolution is likely responsible for the relatively low orbital eccentricities of close-in extra-solar planets. The initial distribution of e for these planets (at the time that tidal evolution became dominant, after the gas disk had dissipated) agrees well with the e distribution for farther-out planets. There is good agreement for ($Q'_* = 10^{5.5}$, $Q'_p = 10^{6.5}$) and ($Q'_* = 10^{5.25}$, $Q'_p = 10^{6.5}$). These Q' values are consistent with estimates from orbital constraints in the Solar System, as well as from models of the physics of gaseous bodies.

Our numerical solutions of the tidal evolution equations demonstrate the importance of retaining all terms representing the tides on both the planet and the star. It is inaccurate, when considering changes in eccentricities, to ignore tides raised on the star. Similarly, it is inaccurate, when considering changes in semi-major axis, to ignore tides raised on the planet. Incorporating these effects significantly improves the accuracy of our results relative to previous studies. We have also shown the significance of the coupling between the evolution of a and e. Previous conclusions reached by considering the "timescale" for changes in e have depended on the assumption that the simultaneous changes in a can be ignored. Using that approximation, the time dependence of e would be exponential, with a corresponding timescale. However, the simultaneous changes in a cause the time variation of e to be more complex, with de/dt not even necessarily changing monotonically over the age of a planet. Similarly, "tidal migration" has generally been considered to be a process of change in semi-major axis. However, such change is often coupled intimately with the changes in e, so tidal migration should always

refer to both aspects of the change in an orbit. In summary, the results of studies that incorporated approximate solutions to Equations (3.1) and (3.2) should be applied with caution.

Our full treatment of tidal evolution has revealed that close-in planets have current orbital semi-major axes typically half as large as they were at the time that the planets had formed and the nebula cleared. Even the closest-in planets we observe today probably started with $a_{initial} > 0.04$ AU. However tides have probably destroyed many planets, so it is unclear where the inner cut-off in initial a-values may have been, if, indeed, there was such a cut-off.

We have neglected interactions between the tidally evolving planet and other planets in its system. Ten of the 36 of the planets in our study are known to be members of a multi-planet system. Models that couple tidal evolution to planet-planet interactions have been developed (Mardling & Lin 2002; Adams & Laughlin 2006), but they require specific assumptions about the tidal response of bodies. The modeling of such complex phenomenon was beyond the scope of this paper, but future work should include these effects.

Since our equations depend sensitively on many uncertain parameters (such as system age, $a_{current}$, and planetary radii), the exact model solution we present here is not exact for any specific planet. However, assuming that errors in our choices for significant parameters are evenly spread about their correct values, our calculations probably provide a reasonable representation of the population as a whole. Similarly, our assumption that all planets have the same Q'_p as one another, and that all stars have the same Q'_* as one

another, surely introduces errors for individual planets and stars, but probably provides a reasonable first estimate of the evolution of the population as a whole.

In the future, our approach can be revised and updated, and the results can be refined. As tidal dissipation mechanisms come to be better understood, particularly their dependence on frequency, we can improve our calculations, and use forms of the governing equations that are more reliable at large e. As more extra-solar planets are discovered, the quality of our statistical analysis will improve. Continued radial-velocity observations will result in better orbital solutions, while transit observations will provide us with more accurate planetary masses and radii. Also, improvements in stellar age estimates will help us to better understand the duration of tidal effects.

As the orbits of the close-in planets evolve, tidal heating rates have also evolved, changing by orders of magnitude. The large variations in heating rates have been suggested to be important in determining internal structures of close-in planets, and in many cases, may explain the discrepancies between model predictions and observations of the radii of transiting planets. In the next chapter, we use the calculations presented in this chapter to determine past and present tidal heating rates of close-in planets.

Name	M_* (solar masses)	R_* (solar radii)	M_p (Jupiter masses)	R_p (Jupiter radii)	$a_{current}$ (AU)	$e_{current}$	Nominal Age (Gyr)	Minimum Age (Gyr)	Maximum Age (Gyr)	References for M_*, R_*, M_p, R_p, $a_{current}$, $e_{current}$, age
51 Peg b	1.09	1.15	0.472	1.20	0.05	0.01	6.76	5.28	8.40	2, 2, 2, …, 2, 2, 18
55 Cnc b	0.92	0.93	0.833	1.20	0.11	0.01	…	7.24	…	2, 2, 14, …, 14, 14, 18
55 Cnc e	0.92	0.93	0.038	0.34	0.04	0.09	…	7.24	…	2, 2, 14, …, 14, 14, 18
BD 10-3166 b	0.92	0.84	0.458	1.20	0.05	0.02	…	…	1.84	2, 2, 2, …, 2, 2, 18
GJ 436 b	0.44	0.46	0.077	0.37	0.03	0.15	…	7.41	11.05	12, 6, 2, 4, 16, 16, 17
GJ 876 c	0.32	0.39	0.619	1.20	0.13	0.22	…	6.52	9.90	18, 7, 16, …, 16, 16, 17
HAT-P-2 b	1.928	1.474	9.04	0.982	0.07	0.52	2.60	1.20	3.40	1, 1, 1, 1, 1, 1, 1
HD 102117 b	1.11	1.26	0.170	0.55	0.15	0.09	9.40	8.04	10.60	2, 2, 2, …, 2, 2, 18
HD 108147 b	1.19	1.25	0.261	0.64	0.10	0.53	3.20	2.32	3.92	2, 2, 2, …, 2, 2, 18
HD 118203 b	1.23	2.13	2.140	1.20	0.07	0.31	4.60	3.80	5.40	3, 3, 3, …, 3, 3, 3
HD 130322 b	0.88	0.85	1.090	1.20	0.09	0.03	…	10.80	…	2, 2, 2, …, 2, 2, 18
HD 13445 b	0.77	0.80	3.910	1.20	0.11	0.04	…	8.48	…	2, 2, 2, …, 2, 2, 18
HD 149143 b	1.10	1.55	1.330	1.20	0.05	0.08	7.60	6.40	8.80	3, 3, 2, …, 3, 3, 3
HD 162020 b	0.78	0.74	15.000	1.20	0.08	0.28	…	…	0.76	19, 19, 2, …, 19, 19,18
HD 168746 b	0.93	1.04	0.248	0.63	0.07	0.11	12.40	10.28	…	2, 2, 2, …, 2, 2, 18
HD 179949 b	1.21	1.22	0.916	1.20	0.04	0.02	2.56	0.92	3.68	2, 2, 2, …, 2, 2, 18
HD 185269 b	1.28	1.88	0.909	1.20	0.08	0.28	4.00	3.00	…	8, 8, 2, …, 8, 8, 15
HD 187123 b	1.08	1.17	0.532	1.20	0.04	0.04	7.40	6.24	8.64	2, 2, 2, …, 2, 2, 18
HD 192263 b	0.81	0.77	0.641	1.20	0.15	0.06	2.56	…	13.36	2, 2, 2, …, 2, 2, 18
HD 195019 b	1.07	1.38	3.700	1.20	0.14	0.01	2.00	…	7.04	2, 2, 2, …, 2, 2, 18
HD 209458 b	1.14	1.14	0.690	1.32	0.05	0.01	2.44	0.80	3.76	2, 2, 2, 9, 10, 10, 18
HD 217107 b	1.10	1.08	1.410	1.20	0.07	0.13	5.84	3.40	7.76	2, 2, 20, …, 20, 20, 18
HD 38529 b	1.47	2.50	0.852	1.20	0.13	0.25	3.28	3.04	3.64	2, 2, 2, …, 2, 2, 18
HD 41004B b	0.40	0.49	18.400	1.20	0.02	0.08	…	1.48	1.64	22, 7, 22, …, 22, 22, 17
HD 46375 b	0.92	0.94	0.226	0.61	0.04	0.06	…	11.88	…	2, 2, 2, …, 2, 2, 18
HD 49674 b	1.06	0.95	0.115	0.49	0.06	0.29	…	..	3.56	2, 2, 2, …, 2, 2, 18
HD 6434 b	0.79	0.74	0.397	1.20	0.14	0.17	13.30	7.00	…	13, …, 13, …, 13, 13, 17, 17
HD 68988 b	1.18	1.14	1.850	1.20	0.07	0.12	3.40	1.40	4.44	2, 2, 21, …, 21, 21, 18
HD 69830 b	0.87	0.90	0.032	0.32	0.08	0.10	…	12.04	…	2, 2, 11, …, 11, 11, 18
HD 75289 b	1.21	1.28	0.467	1.20	0.05	0.03	3.28	2.60	3.88	2, 2, 2, …, 2, 2, 18
HD 76700 b	1.13	1.34	0.233	0.62	0.05	0.10	9.84	8.80	12.76	2, 2, 2, …, 2, 2, 18

HD 83443 b	1.00	1.02	0.398	1.20	0.04	0.01	…	11.68	…	2, 2, 2, …, 2, 2, 18
HD 88133 b	1.20	1.93	0.299	0.67	0.05	0.13	…	6.27	9.56	5, 5, 2, …, 2, 2, 18
HD 99492 b	0.86	0.76	0.109	0.48	0.12	0.25	…	…	1.80	2, 2, 2, …, 2, 2, 18
τ Boo b	1.35	1.43	4.130	1.20	0.05	0.02	1.64	1.12	2.08	2, 2, 2, …, 2, 2, 18
υ And b	1.32	1.42	0.687	1.20	0.06	0.02	3.12	2.88	3.32	2, 2, 2, …, 2, 2, 18

Table 3.1: 1 solar mass = 1.9891×10^{30} kg, 1 solar radius = 695500 km, 1 Jupiter mass = 1.8986×10^{27} kg, and 1 Jupiter radius = 71492 km. R_p values were computed as discussed in the text. References: (1) Bakos *et al.* (2007); (2) Butler *et al.* (2006), (3) Da Silva *et al.* (2006); (4) Deming *et al.* (2007); (5) Fischer & Valenti (2005); (6) Gillon *et al.* (2007b); (7) Gorda & Svechnikov (1996); (8) Johnson *et al.* (2006); (9) Knutson *et al.* (2007); (10) Laughlin *et al.* (2005c); (11) Lovis *et al.* (2006); (12) McArthur *et al.* (2004); (13) Maness *et al.* (2007); (14) Mayor *et al.* (2004); (15) Moutou *et al.* (2006); (16) Rivera *et al.* (2005); (17) Saffe *et al.* (2006); (18) Takeda *et al.* (2007); (19) Udry *et al.* (2002); (20) Valenti & Fischer (2005); (21) Vogt *et al.* (2005); (22) Zucker *et al.* (2004).

Name	nom e	min e	max e
51 Peg b	0.013	0.001	0.025
55 Cnc b	0.01	0.023	0
55 Cnc e	0.09	0.062	0.118
BD 10-3166 b	0.019	0	0.042
GJ 436 b	0.16	0.14	0.18
GJ 876 c	0.2243	0.223	0.2256
HAT-P-2 b	0.52	0.51	0.53
HD 102117 b	0.121	0.039	0.203
HD 108147 b	0.53	0.4	0.64
HD 118203 b	0.309	0.295	0.323
HD 130322 b	0.025	0	0.057
HD 13445 b	0.046	0.042	0.05
HD 149143 b	0.08	0.04	0.12
HD 162020 b	0.277	0.275	0.279
HD 168746 b	0.107	0.027	0.187
HD 179949 b	0.022	0.007	0.037
HD 185269 b	0.3	0.26	0.34
HD 187123 b	0.023	0.008	0.038
HD 192263 b	0.055	0.016	0.094
HD 195019 b	0.0138	0.0094	0.0182
HD 209458 b	0.014	0.005	0.005
HD 217107 b	0.13	0.11	0.15
HD 38529 b	0.248	0.225	0.271
HD 41004B b	0.081	0.069	0.093
HD 46375 b	0.063	0.037	0.089
HD 49674 b	0.087	0	0.182
HD 6434 b	0.17	0.14	0.2
HD 68988 b	0.1249	0.1162	0.1336
HD 69830 b	0.1	0.06	0.14
HD 75289 b	0.034	0.005	0.063
HD 76700 b	0.095	0.02	0.17
HD 83443 b	0.012	0	0.036
HD 88133 b	0.133	0.061	0.205
HD 99492 b	0.254	0.162	0.346

τ Boo b	0.023	0.008	0.038
υ And b	0.023	0.005	0.041

Table 3.2: Ranges of orbital eccentricities allowed by observational uncertainties. The nominal ("nom"), minimum ("min") and maximum ("max") values are taken from the same sources as given in Table 3.1.

Chapter 4
Tidal Heating of Extra-Solar Planets

4.1.   Introduction

In the previous chapter, we demonstrated the importance of the orbital effects of tides on the orbits of extra-solar planets, and discussed implications for the origins and formation of the planets. Tidal evolution of a planet's orbit is necessarily accompanied by dissipation of energy within the planet and its host star. In many cases, the rates of dissipation may be large enough to significantly affect the planet's internal structure and physical properties. In this chapter, we discuss the tidal heating of close-in extra-solar planets that accompanied their orbital evolution and its relevance to observations of transiting extra-solar planets.

During the course of the tidal evolution, tidal distortion of the figure of the planet can result in substantial amounts of internal heating at the expense of orbital energy. As the planet passes from pericenter to apocenter and back, the tidal distortion oscillates between its maximum and minimum size. The rate at which the distortion oscillates at its amplitude depend on the orbital elements e, a, and n (which depends on a), so the heating rate is coupled to the evolution of the orbit. Compared with their current orbits, many close-in planets were probably farther from their host star (larger semi-major axes) at the time that the planetary system formation had ceased and the gaseous nebula dissipated. In a typical case, tidal heating might have begun modest, when a was larger (and n was smaller) but then increased as tides reduced the semi-major axis a (and increased n). As

the tides became stronger, they would circularize the orbit, which in turn would shut down the tidal heating mechanism.

Thus two competing effects are in play: the reduction of *a* which increases tidal heating, and the damping of *e* which decreases the heating. The relative strength and timing of these two effects determines a planet's history, typically with a gradual increase in the heating rate followed by a decrease.

The effects of tidal heating on a planet's internal structure may be critical in determining its physical properties. For example, models of extra-solar planets have considered the effects of heating on their radii, which can be measured directly by transit observations. Heat sources that have been considered in these models include the energy of planetary accretion and radiation from the star, as well as tidal heating (Bodenheimer *et al.* 2003; Mardling 2007; Winn & Holman 2007). In many cases the theoretical predictions match the observations reasonably well. However, there are notable exceptions. HD 209458 b has been observed by Knutson *et al.* (2007) to have a radius of 1.32 Jupiter radii (R_{Jup}), which is about 10-20% larger than predicted by theoretical modeling (Guillot 2005; see also Burrows *et al.* 2007). HAT-P-1 b is also larger than predicted by theory (Bakos *et al.* 2007a). On the other hand, HAT-P-2 b is observed (Bakos *et al.* 2007b) to be about 12% *smaller* than the radius predicted by theory (Fortney *et al.* 2007).

Theoretical models must make multiple assumptions about the behavior of gases at high pressures, atmospheric heat flow, and radiative cooling, among others. Moreover, theoretical models to date have not taken into account the history of tidal heating for

close-in planets. Of course, those are the planets most likely to have radii measurable by transits. To help address the effects of tidal heating, we calculated the tidal heating histories that would accompany the orbital evolution as computed in the previous chapter.

4.2.   Method

The computation of the tidal evolution was described by Jackson *et al.* (2008a) and in the previous chapter. The dissipation of energy within a planet due to tides comes directly from the planet's orbit (except perhaps very early-on while the planetary spin is quickly brought to the equilibrium rate). The orbital energy depends on only one orbital element, the semi-major axis. Thus the term in the equation for *da/dt* that corresponds to tides raised on the planet by the star also gives the heating rate. In this way, the heating rates can be extracted from the same numerical integrations of the tidal evolution of orbits.

We have considered for various planets of interest the range of heating histories, given the range of uncertainties in their current orbital elements. For example, planets with nominal reported eccentricities of zero were not considered by Jackson *et al.* (2008a). If *e* were really zero, there would be no tidal heating as long as the planetary rotation rates were equal to the equilibrium rate. Here we consider the possible heating, even for those planets, using the full range of *e* and *a* values that may be consistent with observational uncertainty. The planets that we discuss here are of particular interest because in each case there is some basis for comparison of thermal models with an observationally measured radius.

4.3.   Tidal Heating Histories

Using the notation and assumptions in the previous chapter, the tidal heating rate

H can be expressed as

$$H = (\tfrac{63}{4}) \frac{(GM_*)^{3/2} M_* R_p{}^5}{Q'_p} a^{-15/2} e^2 \qquad (4.1)$$

As discussed in the previous chapter, tidal evolution of the orbital elements

reduces both *a* and *e*, with competing effects on the heating rate: Reducing *a* increases

the heating, but reducing *e* decreases it. The evolutionary histories presented in the

previous chapter are such that the change in *a* usually dominates earlier on, while the

damping of *e* dominates later. Thus a typical heating history involves an increase to a

maximum rate, followed by a decrease to the current rate. In the next section, we consider

the variation in heating rate for several planets of interest. The orbital and physical

parameters we adopted for our modeling are listed in Table 4.1, in which M_p is a planet's

mass and R_* is the stellar radius. Minimum (min), nominal (nom) and maximum (max)

values of orbital parameters that are allowed by observation are listed there as well.

4.3.1. Planets with published eccentricities

4.3.1.1.   HD 209458 b

Figure 4.1 shows the time history of the tidal heating rate. The solid curve is

based on the nominal current *e* = 0.014 and *a* = 0.0473 AU (Laughlin *et al.* 2005a). The

dashed line is based on the maximum current heating rate consistent with the

observational constraints on the orbital elements, *i.e.* with the maximum plausible current value of *e* (0.042) and the minimum plausible value of *a* (0.0459 AU). The integrations go back 15 Gyr, although the nominal age of the system (shown by the vertical line) is 2.5 Gyr (Takeda *et al.* 2005). Burrows *et al.* (2007) suggest that a heating rate of about 4 x 10^{19} W would be required to maintain the observed planetary radius. Therefore, even with the largest possible current *e* value, the current tidal heating rate is too small to resolve the discrepancy between the large observed planetary radius and theoretical models. However, the history plotted in Figure 4.1 shows that the required heating rate was maintained for about a billion years after the system formed, and dropped off only about a billion years ago. If the lag in the response of the planet to the heating rate were on the order of a billion years, it may explain the observed large radius. Such a lag seems reasonable based on the long duration of the influence of heat of formation on the planet's radius in the modeling by Burrows *et al.* (2007), and more recent work confirms that the lag between heating and response of a planet's radius may be as long as 1 Gyr (Liu *et al.* 2008).

The evolution shown in Figure 4.1 is an example of the most general case of a rising heating rate followed by a decrease. In this case, it is likely that the system was near or at the peak of heating at the end of its formative period. If the current *e* value is less than the nominal value, then the heating rate has probably been decreasing throughout the lifetime of the planet. Note too that for this planet, observations cannot rule out a circular orbit. If that is the case, tidal dissipation could have been negligible.

Nevertheless, the best fit case, with a current $e = 0.014$ or larger, corresponds to a heating history that may help explain the large observed radius of this planet.

We note that some authors have estimated that the tidal circularization timescale for HD 209458 b was so short that a mechanism was needed to explain any planet's current non-zero eccentricity. For example, Mardling (2007) proposed that an additional planet is needed to maintain a non-zero eccentricity. However, transit timing observations rule out the existence of another planet with a period less than 15 days (Miller-Ricci *et al.* 2008). In fact, the issue may be moot, because the calculations from the previous chapter show that tides have taken billions of years to circularize HD 209458 b's orbit. The short circularization timescales estimated by previous workers were based on the exponential solution of the equation for tidal damping (*de/dt*), which ignored concurrent and codependent changes in semi-major axis. Because tides reduce both *a* and *e* together, ignoring changes in *a* significantly underestimated the time required to circularize orbits. Using the coupled equations for tidal evolution, we find it is perfectly reasonable that the eccentricity remains non-zero. Thus, tidal heating has likely been large during the past billion years, perhaps explaining the planet's surprisingly large radius.

4.3.1.2. HAT-P-1 b

Like HD 209458 b, this planet's observed radius of 1.36 R_{Jup} (Bakos *et al.* 2007a) is larger than expected from theoretical modeling that did not include tidal heating (Fortney *et al.* 2007). Figure 4.1 shows the tidal heating history for this planet. Similar to HD 209458 b, the heating rate ~ 1 Gyr ago was substantially higher than the present tidal

heating, based on either the nominal best fit *e* value (solid curve) or the maximum current *e* value (dashed line). In this case the planetary system is somewhat older, so the history extends further back in time, and thus includes a longer period of increasing tidal heating (due to the decrease in semi-major axis), followed by a decrease in heating (as the orbit circularizes). For both HD 209458 b and HAT-P-1 b, the substantial heating rate ~ 3-4 x 10^{19} W about 1 Gyr ago may help account for the discrepancy between the large observed planetary radii and the predictions of physical modeling.

4.3.1.3.   GJ 436 b

This planet has a measured radius consistent with theoretical models which did not include tidal heating (Gillon *et al.* 2007b). The tidal heating history shown in Figure 4.1 is consistent with that result. Compared with the previous two cases, the maximum heating rate was two orders of magnitude less. This lower rate of dissipation may be partially offset by the fact that the duration of the maximum heating was several billion years, *i.e.* the peak is much broader than for the previous planets. However, the total tidal heat is still much smaller than the other cases, and most of it was so long ago that its residual effects are probably negligible, which may explain why the measured radius fits the tide-free physical model.
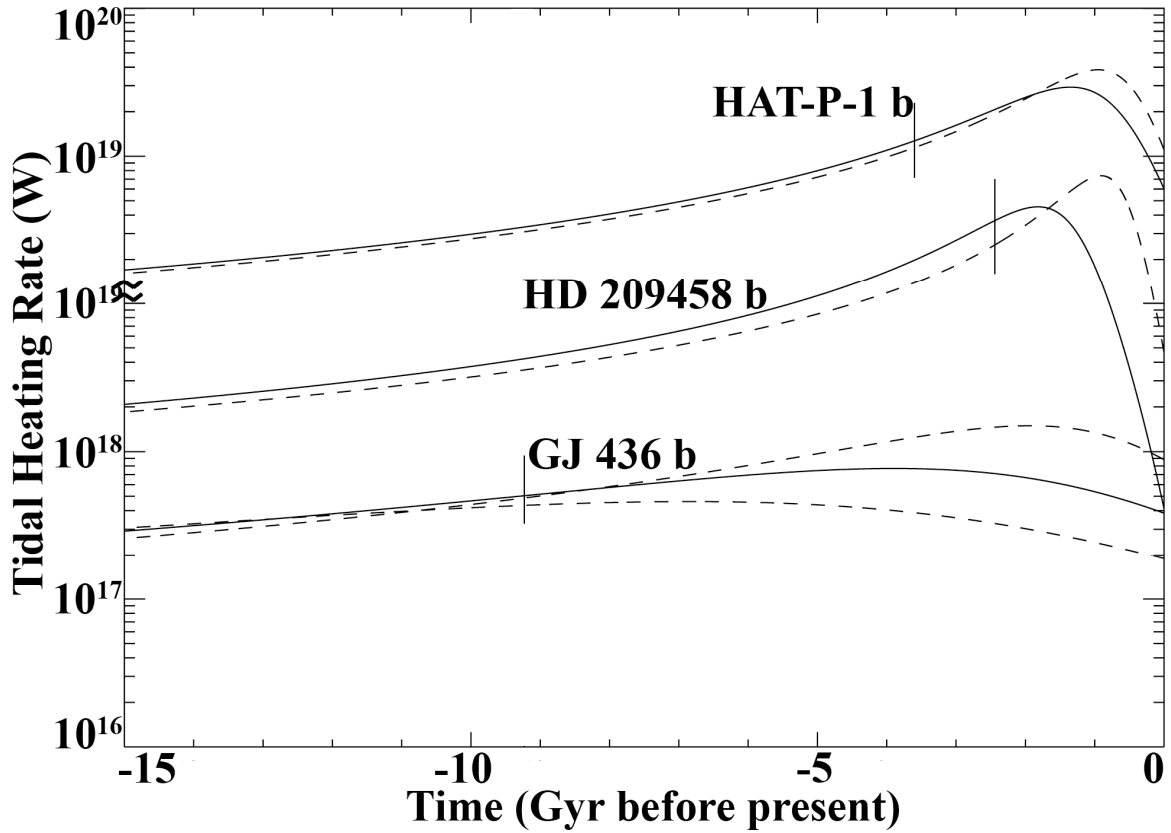
Figure 4.1: The tidal heating rates for planets HAT-P-1 b, HD 209458 b, and GJ 436 b as a function of time. The present time (t=0) is at the right, and the scale indicates the time before the present. Vertical lines indicate the best estimate of the formation time for the planet. Note that the vertical scale has been shifted (by a factor of 10) for HAT-P-1 b to make its curves more visible. For each planet, here and in subsequent figures, the vertical scale that corresponds to each curve is the scale intersected by that curve. The solid curve for each planet is based on the current nominal eccentricity value, while the dashed lines assume the maximum and minimum heating consistent with observational uncertainty in the orbital elements. For HAT-P-1 b and HD 209458 b, observations could not exclude a current eccentricity of zero, so the lower bound on heating rates is formally zero. Hence in those cases only one dashed line is shown, representing the upper limit. The following figures use the same conventions.

4.3.1.4.   TrES-1

This planet may have experienced more tidal heating than any of the previous cases as shown in Figure 4.2. Based on that result, and by analogy with HD 209458 b and HAT-P-1 b, one might have expected the measured radius to be larger than predicted by previous physical modeling. However, Winn *et al.* (2007) report that the measured radius does fit theory. It seems that the expected large amount of tidal dissipation did not affect the radius in this case, a surprising result that calls for an explanation. One possibility is that we have overestimated the tidal heating; another is that the theoretical modeling may need adjustment so as to accommodate more heat without increasing the inferred radius.

4.3.1.5.   HAT-P-2 b

In this case also there has been a substantial amount of tidal heating (Figure 4.2). The current heating rate is similar to the maximum rate attained by HD 209458 b and HAT-P-1 b, so again we might expect a larger radius than predicted by theory that ignored tidal heating. In this case, however, the measured radius is actually smaller than predicted (Bakos *et al.* 2007b). Thus there is a discrepancy between theory and observation even if tidal heating is neglected. Correction to the theoretical modeling seems to be necessary, and the correction would need to be in the same sense as that for TrES-1 (*i.e.*, a smaller radius for a given amount of heating). The fact that there is likely a high rate of tidal dissipation makes the problem even worse.

On the other hand, a key factor in the reconciliation may be that, while the current tidal heating rate is high and increasing, in the recent past the heating rate was much lower. HAT-P-2 b is still on the increasing part of the heating curve, which is unusual among planets considered here, most of which have passed their peaks. The fact that the heating rate was several times smaller a billion years ago than it is now may help explain the small radius.

Compare that result with what we found above for the planets where the observed radii are larger than expected (HD 209458 b and HAT-P-1 b). In those cases, the fact that the heating rate was several times *larger* a billion years ago than it is now may help explain the *large* radius. In all of these cases it seems that the heating rate in the past (~1 Gyr ago) may been the crucial factor in determining the current radius.
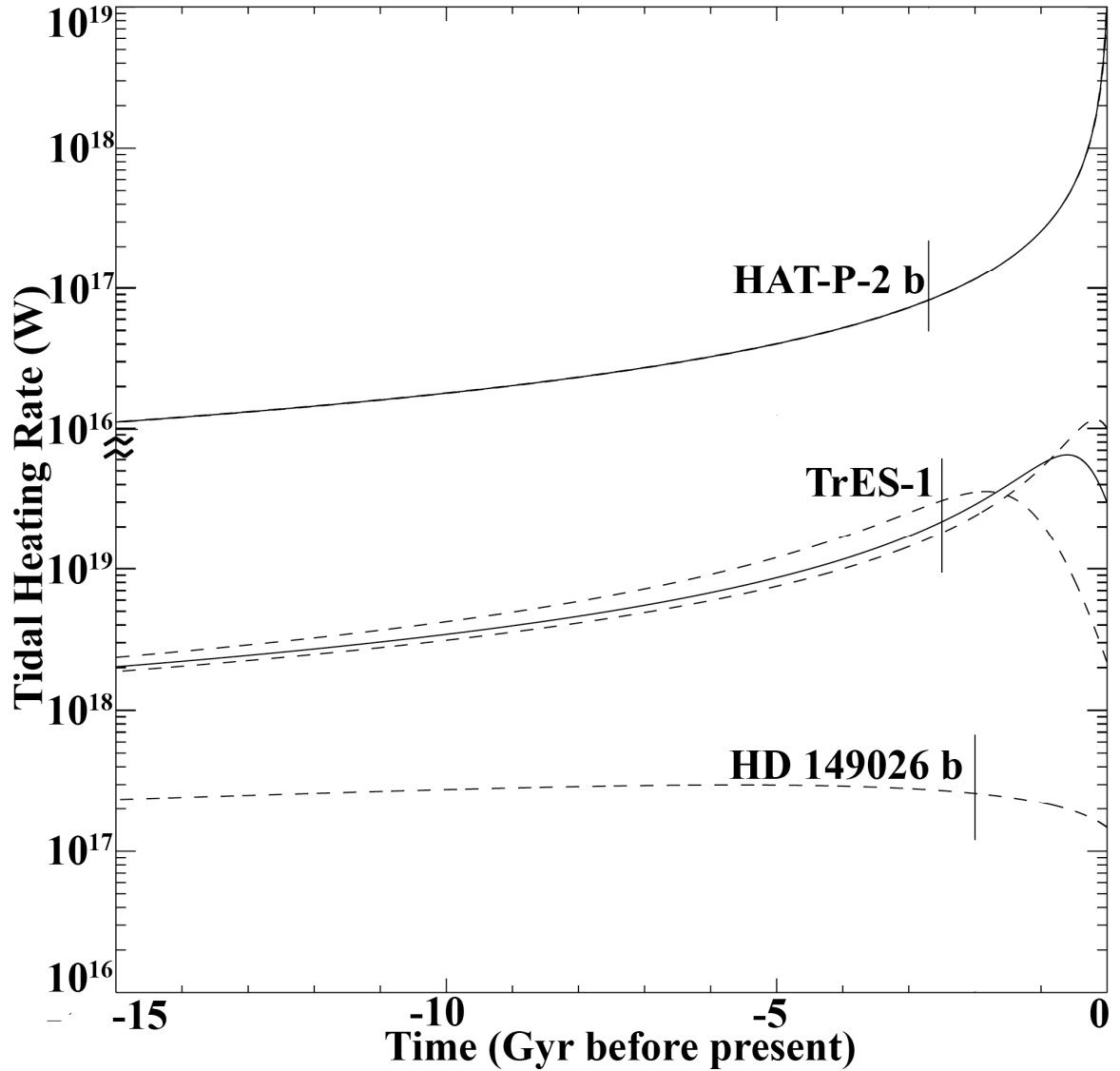
Figure 4.2: The tidal heating rates for planets HAT-P-2 b, TrES 1 b, and HD 149026 b as a function of time, similar to Figure 4.1. Note that the vertical scale has been shifted for HAT-P-2 b to make its curves more visible. The minimum and maximum heating rates for HAT-P-2 b are nearly equal to the nominal rate, and so the corresponding curves are covered up. The solid lines and dashed lines have the same meaning as in Figure 4.1. For HD 149026 b, the dashed line represents the maximum heating consistent with observational limits, while the nominal eccentricity is zero, corresponding to zero heat (off scale) throughout the history.

4.3.1.6.   HD 149026 b

For this planet, the maximum e allowed by observation is 0.02, although the nominal adopted e value is zero. Even assuming a current orbit that would allow maximum heating, (dashed line in Figure 4.2) given observational constraints on the current orbit, tidal heating has been only about 2 x 10^{17} W for most of the lifetime of the system, and has dropped by about 30% during the past 1 Gyr as the eccentricity has damped down. Similarly to GJ 436 b, tidal heating is probably not a factor in determining its radius. In fact, transit observations show HD 149026 b has one of the smallest radii measured for any extra-solar planet, 0.726 R_{Jup} (Charbonneau *et al.* 2006). Interior models require a large core, with a mass ~80 Earth masses, to be consistent with this small observed radius (Sato *et al.* 2005). Conceivably, such a core would have a lower Q_p than we have assumed as the bulk value for this planet because rocky bodies generally have $Q_p \sim 100$. In that case the tidal heating may have been great enough to have been a factor in the planet's geophysical history. However, if additional heat were incorporated into the theoretical modeling, it might tend to increase the model radius, perhaps requiring an even larger core to match the observed radius. In any case the theoretical models need to take into account the possible addition of considerable tidal heating.

4.3.2. Planets with undetermined eccentricities

For most extra-solar planets whose eccentricities have not yet been measurable, the value is customarily tabulated as zero (Butler *et al.* 2006). For at least nine such

planets, radii have been measured and can be compared with theoretical predictions. In most cases the models fit the observations, but in four of the nine cases, the theory predicted radii smaller than observed. Next we consider for each of these planets whether tidal heating, which has not yet been incorporated into the modeling, might potentially play a role. For many planets with tabulated e values of zero, the true values may be as large as 0.03 (Butler *et al.* 2006). Thus, for each of the nine planets, we consider the implications that would follow if the current e actually has a value of 0.001, 0.01, and 0.03, in order to sample a range of possible values. The results are shown in Figures 4.3 and 4.4. For each planet, the results for a current value for e of 0.01 are shown with a solid line, and the results for the smaller and larger values (and thus smaller and larger current heating rates, respectively) are shown with dashed lines.

The following planets seem to have larger radii than had been predicted by models: TrES-2 (Sozzetti *et al.* 2007), WASP-2 b (Sozzetti *et al.* 2007), OGLE-TR-56 b (Pont *et al.* 2007), and XO-1 b (Holman *et al.* 2006). As shown in Figure 4.3, the first three may have had tidal heating well in excess of 10^{19} W within the past 1 Gyr and probably lasting for at least ~ 1 Gyr, assuming their current e is actually > 0.01 (and probably even if their current e is as small as a few times 10^{-3}). Thus tidal heating needs to be included in the physical modeling and may help reconcile the difference between theory and observation. For XO-1 b, tides are unlikely to have played a significant role unless the current e is larger than 0.03. Thus, for this case, the reconciliation probably requires some other correction to the theoretical models, so as to give a smaller radius, which is the same trend suggested for several other cases discussed above.

The five cases that have radii consistent with theoretical models (Burrows *et al.* 2007, Winn *et al.* 2007) are OGLE-TR-10 b, -111 b, -113 b, and -132 b and HD 189733 b. As shown in Figure 4.4, in all cases except -111 b, heating rates may have been greater than 10^{19} W during the past Gyr even if the current *e* values are only 0.01. What is more, Figure 4.4 shows that two planets (OGLE-TR-113 b and HD 189733 b) would have reached 10^{20} W even if their current *e* is only 0.001. (OGLE-TR-111 b would require the current *e* to be > 0.03 to have peaked at 10^{19} W, but even in that case the burst of heat was several billion years ago.) For several of these planets, there has likely been enough heating to be a factor in determining the physical properties. Thus the fact that the measured radii fit the models suggests that either the current *e* values are smaller than the values considered here, or, once again, the theoretical models need to be revisited so as to keep the same radii while accommodating the additional heating due to tides.
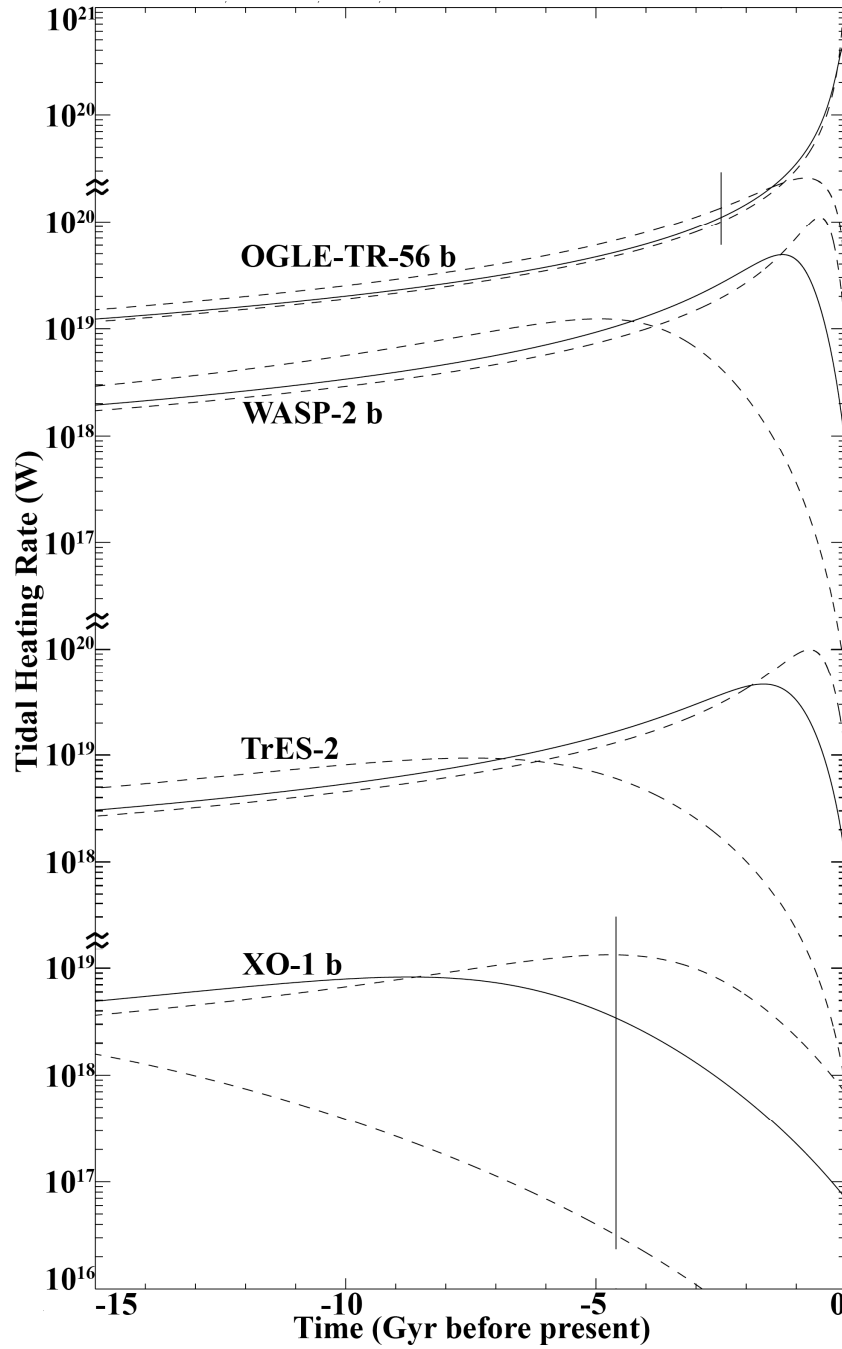
Figure 4.3: The tidal heating rates for four planets for which the nominal (tabulated) current *e* value is zero, but non-circular orbits are possible. For each planet, a heating curve is computed for an assumed current *e* of 0.001, 0.01, and 0.03. The solid line is for 0.01, and greater current *e* corresponds to greater current heating. The scale on the ordinate is shifted by factors of ten to allow the separate results to be displayed clearly. For planets where the vertical age bar is missing, no age estimate is available.
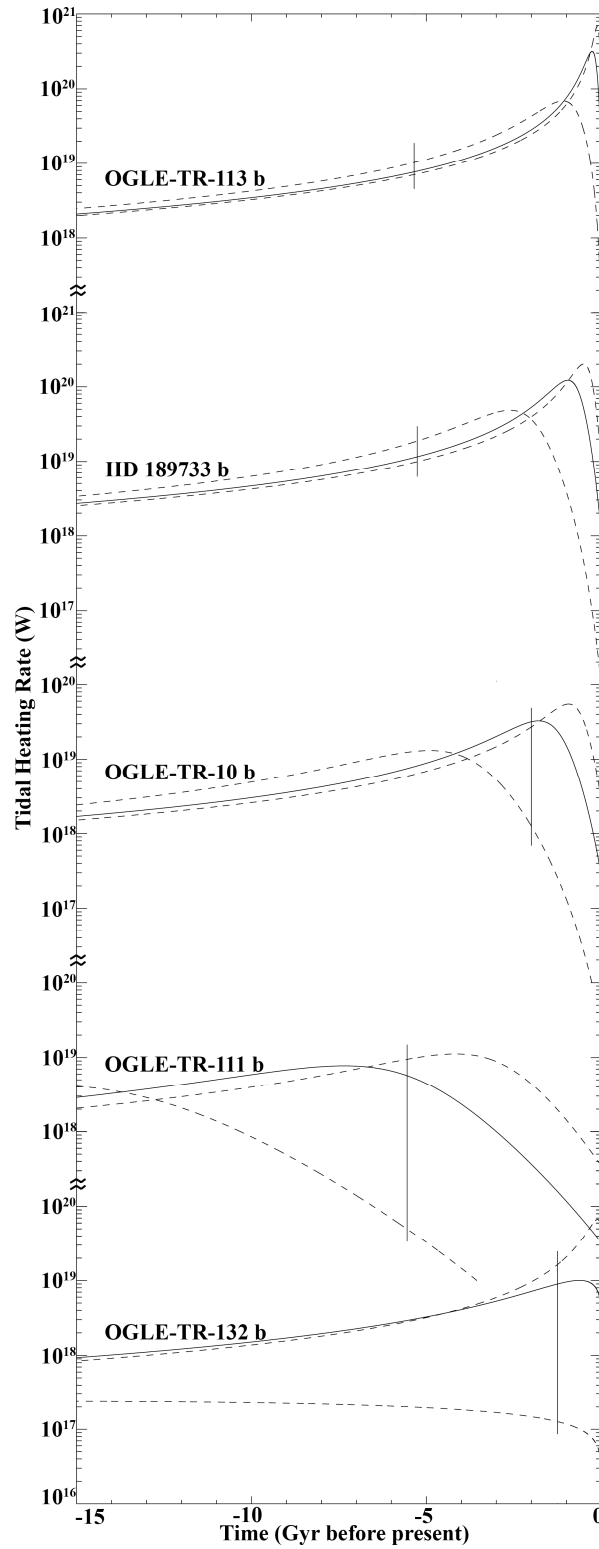
Figure 4.4: The tidal heating rates for five more planets for which the nominal (tabulated) current *e* value is zero, but non-circular motion is likely (similar to Figure 4.3).

4.4. Terrestrial-scale planets

As observational data improve, observers have begun to find extra-solar planets with masses comparable to Earth's, planets that may be terrestrial in nature. Among known planets with masses less than about ten times that of the Earth, tidal heating could have played some role in the geophysical evolution. Here we consider the tidal heating of a few planets with masses comparable to the Earth's, possibly with similar compositions. We assume that the planetary Q_p is 100 and the Love number k is 0.3, giving $Q'_p = 500$, reasonable choices for a rocky planet (Lambeck 1977; Dickey *et al.* 1994; Mardling & Lin 2002; Barnes *et al.* 2007).

For GJ 876 d, the estimated mass is about 6 Earth masses, and the nominal e is zero, so following the same procedure as in the previous section for such cases we consider the heating history under the assumption that the current e value is actually 0.001, 0.01, or 0.03, as shown by the curves so labeled in Figure 4.5. No direct determinations of its radius are available, so we assume $R_p \sim 10,200$ km, based on the mass/radius relationship for terrestrial planets given by Sotin *et al.* (2007). In addition, we consider the implications of the upper limit to e of 0.28, reported by Rivera *et al.* (2005). The implied heating history in that case is given by the curve labeled "0.28" in Figure 4.5. In each of these four cases, the heating rate is well over 10^{19} W for tens of millions of years, and peaks at $\sim 10^{20}$ W. The main difference among the four cases, depending on the assumed current e value, is the timing of the peak, although it is within the past ~ 30 Myr in all four cases.
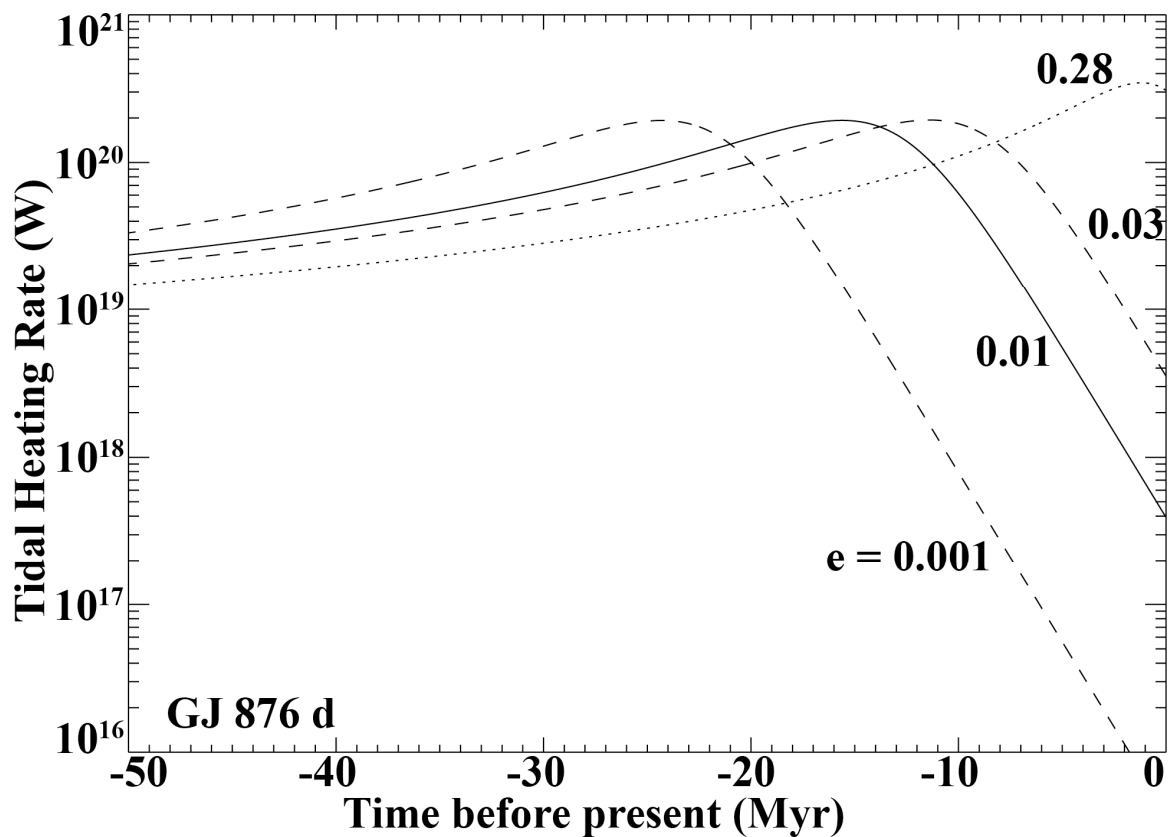
Figure 4.5: The tidal heating rates for GJ 876 d, a possibly terrestrial-scale planet for which the nominal (tabulated) current *e* value is zero, but a non-circular orbit is possible. A heating curve is computed for an assumed current *e* of 0.001, 0.01, and 0.03, as well as for a possible maximum value of 0.28. Extensive internal melting might be expected if the heating rate were greater than $\sim 10^{18}$ W. Tidal heating may have been a significant factor in the geophysical history of this planet.

To put these numbers in context, consider the geophysical modeling of this planet by Valencia *et al.* (2007a) who report that 7×10^{17} W would be adequate to induce substantial internal melting of the mantle. According to that result, for GJ 876 d tidal heating has likely been 2 orders of magnitude greater than needed for melting. At the surface, in a steady state the tidal heating would correspond to a heat flux of $\sim 10^{4\text{-}5}$ W/m^2. For comparison the surface heat flux for spectacularly active Io is ~ 3 W/m^2 (McEwen *et al.* 1992) and is largely due to tides. For the Earth the flux is ~ 0.08 W/m^2 (Davies 1999), which is largely due to radiogenic heat. Valencia *et al.* (2007b) suggested that radiogenic heating of GJ 876 d might have been adequate to initiate plate tectonics, but our results indicate that tidal heating may have been a major contributor to the geological and geophysical character of the planet. Tidal heat has provided an important component of the heat budget for this planet, perhaps the dominant component during at least the past $\sim 10^8$ yr. The tidal heating rate would be so large, in fact, that GJ 876 d is unlikely to be a solid, rocky body, or the planet's orbital eccentricity is much smaller than considered here.

For the nominal current orbit of Gl 581 c (Butler *et al.* 2006), the tidal heating is about 10^{16} W, assuming the best-fit current *e* and *a*. It has been nearly constant over the past billion years, and was only slightly larger early in its history 9 Gyr ago. Considering the range of uncertainty of the current orbit, the values could have been a few times higher or lower, but still $\sim 10^{16}$ W, far less than GJ 876 d. Nevertheless, this rate could be geophysically important. Assuming $R_p \sim 10,000$ km (again scaling from the mass), the

tidal contribution to the geophysical heat flux would be ~ 10 W/m^2 at the surface, more than twice that of Io and 100 times the heat flux at the surface of the Earth.

HD 69830 b is greater than 10 Earth masses, so it is more likely a Uranus/Neptune class planet than a terrestrial one. Nevertheless, Valencia *et al.* (2007a) considered the possibility that it is terrestrial in character, so we consider the implications for tidal heating if its $Q'_p=500$. For the best-fit current e value, we find that tidal dissipation may generate ~10^{17} W, or up to a few times more given the range allowed for the current orbital parameters. The heating rate has been fairly constant over the past billion years, but it had decreased by a factor of a few since the planet's formation ~10 Gyr earlier (Lovis *et al.* 2006). Assuming a radius of ~12,000 km (based on its mass), the surface heat flux over the past 1 Gyr would be 55 W/m^2 (20 times Io's). If HD 69830 b is a terrestrial planet, tidal heat must have been a major factor in its geophysics throughout its history.

Note that in these calculations we have ignored the effect of interactions between these planets and other known (and probably still unknown) planets in their systems. Secular interactions and orbital resonances may well have affected the orbital evolution in ways that modified the tidal heating histories. These effects would be in addition to the other uncertainties and assumptions intrinsic to the results presented here. Nevertheless, the point of our results is that tidal dissipation is likely to have been a significant factor in the geophysical evolution of extra-solar terrestrial-type planets.

4.5.   Discussion

The calculations here suggest that tidal heating may well have played an important role in the evolution of the physical properties of many extra-solar planets, the physical property for which we have the best constraints at present being the planetary radius. We caution that the specific calculations displayed here depend on numerous assumptions and several uncertain parameters. The heating rates correspond to many of the orbital evolution trajectories presented in the previous chapter, and the same caveats for those calculations apply here. In particular, the exact tidal histories presented here depend on the choice of Q'_*. However most of the tidal histories presented here are not very sensitive to the choice of Q'_* since tides raised on the planet usually dominate the evolution. HAT-P-2 b is an important exception. Owing to the planet's unusually large mass ($\sim 9\ M_{Jup}$), tides raised on the star may dominate the tidal evolution. As a result, the rate of tidal evolution depends sensitively on Q'_*, *e.g.,* larger Q'_* results in significantly slower tidal evolution. If tidal evolution were slower for this planet, it would mean that the past heating rate was closer to the current, large heating rate since the orbital parameters would not have changed much.

In any case, it is quite likely that the actual thermal history of any particular planet was different to some degree from what we show here. However, the unavoidable point is that tidal heating may be significant even for small current eccentricities and should be considered as a factor in theoretical modeling of physical properties.

As shown in Section 4.3, in most cases where the measured radius is greater than the theoretically predicted value (HD 209458 b, HAT-P-1 b, TrES-2, WASP-2 b, and

OGLE-TR-56 b), the tidal heating has been significant and may thus resolve (or at least contribute to resolving) the discrepancy, once it is incorporated into the physical models. The greatest heating was typically ~ 1 Gyr ago, so it may be that current planetary radii reflect the heating rate at that time in the past.

In only one case where the measured radius is greater than theoretically predicted (XO-1 b) is the tidal heating too small to be a significant factor. Some other correction is probably needed to bring the model into agreement with the observation.

Among cases where the theoretical models have seemed to be in good agreement with measured radii, two have experienced negligible tidal heating (GJ 436 b and OGLE-TR-111 b), so the agreement is preserved even when tides are taken into account. However, five cases may have undergone considerable tidal heating (TrES-1, HD 189733 b, OGLE-TR-10 b, -113 b, and -132 b). Physical models may need to incorporate this heat source, which is likely to increase the radius predicted by the models. If the change is significant, other modifications will be required before the theory can be considered in agreement with observations.

In two of the cases considered here, the theoretical models predicted radii larger than actually measured. For HD 149026 b, tidal heating is probably not a factor. For HAT-P-2 b, the tidal heating exacerbates the discrepancy between theory and observation. However, the problem is less severe if (as suggested by the other cases above) the current radius reflects the heating rate ~1 Gyr ago, when the heating rate (in this case) was a few times less than at present.

Our study also suggests that the current state of physical modeling often gives radii that are too large for a given assumed amount of heating (or equivalently underestimating the amount of heat needed to yield a given radius). Tidal heat may resolve the discrepancy between theory and observations for most of the cases where measured radii were larger than expected, but it may make things worse in most of the cases where measured radii seemed to fit the current models. In two cases, whether tidal heating is significant or not, the observed radii are smaller than predicted by the models. In summary, some discrepancies may be resolved by taking into account tidal heating, some remain even when tidal heating is taken into account, and some are exacerbated by tidal heating. Even when tidal heating is included, theoretical models will generally need to be adjusted and improved so as to yield smaller radii for a given amount of internal heat, if they are to agree with measured values. Certainly, theoretical studies of the evolution of the physical properties of planets need to account for tides as a significant source of heat, and one that varies over time. Unlike heat of accretion, tidal heating varies over time, often reaching its maximum considerably later in the life of the planet.

Among terrestrial-scale planets, we find that tidal heating may have dominated the geological and geophysical evolution of the planets and control their current character. The tidal heating rate for GJ 876 d may be orders of magnitude greater than the magnitude considered by Valencia *et al.* (2007) to be geophysically significant. For Gl 581 c tidal heating may yield a surface flux about three times greater than Io's, suggesting the possibility of major geological activity. The surface flux of tidal heat on HD 69830 b would be yet an order of magnitude larger if it is a rocky planet. These

heating rates are so large (especially for GJ 876 d) that either the orbital eccentricity is different from what we've considered here, or the extensive melting implied may not be consistent with the tidal dissipation parameters that we have assumed. Some melting might increase the rate of tidal heating as the tidal amplitude increases, but deep global melting would increase Q'_p and limit the heating to rates lower than what we have calculated. Another caveat is that the masses of these planets are minimum masses from radial velocity studies, so they may not be rocky, terrestrial scale bodies after all. Finally we emphasize that we have ignored the effects of mutual interactions among planets, which may affect orbital and tidal evolution in interesting ways.

These results demonstrate the importance of using the coupled equations of tidal evolution of e and a. Here we have seen that the slower circularization has likely resulted in significant heating rates at present and in the relatively recent past.These results show that tidal heat may be a major factor in determining the character of extra-solar planets. The extent to which a given amount of heat affects the physical state of the planet must depend on where the heat is dissipated. Heating near the surface may have less effect than if it is deep in the interior. Despite these uncertainties, the results presented here do demonstrate that tidal heat must be considered in theoretical modeling.

The magnitudes of the heating rates determined for the super-Earths considered here suggest that tides may have an important influence on the geophysical states for rocky extra-solar planets close to their host stars. Such effects will also undoubtedly have consequences for the habitability of these planets. In the next chapter, using the same methodology as this and the previous chapter, we present calculations of the tidal

evolution and heating for many hypothetical rocky extra-solar planets, spanning a range of orbital and physical properties, and discuss possible implications for their physical properties and habitability.

Planet Names	M∗ (M$_{sol}$)	R∗ (R$_{sol}$)	M$_p$ (M$_{Jup}$)	R$_p$ (R$_{Jup}$)	a (AU) min	a (AU) nom	a (AU) max	e min	e nom	e max	Age (Gyr)	References M∗, R∗, M$_p$, R$_p$, a, e, Age
HD 209458 b	1.14	1.13	0.64	1.32	0.0459	0.0473	0.0487	0	0.014	0.042	2.44	1, 1, 2, 2, 3, 3, 4
HAT-P-1 b	1.12	1.15	0.53	1.36	0.0536	0.0551	0.0566	0	0.09	0.11	3.6	5 (all)
GJ 436 b	0.44	0.44	0.0706	0.3525	0.0276	0.025b5	0.0293	0.14	0.16	0.18	9.23[a]	6 (all)
TrES-1	0.88	0.81	0.75	1.08	0.0386	0.0393	0.04	0.039	0.135	0.231	2.5	8, 8, 8, 8, 8, 8, 9
HAT-P-2 b	1.35	1.8	9.05	0.982	0.0673	0.0685	0.0697	0.495	0.507	0.519	2.7	10 (all)
HD 149026 b	1.3	1.45	0.36	0.73	0.042	0.043	0.044	0	0	0.02	2	11 (all)
TrES-2	1.08	1	1.25	1.24	0.0362	0.0367	0.0379	0.001	0.01	0.03	…	12, 12, 12, 12, 12, …, …
WASP-2 b	0.79	0.81	0.88	1.04	0.0296	0.0307	0.0318	0.001	0.01	0.03	…	13, 13, 13, 13, 14, …, …
OGLE-TR-56 b	1.17	1.32	1.29	1.3	0.0221	0.0225	0.0229	0.001	0.01	0.03	2.5	15, 15, 15, 15, 15, …, 9
XO-1 b	1	0.93	0.9	1.18	0.0483	0.0488	0.0493	0.001	0.01	0.03	4.6	16, 16, 16, 16, 17, …, 17
OGLE-TR-10 b	1.02	1.16	0.63	1.27	0.0423	0.043	0.0436	0.001	0.01	0.03	2	15, 15, 15, 15, 15, …, 9
OGLE-TR-111b	0.81	0.83	0.52	1.07	0.046	0.047	0.048	0.001	0.01	0.03	5.55	18, 18, 18, 18, 18, …, 23
OGLE-TR-113 b	0.78	0.77	1.32	1.09	0.0227	0.0229	0.0231	0.001	0.01	0.03	5.35	19, 19, 19, 19, 19, …, 23
OGLE-TR-132 b	1.35	1.43	1.19	1.13	0.0298	0.0306	0.0314	0.001	0.01	0.03	1.25[a]	20, 20, 20, 20, 20, …, 6
HD 189733 b	0.82	0.76	1.15	1.15	0.0309	0.0313	0.0317	0.001	0.01	0.03	5.26	21, 21, 21, 21, 22, …,23
GJ 876 d	0.32	0.36	0.018	0.143	0.0208	0.0208	0.0208	0.001	0.01	0.03	9.9	24, 24, 24, 25, 24, …, 7
Gl 581 c	0.31	0.38	0.016	0.138	0.0714	0.073	0.0746	0.09	0.16	0.23	2.0[b]	26, 26, 27, 25, 27, 27, 27
HD 69830 b	0.86	0.895	0.032	0.167	0.0785	0.0785	0.0786	0.06	0.1	0.14	7.0[a]	28, 28, 28, 25, 28, 28, 28

Table 4.1: References. - (1) Butler *et al.* (2006); (2) Knutson *et al.* (2007); (3) Laughlin *et al.* (2005); (4) Takeda *et al.* (2007); (5) Bakos *et al.* (2007a); (6) Gillon *et al.* (2007b); (7) Saffe *et al.* (2006); (8) Winn *et al.* (2007b); (9) Melo *et al.* (2006); (10) Bakos *et al.* (2007b); (11) Sato *et al.* (2005); (12) O'Donovan *et al.* (2006); (13) Charbonneau *et al.* (2007b); (14) Collier Cameron *et al.* (2007); (15) Pont *et al.* (2007); (16) Holman et al (2006); (17) McCullough *et al.* (2006); (18) Winn *et al.* (2007a); (19) Gillon *et al.* (2006); (20) Moutou *et al.* (2004); (21) Bakos *et al.* (2006); (22) Bouchy *et al.* (2005); (23) Burrows *et al.* (2007); (24) Rivera *et al.* (2005); (25) Sotin *et al.* (2007); (26) Bonfils *et al.* (2005); (27) Udry *et al.* (2007); (28) Lovis *et al.* (2006).

Notes: a – This value is the average of the minimum and maximum ages reported. b –This value is the minimum age reported

Chapter 5
Tidal Heating of Rocky Extra-Solar Planets and Implications for their Habitability

5.1.   Introduction

As observational technology and techniques improve, it is anticipated that Earth-like planets may be found orbiting stars other than the Sun. Such a discovery would be a milestone in the search for extra-terrestrial life. One technique for finding extra-solar planets, the radial-velocity observations of distant stars, is sensitive to Earth-mass planets if they orbit close to inactive, low-mass M-stars. Also, since M stars are less luminous than more massive stars, the conventional habitable zone (HZ, as defined by Selsis *et al.* 2007; see also Kasting *et al.* 1993) lies closer to the star than for a star of a greater mass. Planets must be closer to their M star host in order to have a surface temperature suitable for life. Taken together, these criteria suggest that the first Earth-like, habitable planets may be discovered around M stars (Tarter *et al.* 2007).

The effects of tides on rocky (or "terrestrial") planets close to their host stars are likely to be important (Mardling & Lin 2004; Mardling 2007; Barnes *et al.* 2008b; Jackson *et al.* 2008b). If such a planet is on an eccentric orbit, the dissipation of tidal energy within the planet will tend to circularize the planet's orbit and probably lead to substantial internal heating. As we show in this chapter, such heating may have important consequences for the habitability of these bodies.

In the previous chapter, we considered the effects of tidal heating on observed extra-solar planets. The tidal heating that accompanies orbital evolution was considered

for jovian-scale extra-solar planets, where it may have major effects on physical properties. For example, the radii of some transiting extra-solar planets are observed to be larger than theoretical modeling predicts (*e.g.*, Bodenheimer *et al.* 2003; Burrows *et al.* 2007), but tidal heating of the interiors of these planets may have been enough to pump up their radii (Jackson *et al.* 2008b; Liu *et al.* 2008). In the previous chapter, we also showed that tidal heating of some known extra-solar planets, if they were terrestrial, may be enough to completely melt some planets. Many such planets could be at least as volcanically active as Jupiter's moon Io, the most volcanically active body in our solar system, with massive volcanic plumes and frequent global resurfacing (Peale *et al.* 1979; McEwen *et al.* 2004). In fact, tidal heating of the innermost planet in the recently discovered system HD 40307 (Mayor *et al.* 2009a) may exceed Io's, suggesting that, if the planet is rocky, it may be volcanically active (Barnes *et al.* 2008b). The same may hold for Gl 581 e (Mayor et al. 2009b), for which perturbations from the other planets in the system may induce tidal heating of 100s W/m^2.

Other sources of internal heating may drive geophysical processes. For example, on the Earth, tidal heating is negligible, and instead much of the heating that drives geophysical processes is provided by decay of radionuclides. This internal heating drives convection in the mantle, and thus, contributes to the process of plate tectonics, although this process is not completely understood (O'Neill & Lenardic 2007). Plate tectonics helps stabilize the planet's atmosphere and surface temperature over hundreds of millions of years (Walker *et al.* 1981). Because a stable surface temperature is probably a prerequisite for life, plate tectonics or another geophysical process for buffering the

atmospheric content of greenhouse gases may also be required for a planet to be habitable (Ragenauer-Lieb *et al.* 2001).

These considerations suggest that, in order to be habitable, terrestrial planets may require a significant source of internal heating. However, models of *in situ* planet formation predict that terrestrial planets that form around M stars would have masses much less than the Earth (Raymond *et al.* 2007), although shepherding of planet-forming material by migrating gas giants may result in larger terrestrial planets around these stars (Raymond *et al.* 2008a). Thus, if *in situ* formation of terrestrial planets is common, many terrestrial planets we find may have too little radiogenic heating to drive long-lived plate tectonics (Williams *et al.* 1997). However, even without radiogenic heating, as we show, tides may provide adequate internal heating and hence may be critical in determining planetary habitability.

In many cases tidal heating may even be too great to allow habitability. For example, tides on planets with masses comparable to or larger than the Earth's may generate more internal heat (per unit surface area) than Io, even for small orbital eccentricities. Even planets with masses smaller than Mars may experience similarly large heating with eccentricities ~ 0.3, the average value for observed extra-solar planets. Thus, many extra-solar terrestrial plants may be extremely volcanic, perhaps enough to preclude habitability.

Tidal heating may also be important for the creation and maintenance of the atmospheres of terrestrial planets. As heat induces internal convection within the mantles of these planets, volatiles trapped in the mantle may be outgassed, feeding the

atmosphere. In the HZ of M stars, atmospheres may be depleted by vigorous stellar activity (West *et al.* 2008) or impact erosion (Melosh & Vickery 1989), so tides may play an important role in driving outgassing adequate to replenish the atmosphere, enabling the planet to remain habitable.

In other cases, planets may be habitable even without an atmosphere. Tidal heating of an icy planet may generate a habitable subsurface ocean, analogous to Jupiter's moon Europa. For these planets, an atmosphere may not be necessary for habitability if, as proposed for Europa, life could exist below the icy surface.

To determine the potential impact of tidal heating on the geophysics, surfaces and atmospheres of possible extra-solar terrestrial planets, and thus ultimately on their habitability, we model the tidal evolution of a suite of hypothetical terrestrial planets in the HZ of their host stars. We explore a range of planetary and stellar masses and orbital parameters, using the model for tides from previous chapters, and track the tidal evolution for each planet over billions of years. Tides raised on the planet tend to damp down the orbital eccentricity e at the same time as they heat the planet and reduce the semi-major axis a. If a tidally evolving terrestrial planet begins with a non-zero eccentricity, it may take billions of years for tides to damp that eccentricity to near-zero, even without gravitational interactions with other planets. Consequently, we find tidal heating can be very long-lived, even for an isolated planet, in contrast to previous studies that used the "circularization timescale" formulation. (See Chapter 3.)

In the next section, we give the details of our model. In Section 5.3, we present the results of our calculations, while in Section 5.4, we discuss the implications of these results. In Section 5.5, we summarize our results.

5.2.   Methods

To calculate the tidal heating of hypothetical extra-solar terrestrial planets, we performed a suite of integrations of the tidal evolution equations, for a range of stellar and planetary masses and a range of orbital elements. We considered stellar masses M_* from 0.1 to 0.5 solar masses (M_{Sun}), which is the range of masses for M stars. We sampled planetary masses M_p from 0.01 to 10 Earth masses (M_{Earth}). For each star, we assumed a radius based on the star's mass, according to Gorda & Svechnikov (1998). For each planet, we assumed a radius (R_p) based on geophysical models by Sotin *et al.* (2007): $R_p = M_p^{0.27}$ for $1 < M_p < 10$ Earth masses and $R_p = M_p^{0.3}$ for $0.1 < M_p < 1$, Earth masses where R_p is in Earth radii (R_{Earth}).

We also considered a range of initial orbital eccentricities e_0 from 0.01 to near unity, a range similar to known extra-solar planets (*e.g.*, Butler *et al.* 2006). Each planet was also assigned an initial orbital semi-major axis a_0 in the middle of its host star's HZ, as defined by Barnes *et al.* (2008) who modified the definition from Selsis *et al.* (2007). Selsis *et al.* related a star's HZ to its mass, a planet's cloud cover, and a planet's semi-major axis. Barnes *et al.* (2008) expanded the relationship to include the effects of non-zero eccentricities on the range of habitable semi-major axes, using the results from

Williams & Pollard (2002). For each planet, we chose the HZ range for no cloud cover on the planet (Selsis *et al.* 2007).

Figure 5.1 shows the dependence of a_0 (at the middle of the HZ) on e_0 from Barnes *et al.* (2008). For large e_0, the HZ shifts slightly outward (*i.e.* a_0 is slightly larger) so that the planet does not receive a sterilizing dose of stellar insolation near pericenter. As in previous chapters, each planet was assumed to have zero obliquity and a rotation that had spun-down so early that exchange of angular momentum between the planet's orbit and its rotation is not a factor.

For terrestrial planets, we assume $Q_p' = 500$, which incorporates a conventional value for the planetary Love number of 0.3 (Dickey *et al.* 1994; Mardling & Lin 2004), although actual values could vary, depending on the planet's structure and composition.

The tidal heating rate of the planet is equal to the portion of the loss of orbital energy due to tides raised on the planet, which is proportional to the first term in the equation for *da/dt*. Thus, the heating rate is given by

$$h = \left(\frac{63}{16\pi} \right) \frac{(GM_*)^{3/2} M_* R_p^3}{Q_p'} a^{-15/2} e^2 \tag{5.1}$$

Here, *h* is expressed in terms of the internal heating per unit surface area of the planet for convenience in considering the various effects on planetary surfaces later.
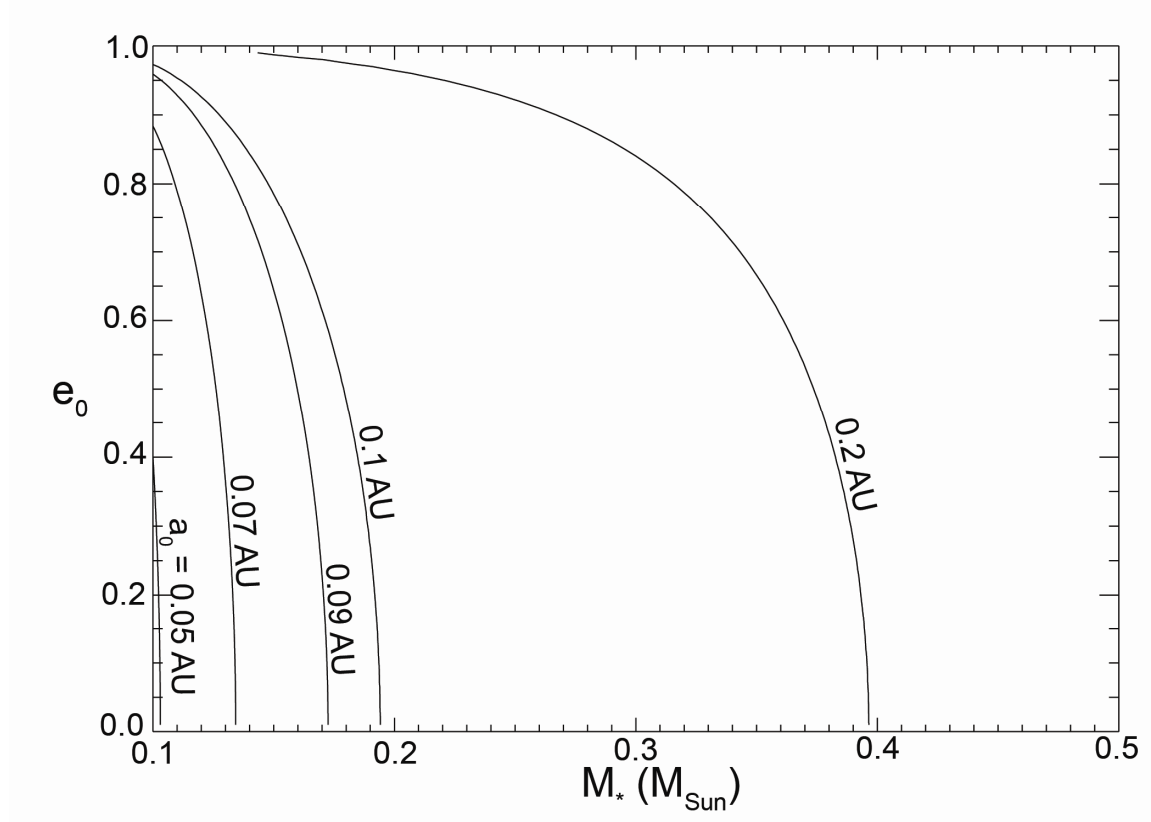
Figure 5.1: For circular orbits ($e_0 = 0$), the orbital semi-major axis at the center of the HZ (a_0) depends only on the stellar mass M_*. For $e_0 > 0$, the value of a_0 shifts to larger values as shown.

As in previous chapters, we numerically integrated the tidal equations, Equations (3.1) and (3.2), forward in time, beginning at a_0 and e_0, and calculated the heating that accompanies the evolution, using Equation (5.1). For the range of parameters considered here, we find that the effects of the tides raised on the star by the planet, given by the second terms in Equations (3.1) and (3.2), are small. Because tides on the star don't contribute, the orbital angular momentum is conserved.

As tides cause a planet's orbit to evolve, h often passes through a maximum. Initially tides reduce a without significantly reducing e, and h increases. As a becomes smaller, the rate of tidal circularization increases, and eventually e decreases enough that h decreases as well.

The maximum value of h occurs where $dh/dt = 0$. Differentiating Equation (5.1) and setting dh/dt equal to zero yields:

$$2e\frac{de}{dt}a^{-15/2} - \frac{15}{2}e^2 a^{-17/2}\frac{da}{dt} = 0 \tag{5.2}$$

With conservation of orbital angular momentum $l = (G\,M_* \,a\,(1\text{-}e^2))^{1/2}$, we have

$$\frac{d(l^2)}{dt} \propto \frac{da}{dt}(1-e^2) - 2ae\frac{de}{dt} = 0 \tag{5.3}$$

which yields

$$\frac{da}{dt} = \frac{2ae}{1-e^2}\frac{de}{dt} \tag{5.4}$$

Substituting da/dt from Equation (5.4) into (5.2) yields $e = \sqrt{2/17} \approx 0.34$. Thus whenever h reaches a maximum, e is equal to this particular numerical value.

5.3.   Results

Figures 5.2 and 5.3 show the tidal heating rates and tidal evolution of e and a over time for planets of various masses and various values of e_0 in the HZ of an M star with a mass of 0.1 M_{Sun} and 0.2 M_{Sun}, respectively. In none of our cases do we find that the tidal evolution carries the planet out of the HZ. (See Barnes *et al.* 2008a for a discussion of this possibility.)

In Figure 5.2, qualitative, as well as quantitative, differences appear in the history of h, depending on the value of e_0. Because h peaks when $e \approx 0.34$, planets that begin with $e_0 < 0.34$ have their heating rates drop monotonically with time. For larger e_0 (above 0.34), the initial and peak values of h are larger. However, for $e_0 > 0.6$, we see that the initial value of h is smaller, and, while the peak in h is larger, it occurs later. It may seem surprising that these largest values of e_0 give less initial heating. However, this effect arises from our requirement (for this study) that a_0 be in the middle of the HZ. From Figure 5.1, we see that a_0 is considerably larger for larger e_0. The larger a_0 means the initial value of h is reduced (Equation (5.1)). Similarly the initial value of de/dt is smaller, so it takes longer for e to reach 0.34, the value at which h reaches a maximum.

Figure 5.2 also shows how h depends on M_p. Since h is proportional to $R_p{}^3$ and $R_p \sim M_p{}^{1/3}$, it depends almost linearly on M_p (Sotin *et al.* 2007). For example, for $M_p = 0.3$ M_{Earth} and $e_0 = 0.1$, (Figure 5.2 (a)), the initial value of h is about 0.3 W/m^2. By comparison, for a planet three times as massive (Figure 5.2 (b)), h begins at about 1 W/m^2. For the range of M_p we consider here, the orbits of larger planets evolve more quickly than those of smaller planets, and so are eccentric for less time.
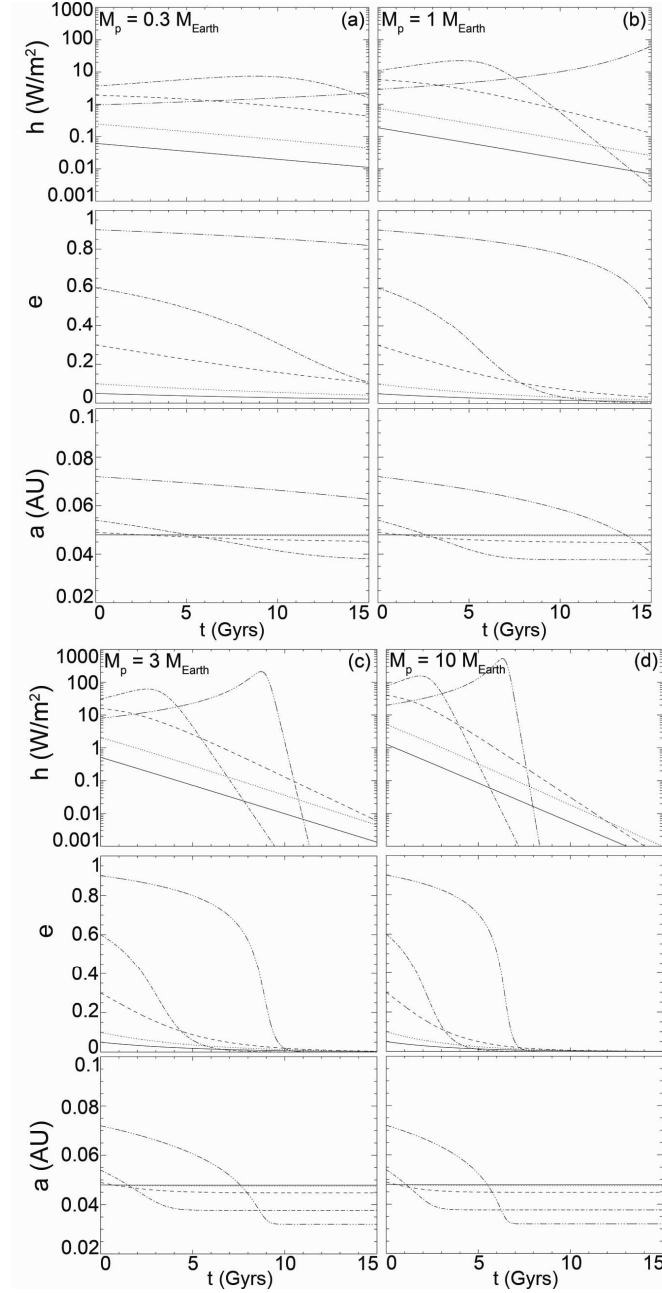
Figure 5.2: Tidal heating histories and tidal evolution of *e* and *a* for planets of various masses with various values of initial eccentricity e_0 orbiting a star with mass 0.1 M_{Sun}. Parts (a) - (d) illustrate histories for planets with masses 0.3, 1, 3, and 10 M_{Earth}, respectively. These planets are assumed to be in the HZ of the star. For all panels for a given M_p, solid lines correspond to $e_0 = 0.05$, dotted lines to 0.1, dashed to 0.3, dashed-dotted to 0.6, and dashed-dot-dot-dot to 0.9. The tidal heating rate is expressed in terms of *h*, the heating per area. For comparison, internal heating rates for Io and the Earth are 2 and 0.08 W/m^2, respectively.

In Figure 5.3, we show the tidal heating for a planet with $M_p = 10$ M_{Earth} orbiting a star with $M_* = 0.2$ M_{Sun}. Since stars with larger masses are more luminous, planets in the HZ of more massive stars are farther from the star. The rate of tidal evolution for planets in the HZ of these stars is much smaller since a is larger. Thus, while the heating rates for these planets may be significant, they change very slowly. For $M_p < 10$ M_{Earth}, even after 15 Gyrs, h remains essentially unchanged from its initial value, which depends on M_p, M_* and the initial eccentricity.

The contours in Figures 5.4 and 5.5 show how h depends on M_p, M_* and e, at a fixed moment in time for a planet in the center of the HZ. (The nearly constant heating rates for planets with $M_p < 10$ M_{Earth} orbiting a star with $M_* > 0.2$ M_{Sun} can be read off Figures 5.4 and 5.5.) In both figures, h increases as e increases from zero, but then decreases as e becomes larger than ~0.6. The increase with e is due to the e dependence in Equation (5.1), but the decrease in h as e gets very large arises, again, because the HZ moves farther from the star (see Figure 5.1).
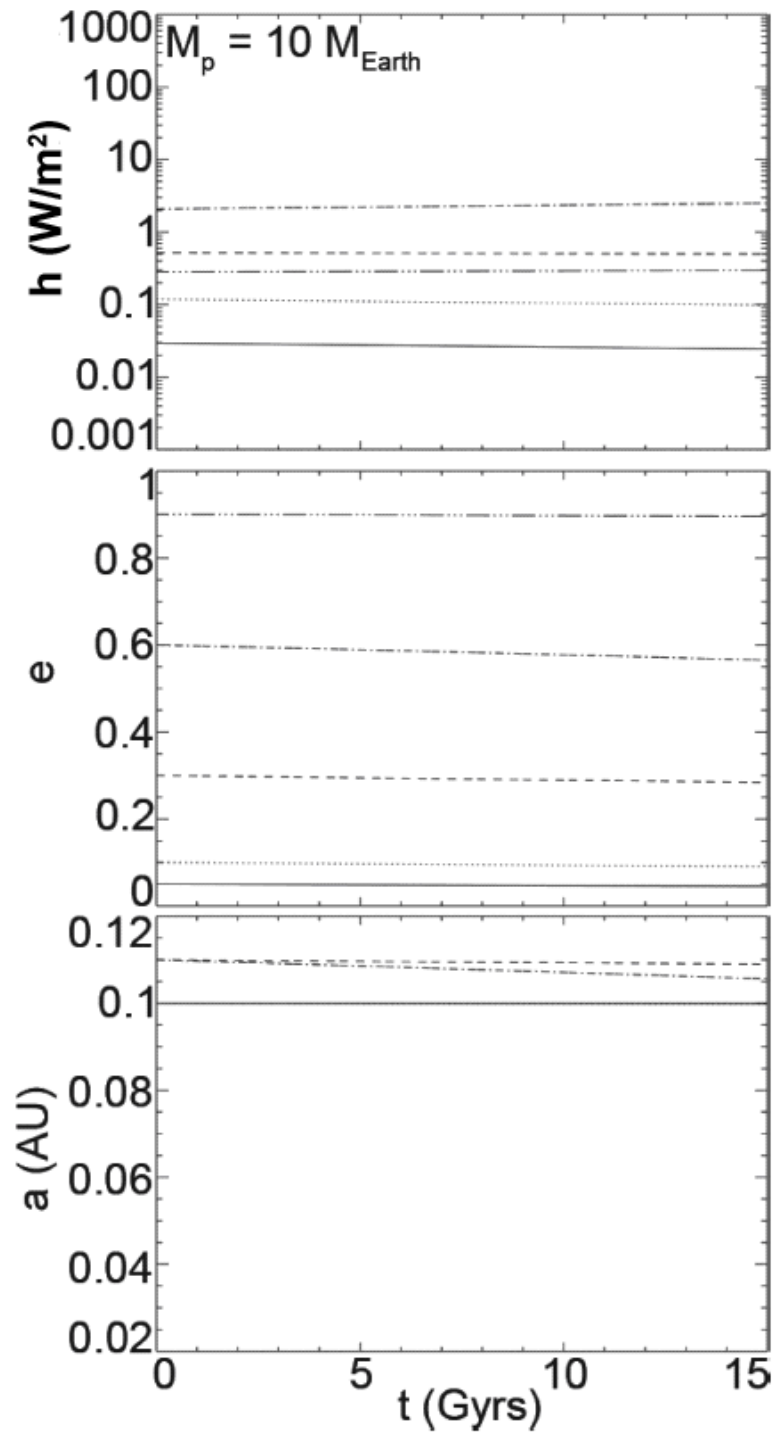
Figure 5.3: Tidal heating histories and tidal evolution of *e* and *a* for a planet with mass $M_p = 10$ M$_{\text{Earth}}$ with various values of e_0 orbiting a star with mass 0.2 M$_{\text{Sun}}$. The various linestyles correspond to the same values of e_0 as in Fig. 2. For smaller planetary masses, tidal heating changes very little over 15 Gyr.

5.4.   Discussion

Tidal heating may affect a planet's habitability in various ways: (1) It may be great enough to drive plate tectonics for a length of time that depends sensitively on the host star and planet's masses and the planet's initial orbit. (2) It may be so great as to make the planet uninhabitably volcanic. (3) It may drive outgassing from the planet's interior, continually replenishing the planet's atmosphere against loss. (4) It may also be sufficient to produce a habitable subsurface ocean on an icy planet, or to mitigate life-challenging "snow-ball" conditions on a terrestrial planet.

Interpretation of the heating rates computed here is facilitated by comparison with known planetary bodies. The Earth emits ~ 0.08 W/m^2 of internal (radiogenic and primordial) heat (Davies 1999), which is apparently adequate for plate tectonics. For an estimate of the minimum heating required for tectonic activity, consider the geologic history of Mars. When Mars was last tectonically active, its radiogenic heat flux was ~ 0.04 W/m^2 and has dropped steadily since then (Williams *et al.* 1997). This reasoning suggests 0.04 W/m^2 is a minimum amount required for tectonics in a rocky planet. At the opposite extreme, Jupiter's moon Io emits 2 – 3 W/m^2 of internally generated heat mostly from tides (Peale *et al.* 1979; McEwen *et al.* 2004), which results in extreme planet-wide volcanism, including active volcanic plumes and rapid resurfacing. Jupiter's moon Europa, a rocky body covered by 150 km of H_2O, may generate as much as 0.19 W/m^2, scaling from tidal heating on Io (O'Brien *et al.* 2002). Tidal heating in Europa maintains a sub-surface water ocean, and with that value of *h*, the surface ice would be only a few km thick (Greenberg *et al.* 2002; Greenberg 2005).

By comparing our calculations of h for hypothetical planets to the above heating rates for known planets, we can estimate the range of masses and orbital elements that correspond to each of these physical effects. Of course, these geophysical processes are complicated, and the various processes may be very different on extra-solar planets than on planets in our solar system. For example, O'Neill & Lenardic (2008) show that plate tectonics may be less likely on terrestrial planets more massive than the Earth, even though they would probably experience more radiogenic heating, while Valencia *et al.* (2007) suggest just the opposite. To conclude that these processes discussed here actually occur on a given planet requires more complete modeling than we present here. However, our calculations provide a starting point for such work by identifying ranges of possible planets for which tidal heating may be critical in establishing habitable conditions.

With reference to Figures 5.4 and 5.5, we next consider how various heating-rate regimes in the (e, M_p, M_*) space affect prospects for habitability.
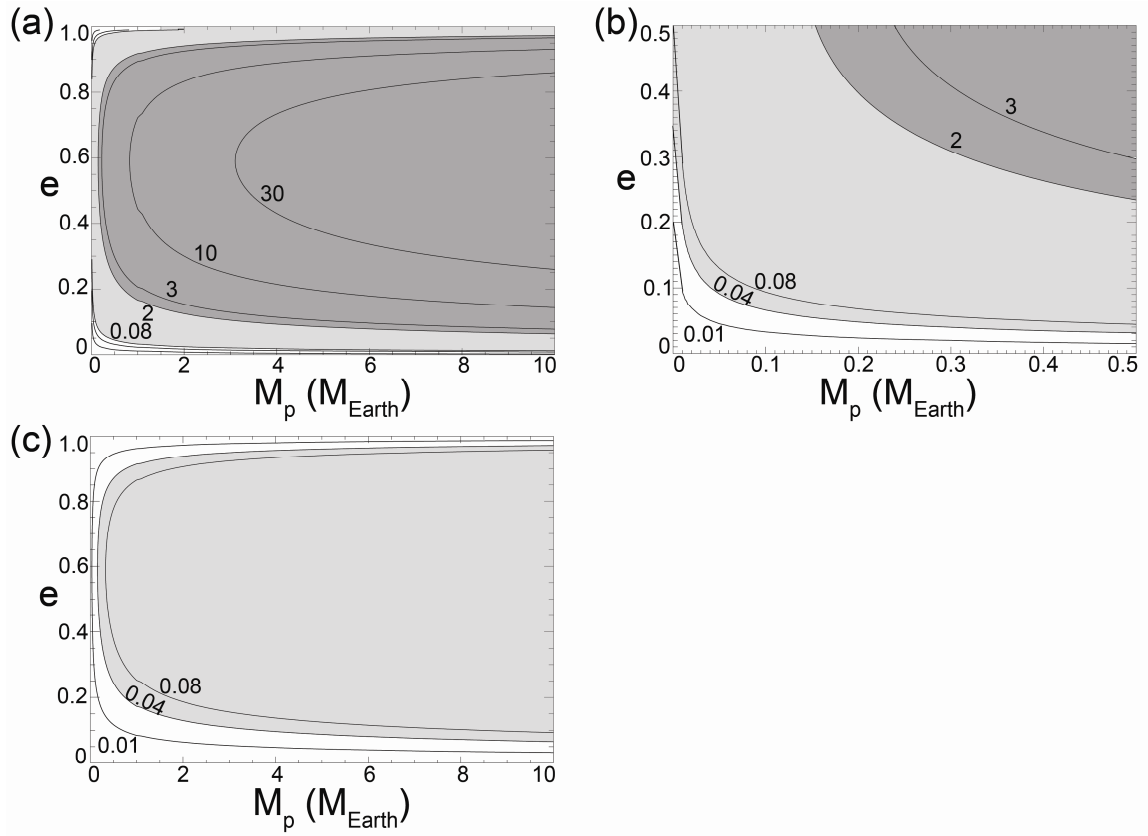
Figure 5.4: Contours of heating in W/m^2 for a range of M_p and e. For panels (a) and (b), $M_* = 0.1$ M$_{Sun}$, and $M_* = 0.2$ M$_{Sun}$ for panel (c). Panel (b) shows a close-up of the bottom left corner of panel (a). White areas indicate $h < 0.04$ W/m^2. Light gray areas indicate 0.04 W/m$^2 < h < 2$ W/m^2 (perhaps adequate for tectonic activity), while dark gray indicates $h > 2$ W/m^2 (more than Io).
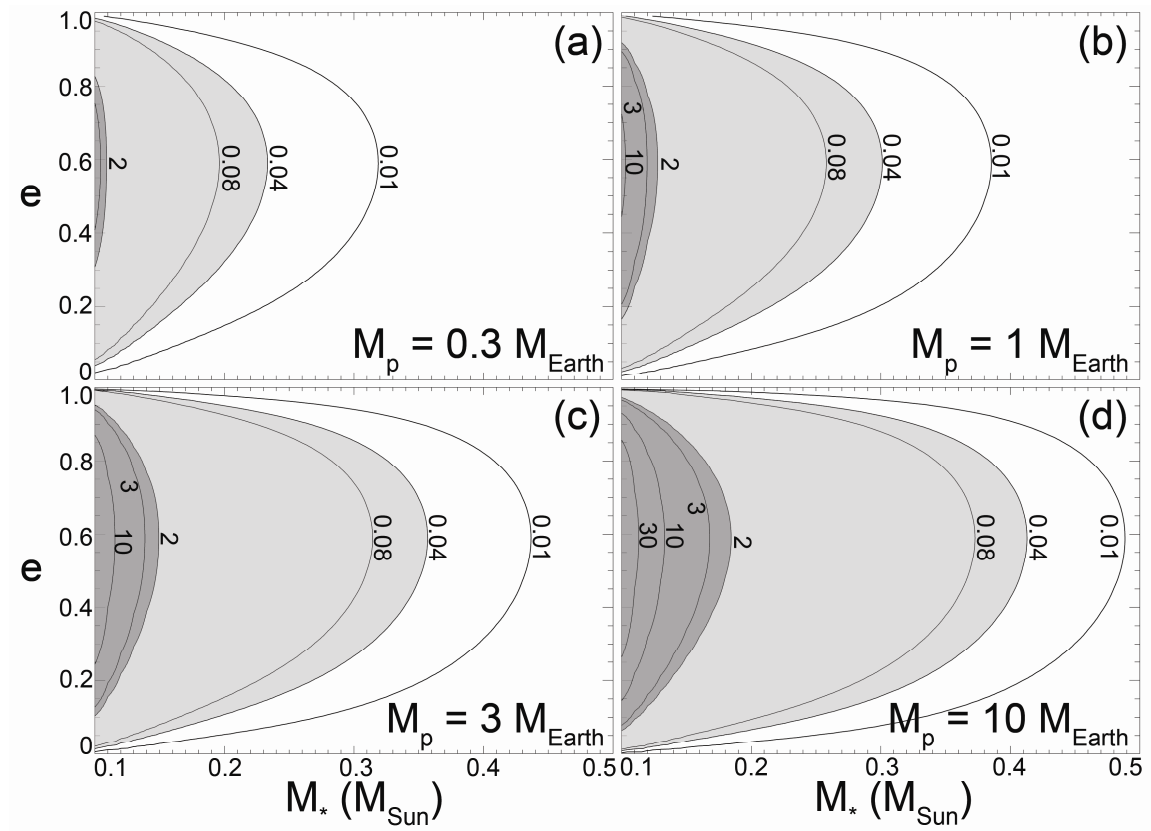
Figure 5.5: Contours of heating in W/m^2 for a range of M_* and e. For panels (a) – (d), M_p = 0.3, 1, 3, and 10 M_{Earth}. White and gray areas have the same meanings as in Figure 5.4.

5.4.1. Planets with Sufficient (but not Excessive) Tidal Heating for Plate Tectonics

First, we consider requirements for enough heating for plate tectonics, but not so much that there is devastating volcanism. As described above, this range is perhaps between ~0.04 and ~2 W/m^2. The light gray shading in Figures 5.4 and 5.5 indicate the range of parameters for which h lies in this range. Figure 5.4 (a) and (b) show that tidal heating might drive plate tectonics on a Mars-sized planet (M_p = 0.3 M$_{Earth}$) orbiting a star of mass 0.1 M$_{Sun}$, even with e as small as 0.04. For planets around larger stars (Figure 5.4 (c)), larger eccentricities are required for sufficient internal heating. Figure 5.5 shows that sufficient but not excessive heating also requires a specific range of M_* and e.

In order to consider whether life might develop and evolve on a given planet, it is also useful to estimate how long h lies in the acceptable range of values as the planet tidally evolves. Figures 5.6 and 5.7 show how long h lies in this range between too little for plate tectonics and so much that volcanism is intolerable. It is important to note that, for many of our modeled planets, the initial value of h is above the acceptable range, and only later, when the eccentricity is sufficiently small, does h enter the acceptable range. For these cases, the time during which h lies in the acceptable range, as depicted in Figures 5.6 and 5.7, begins several Gyrs after the start of the simulation.

Figure 5.6 (a) shows that with M_* = 0.1 M$_{Sun}$ and M_p < 8 M$_{Earth}$, increasing e_0 results in an increasing duration of acceptable h values until e_0 reaches a critical value between 0.3 and 0.6 (depending on M_p), at which point the duration drops again. For these largest values of e_0, the orbital circularization is fast. On the other hand, for M_* =

0.2 M_{Sun} (Figure 5.6 (b)), the HZ is far enough from the star that planets can remain in the acceptable h range longer than 10 Gyr, even in excess of 100 Gyr.

Figure 5.7 shows how the heating lifetime depends on M_*. There is an abrupt transition from planets that never undergo habitable heating to planets with heating lifetimes greater than 10 Gyr, again as a result of the dependence of a_0 on M_*. Moving from panel (a) to (d), M_p increases from 0.3 to 10 M_{Earth}. An island of small heating lifetimes centered around $e_0 = 0.7$ and small M_* grows larger with larger M_p, as the initial heating rate is larger. After billions of years, however, the eccentricities of these large planets drop, and the heating rates eventually pass through the habitable range.

Figures 5.6 and 5.7 suggest that determining the habitability of a terrestrial planet will require tight constraints on the planet's orbital and physical parameters to keep h in the acceptable range for a reasonable amount of time. These calculations suggest that for plausible initial conditions, even small terrestrial planets might retain sufficient internal heating to remain habitable for longer than the age of the Earth.
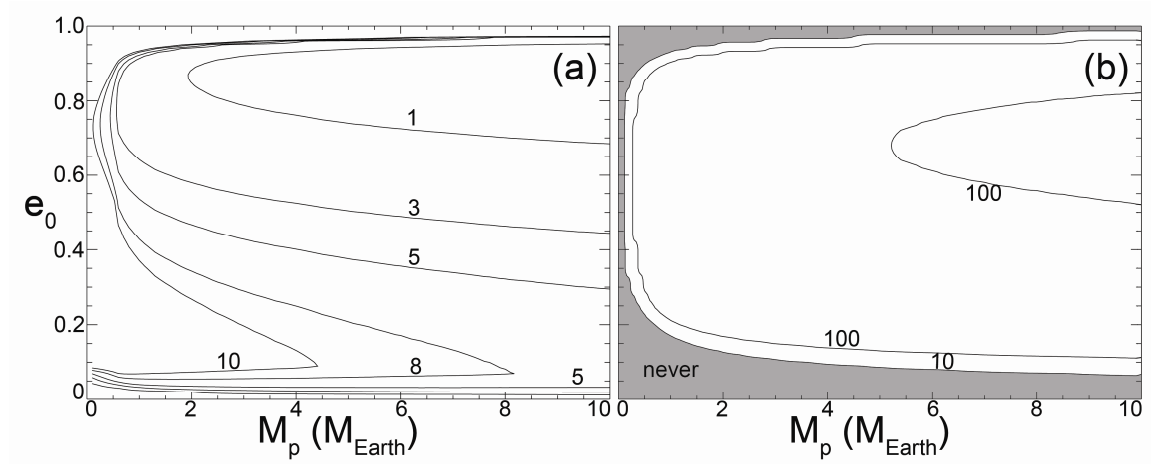
Figure 5.6: Duration of tidal heating in the "habitable range" (*i.e.* enough for plate tectonics, but not enough for sterilizing, Io-like volcanism) for various M_p and e. For panels (a) and (b), the corresponding values of M_* are 0.1 and 0.2 M_{Sun}. The contours of heating lifetimes are labeled in Gyrs, and contours levels for 1, 3, 5, 8, and 10 Gyrs are shown. In panel (b), since the change in tidal heating rate is very slow, planets that begin with sufficient tidal heating have sufficient heating for longer than 10 Gyr, longer than 100 Gyr in some cases. In the region shaded gray and labeled "never", planets start out with too little heating and always have too little heating.
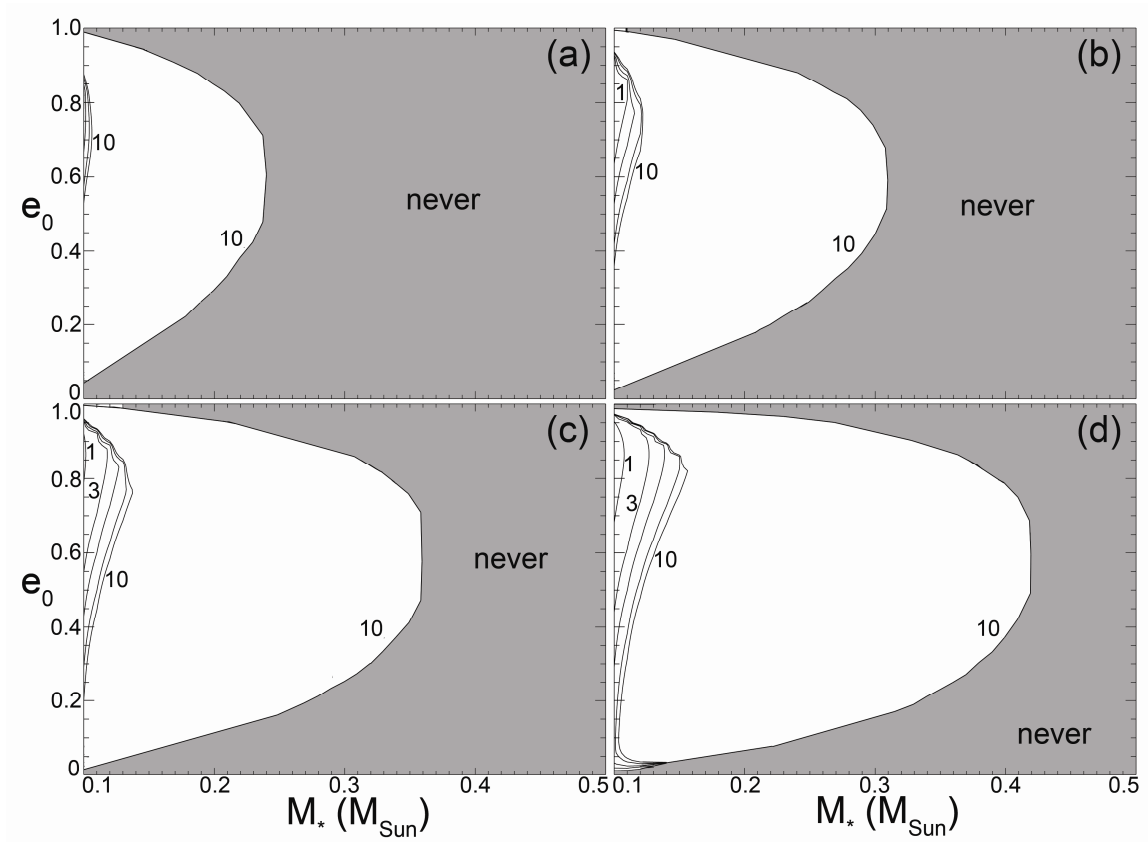
Figure 5.7: Tidal heating lifetimes for various M_* and e. Panels (a) – (d) correspond to M_p = 0.3, 1, 3, and 10 M_{Earth}, respectively. Again, the contours of heating lifetimes are labeled in Gyrs and are shown for 1, 3, 5, 8, and 10 Gyr, and planets in the shaded gray region, labeled "never", never have high enough heating rates for habitability.

5.4.2. Planets with Excessive Volcanism

For $h > 2$ W/m^2, by analogy with Io, habitability may be unlikely, because tidal heating may drive volcanic and tectonic activity too vigorous to allow life. The dark gray shading on Figures 5.4 and 5.5 shows the range of M_p, M_* and e for which h exceeds 2 W/m^2. For $M_* = 0.1$ M$_{Sun}$ (Figure 5.4 (a) and (b)), a very wide range of e and M_p result in this overheating. However, for $M_* = 0.2$ M$_{Sun}$ (Figure 5.4 (c)), planets in the HZ are unlikely to experience heating as large as Io's.

Figure 5.5 gives another perspective on the range of M_p, M_* and e values that give overheating. Planets with $M_p = 0.3$ M$_{Earth}$, for example, only experience heating comparable to Io's when in the HZ of very small star, *e.g.* with $M_* \sim 0.1$ M$_{Sun}$. For a larger planet in the HZ of such a small star, h could be far greater, *e.g.* with $M_p = 10$ M$_{Earth}$, $h > 30$ W/m^2 (Figure 5.5 (d)).

Given the wide range of masses and eccentricities that potentially give rise to extreme volcanism, we might expect that many terrestrial planets will be too volcanically active for life. In fact, as Figure 5.5 (d) shows, the most massive terrestrial planets may also be the most heated and thus the most volcanically active. Since the first extra-solar terrestrial planet that is likely to be confirmed will probably be more massive than the Earth, we might expect it will be volcanically active. Such volcanic activity may be recognizable in the planet's atmospheric transmission spectrum, similar to Io, whose tenuous atmosphere is largely made of sulfur (Geissler *et al.* 1999).

Our calculations also suggest the interesting possibility that a tidally evolving planet may pass through alternate epochs of sufficient heating and excessive heating,

even without interactions with other planets. Consider the $e_0 = 0.9$ curve in Figure 5.2 (a). The initial value of h is ~ 1 W/m^2, sufficient for plate tectonics but not excessive. As time progresses and tides bring the planet closer to the star (smaller a), h slowly grows larger than 2 W/m^2. Eventually after tens of billions of years (beyond the time shown in Figure 5.2 (a)), the orbit will circularize so that h drops below 2 W/m^2 again. Thus, such a planet may begin habitable, then become too violently volcanic, and then, tens of billions of years later, become habitable again. Perhaps life on such a planet would arise in two separate epochs, billions of years apart.

5.4.3. Tidal Heating and Planetary Atmospheres

Tidal heating may also help some extra-solar terrestrial planets to retain atmospheres long enough to allow life to develop and evolve. In some cases such help may be essential, because at least two other processes might otherwise quickly remove the atmospheres. Planets with masses comparable to Mars' will have such low surface gravity that impactors may quickly erode their atmospheres. Melosh & Vickery (1989) found that impact erosion may have reduced the atmosphere of Mars to its current surface pressure from an initial pressure of 1 bar over solar system history. The atmospheres of extra-solar terrestrial planets may also be depleted by stellar activity. Some M stars are so active (Hawley *et al.* 1996; Tarter *et al.* 2007; West *et al.* 2008) that coronal mass ejections (CMEs) could remove atmospheres from planets in the HZ. Lammer *et al.* (2007) showed that, without sufficient shielding by a planetary magnetosphere, an Earth-like planet with $a < 0.2$ AU may lose its entire atmosphere in a billion years, perhaps

limiting prospects for long-term habitability and evolution. On the other hand, tidal heating of the planet may enhance internal convection and help to generate a magnetic field, which could shield the planet's atmosphere.

Tidal heating may also supply or replenish atmospheres that would otherwise be lost. For example, the radiogenic heating of the Earth is sufficient to induce outgassing of volatiles from the Earth's mantle (Williams *et al.* 1997). Papuc & Davies (2008) modeled the thermal and tectonic evolution of hypothetical terrestrial planets, and found that, for a wide range of planetary masses, volcanic outgassing may provide an atmosphere as massive as the Earth's in a few Gyrs.

However, those calculations considered radiogenic heating as the only heat source. Our calculations show that tidal heating may easily exceed radiogenic heating, so it may significantly increase the mantle outgassing rate, in many cases enough to resupply atmospheres that otherwise would be lost to erosion by impactors or CMEs. The habitability of terrestrial planets probably requires a suitable balance between internal and atmospheric processes, and tidal heating is potentially great enough that it plays a critical role.

5.4.4. Ice-covered Planets

Tidal heating could also enhance the habitability of planets with large water components, by maintaining a liquid ocean just below the surface (Vance *et al.* 2007), even if the exposed surface is frozen. Such a planet would be similar to Europa, where (as described above) tides keep most of the water liquid under a thin ice shell. The sub-

surface ocean might be suitable for life (Reynolds *et al.* 1983; Chyba 2000; Greenberg 2005). Europa has a mass of 0.008 M_{Earth} and is composed of a rocky interior below a ~ 150-km-thick layer of water, mostly liquid due to tidal heating (Greenberg *et al.* 2002; Greenberg 2005). The chemicals required for life, including oxidants, may be generated on Europa's surface by energetic charged particles trapped in Jupiter's magnetosphere (Johnson *et al.* 2004). These substances may be transported into the sub-surface ocean by various processes (Greenberg 2005), including impacts (Chyba & Phillips 2002) or local melt-through of the surface ice (O'Brien *et al.* 2002). It has also been speculated that the tidal heating may also give rise to underwater volcanic vents that could support life directly with thermal and chemical energy, by analogy to deep ocean life on the Earth (Baross *et al.* 1982).

Tidal heating may be adequate to drive processes on similar extra-solar ice-covered worlds. Figure 5.4 shows that planets with M_p ~ 0.01 M_{Earth} can experience $h >$ 0.08 W/m^2 with e ~ 0.3, and hence might support a subsurface ocean if there were water present. Also similar to Europa, energetic charged particles, in this case from stellar CMEs rather than from Jupiter's magnetosphere, might give rise to oxidants and other biologically useful substances. In this way, as for Europa, the energetic particles that endanger surface life on Earth-like worlds may enable sub-surface life under an icy crust. Whether a planet as volatile-rich as Europa could actually form around an M star is speculative (Lissauer 2007; Raymond *et al.* 2007), but if they do form, the same processes that may make Europa habitable may also make these planets habitable.

5.5.   Conclusions

From our calculations, we can draw several important conclusions. Many extra-solar terrestrial planets may experience sufficient internal tidal heating to drive plate tectonics. Planets as small as Mars could maintain tectonic activity, even if radiogenic heating alone would be insufficient. Over a wide range of planetary and stellar masses and orbital elements, tidal heating may maintain tectonic activity for billions of years, as a planets orbit evolves and its eccentricity damps down. To maintain such long-lived geophysical activity, it is not necessary to invoke interactions with other planets to pump the eccentricity.

Under a different range of circumstances, tidal heating may be so great as to drive extreme, life-challenging volcanism. For example, we have shown how planets with masses comparable to or larger than the Earth may experience more tidal heating per unit surface area than Io. Because extreme heating may be common among close-in planets with masses larger than the Earth's, the first extra-solar terrestrial planets to be confirmed may prove to be inhospitable to life. The recently discovered planet Gl 581 e, with $M_p = 2$ M_E (Mayor *et al.* 2009b) may represent the first test case for the hypothesis that tides can drive volcanism on extra-solar planets.

Tidal heating may enhance the prospects for life on other planets in various ways. It may enhance the outgassing of volatiles, counteracting the removal of gas by impact erosion and stellar CMEs. In that way tidal heat may be critical to maintaining atmospheres and thus habitability. With or without an atmosphere, if a planet is ice-covered, like Europa, tidal heating may give rise to a habitable subsurface ocean,

protected from organism-damaging CMEs by the surface ice. At the same time, CMEs may actually enable some planets to be habitable by creating essential substances, such as oxidants.

Even with the many simplifying assumptions employed here, the results suggest a wide range of geophysical scenarios. As advancement is made in the understanding of the processes of tidal evolution, in modeling of the geophysics of hypothetical planets, and eventually in the discovery and characterization of actual terrestrial-type planets, these calculations will need to be revisited. In any case, the calculations here show that tidal heating has the potential to be a major factor in governing the internal structures, surfaces and atmospheres of extra-solar terrestrial planets. Accordingly, the effects of tidal heating must be given consideration when evaluating the habitability of such planets.

Chapter 6
Observational Evidence for Tidal Destruction of Extra-Solar Planets

6.1.   Introduction

As discussed in Chapter 3, the distribution of the orbits of close-in exoplanets provides important constraints on models of planet formation and evolution. These planets are unlikely to have formed in their current orbits (with semi-major axis $a < 0.1$ AU) because the protoplanetary gas disk from which they accreted was probably too warm so close to the host star (Lin et al. 1996). For example, the core-accretion model requires coagulation of solid material into a planetary core (Pollack et al. 1996). Within a few 0.01 AU of a star, however, temperatures are too high for condensation of solid material. Instead, the exoplanets observed today in close-in orbits likely formed several AU from their host stars, where temperatures were low enough for condensation of solid material, and later migrated inward (Lin & Papaloizou 1985). An important process driving the migration to ~ 0.1 AU was probably gas drag in the protoplanetary gas nebula (Lin *et al.* 1996). Once planets are inside 0.1 AU, tides can play an important role (Rasio & Ford 1996; Weidenschilling & Marzari 1996; Barnes *et al.* 2008a; Jackson *et al.* 2008a, b; Nagasawa *et al.* 2008). Here we consider the role of tides in shaping the observed orbital distribution.

Figure 6.1 shows the semi-major axes and estimated ages for many close-in exoplanets. (The data for Figure 6.1 are given in Table 6.1.) Most of these planetary systems are younger than 6 Gyrs, and *a*-values are concentrated between 0.03 and 0.7 AU,

centered on about 0.05 AU, which corresponds to an orbital period of about 3 days for a star with a solar mass. Older planets tend to be farther away from their host stars, although there is considerable uncertainty regarding stellar ages (*e.g.* Saffe *et al.* 2005, Soderblom 2009) and the sample size is limited. Also, transiting planets (filled squares in Figure 6.1) tend to be younger than non-transiting planets: all but one transiting planet (XO-5 b) are younger than 6 Gyrs, while there are many older non-transiting planets. Perhaps most significant, there are no planets with $a < 0.017$ AU, and this lower cut-off (approximated by the dashed line in Figure 6.1) increases with age. For example, among planets younger than 5 Gyrs, a-values are as small as 0.017 AU, whereas among planets older than 5 Gyrs, a-values are all greater than 0.036 AU. Given the uncertainty in stellar ages, we performed Monte Carlo simulations that incorporated uncertainties in age and a and found that this trend is persistent. (See Appendix A.) As we will show, these trends are all consistent with the evolution and eventual destruction of planets by tides.

Previous studies have addressed the apparent of a-values concentration centered at 0.05 AU. This concentration is often called the "three-day pile-up" (*e.g.* Rasio & Ford 2006; Cumming *et al.* 2008), a term that reflects an implicit assumption that inward migration deposited these planets at their current orbits, like rocks deposited in a moraine at the front edge of a glacier. Thus, studies of the inward migration have tried to account for a stopping mechanism at around 0.05 AU.

Models in which interactions between planets and a protoplanetary gas disk caused the planets to migrate often invoke a clearing of the gas close to the star to halt the migration (Lin *et al.* 1996; Trilling *et al.* 1998; Ward 1997; Papaloizou 2007). These

studies have suggested a host star's magnetosphere can clear out the gas disk within a few 0.01 AU of the star, and once the migrating planets enter the cleared region, they stop migrating, resulting in a "pile-up".

Other studies have invoked a combination of gravitational scattering and tidal evolution to move planets inward to the "pile-up" (Rasio & Ford 1996; Weidenschilling & Marzari 1996; Ford & Rasio 2006; Nagasawa *et al.* 2008). In such scenarios, interactions between planets in a dynamically unstable nascent planetary system scatter one of the planets into a highly eccentric orbit, with a pericenter distance close enough to the star that tides would affect the orbits. Ford & Rasio (2006) showed that, if scattering resulted in $e \sim 1$ and pericenter distances close to the Roche limit of the star, tides raised on the planet by the host star would drive a-values to nearly twice the Roche limit as the eccentricity dropped to zero, at which point tidal evolution resulting only from tides raised on the planet would cease. This process would typically deposit a planet close to 0.05 AU.
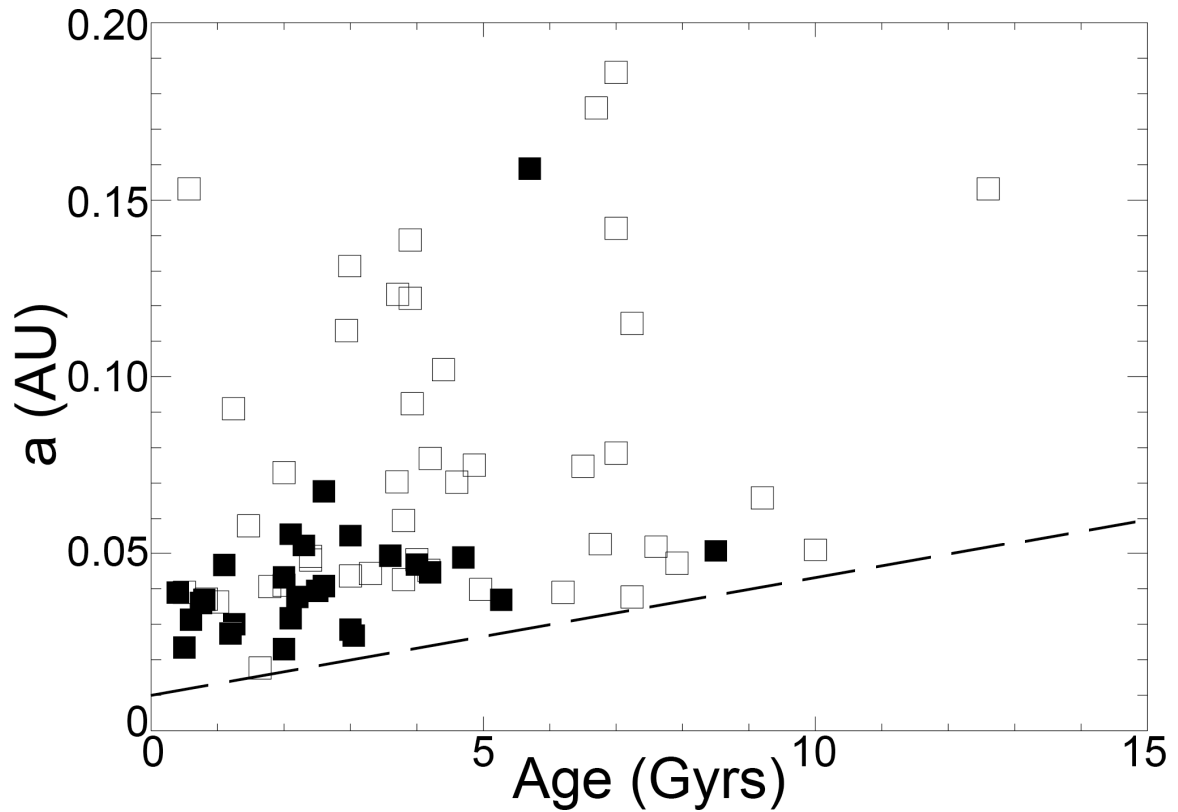
Figure 6.1: The observed distribution of *a*-values and ages for close-in planets for which some estimate of the age is available. Filled squares represent transiting planets, while open squares represent non-transiting planets. For 9 of the 70 planets in the sample, we only have a lower limit on the age. In those cases, we have plotted the age as the available lower limit. Where only the minimum and maximum values for the age were available, we plotted the average of these values. Sources for the data are listed in Table 6.1. The dashed line indicates the apparent lower cut-off boundary in observed *a*-values.

However, such models have generally ignored the effect of the tide raised on the host star, which plays a significant role in the evolution of the orbits of close-in exoplanets (Trilling *et al.* 1998; Dobbs-Dixon *et al.* 2004; Adams & Laughlin 2006; Jackson *et al.* 2008a; Levrard *et al.* 2009; Barker & Ogilvie 2009). In this paper, we consider the effect of the tides raised on the star, which can dominate the orbital evolution for $a < 0.05$ AU. We find that the concentration of observed planets near 0.05 AU may represent the result of inward migration and destruction of closer-in planets, rather than a pile-up of planets that migrated in from farther out. Previous theoretical studies have shown that tides may pull planets into stars in only a few Gyrs (Mardling & Lin 2004; Raymond *et al.* 2008a; Levrard *et al.* 2009). In this chapter, we present observational evidence that this destruction has already occurred.

By modeling the tidal evolution of a hypothetical population of close-in planets, we show how the distribution of observed a-values with age provides evidence for tidal destruction. We find that many of the features of the observed distribution agree with our models if the ages of our model planetary systems are distributed uniformly. However, in the solar neighborhood, there are observed to be more younger than older stars, and the agreement between the observed and modeled distributions of a-values is significantly improved if we account for the prevalence of younger planetary systems. We also find that our model can reproduce the observed clustering of a-values if we assume the distribution of initial a-values was weighted to smaller a.

As we demonstrate below, the tendencies for older exoplanets to be farther from their host stars and for transiting planets to be young likely result from tidal evolution of

orbits. We also show that the apparent clustering of orbital periods near three days does not require a mechanism to stop the inward migration of close-in exoplanets. Rather the observed cut-off in a-values is a natural result of tidal evolution. Our results indicate that many observed close-in exoplanets will probably be destroyed by tides in a few billion years.

6.2.   Timescales for Tidal Destruction of Observed Planets

As discussed in previous chapters, tidal changes in orbital semi-major axes a can be large and thus plays a key role in producing the observed distribution of a-values. In fact, tides can reduce a-values so much that many exoplanets have probably already crossed the critical distance (*e.g.* the Roche limit) inside of which there would be tidal disruption of the planet. As shown below, this tidal removal and disruption leads to the observational trends pointed out in Figure 6.1.

Several previous studies overestimate the time for a planetary orbit to decay into the star, the so-called "orbital decay timescale". These studies attempted to simplify the tidal evolution equations by calculating the current values of $a/(da/dt)$ and using it to estimate the timescale, essentially assuming a damps exponentially with time. For example, Rasio *et al.* (1996) estimated that the orbital decay timescale for 51 Peg b was a trillion years, longer than the main sequence lifetime of its host star. However, the strong dependence of *da/dt* on a (Equation (3.1)) means the ratio $a/(da/dt)$ is not constant, and therefore a does not damp exponentially. Instead, a numerical solution of the coupled Equations (3.1) and (3.2) shows that *da/dt* rapidly increases in magnitude as a drops. The

orbit decays more and more rapidly, as was also pointed out in previous chapters and by Levrard *et al.* (2009). In fact, 51 Peg b's orbit could decay in only a few billion years.

Presumably, once the planet's pericenter distance $p = a(1-e)$ is close enough to its host star, the tidal gravity of the star will disrupt the planet, and the planet will be destroyed. Figure 6.2 shows the coupled tidal evolution of pericenter p and eccentricity e from their current values forward in time for two close-in exoplanets for a range of stellar dissipation parameters Q'_*. The horizontal line near the bottom of each plot is the Roche limit a_R for that system, given by $a_R = (R_p/0.462) (M_*/M_p)^{1/3}$ (Faber *et al.* 2005). The classical Roche limit involves many important assumptions about the planet's density, structure, and strength, so the actual distance of tidal break-up may be different, depending on physical parameters. However, the exact value for the Roche limit is not important because once a tidally evolving planet gets within a few 0.01 AU of its host star, its orbit evolves so quickly that the timescale for the destruction of the planet is not sensitive to the exact break-up distance.

In Figure 6.2 (a), we show the tidal evolution of CoRoT-7 b, which is a transiting exoplanet with the smallest radius found to date, about 2 Earth radii (exoplanet.eu), indicating it may be a rocky planet. Its current orbital eccentricity has been reported as zero, so $p = a$. As a result, only the tide raised on the star by the planet contributes to its tidal evolution (Equation (3.1)). As p begins to decrease, the rate of decreases accelerates rapidly. For the commonly adopted value $Q'_* = 10^5$ (Matheiu 1994; Lin *et al.* 1996), CoRoT-7 b's orbit crosses the Roche limit in a few tens of millions, but even for $Q'_* = 10^7$, CoRoT-7 b would be doomed in the next few billion years.
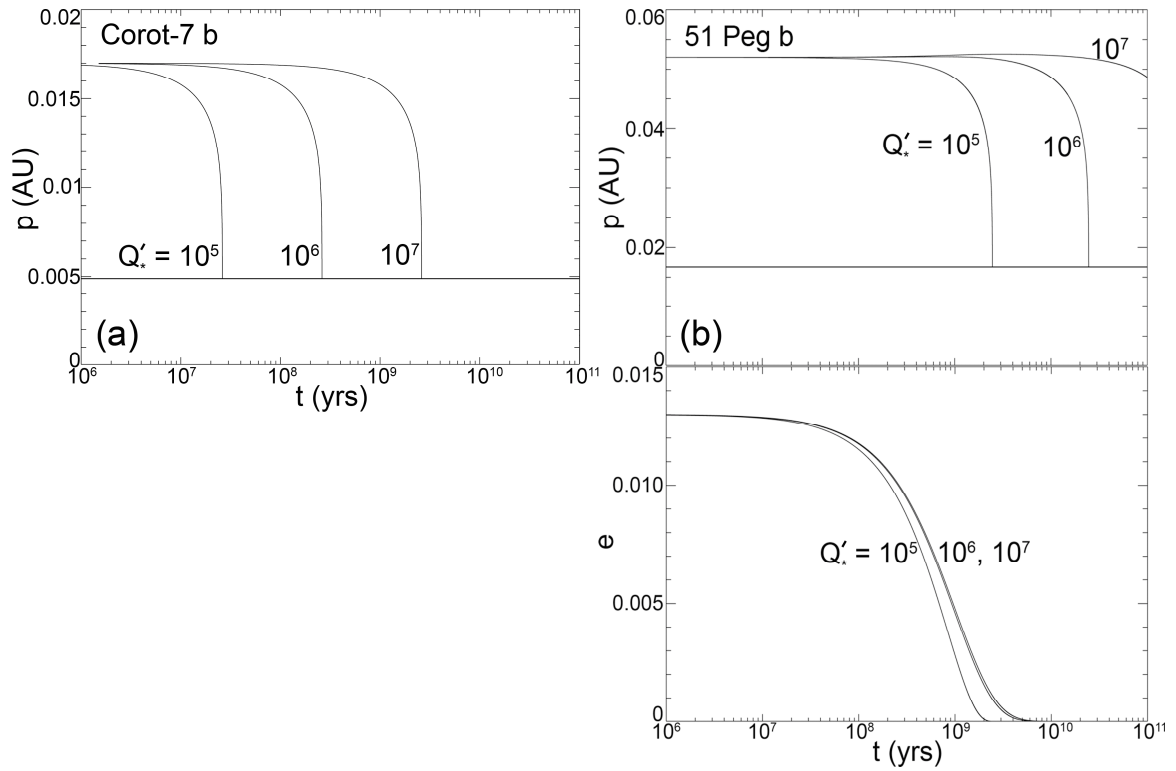
Figure 6.2: Tidal evolution of the pericenters p and eccentricities e of CoRoT-7 b and 51 Peg b. Each line is labeled with its corresponding Q'_* value, and Q'_p is fixed at $10^{6.5}$. The solid, horizontal line indicates to the Roche limit for each planet and star.

For 51 Peg b (Figure 6.2 (b)), recent estimates give $e = 0.013$ (Butler *et al.* 2006). Again, as shown in Figure 6.2 (b), tidal destruction is possible within the lifetime of the star. However, for this planet, the non-zero *e*-value means that the tide raised on the planet contributes slightly to the orbital evolution. As a result, before 51 Peg b plummets to the Roche limit, its eccentricity decreases, and *p* can rise a bit temporarily. While the pericenter distance does not decrease monotonically, it does eventually accelerate toward the star.

These examples show how dependence of *da/dt* on *a* can accelerate the removal of a planet. Consequently, it is the initial *a*-value that determines the time before a planet's orbit crosses the Roche limit, and not so much the initial eccentricity. The acceleration of tidal evolution with decreasing *a* means that a population of planets with small initial *a*-values (orbiting similar stars) would have their *a*-values spread apart more quickly than a group with large initial *a*-values. This process must have a strong effect on the density distribution of those planets as a function of *a* and age, and thus can help shape the observed distribution shown in Figure 6.1.

6.3.   Observable Consequences of Tidal Evolution

6.3.1. Effects of Decreasing *a*

We can illustrate this spreading process and its effect on the orbital distribution by considering a hypothetical population of Jupiter-like planets (with M_p = 1 Jupiter mass and R_p = 1 Jupiter radius) in initial orbits around Sun-like stars (with M_* = 1 solar mass, R_* = 1 solar radius and Q'_* = 10^6) with a range of *a*-values uniformly distributed between 0.01 AU (near the Roche limit) and 0.2 AU. We set initial *e*-values to zero, because (as discussed above) they have little effect on the lifetime before the orbits cross the Roche limit. Here we are considering the evolution of many individual planets, each in its own planetary system, rather than many planets in a single system. For each planet in the model population, we modeled the tidal evolution forward in time according to Equation (3.1). (Equation (3.2) is not relevant in this case of circular orbits.) Figure 6.3 shows the evolution of the population over 15 Gyrs. The closest planets plunge rapidly in toward their stars, while planets farther out hardly evolve. The planets closest to their stars become less densely distributed in *a*-values.

The decrease in the density of planets for smaller *a*-values is quantified in the histogram in Figure 6.4, which shows the evolution of number density (# of planets/increment in *a*) as a function of semi-major axis, and the way in which this function changes with age. The results shown in Figure 6.4 are based on calculations similar to Figure 6.3, but with many more planets: 10,000 planets spread initially from *a* = 0.01 to 0.2 AU. For Figure 6.4, planets are binned by *a*-value in bins 0.005 AU wide, and then the number of planets in that bin is normalized by dividing by the total number

of planets in the original population, giving the normalized number density. Initially ($t =$ 0), all bins are filled evenly, reflecting the assumed uniform spread in a-values. However, as time passes, the innermost bins are rapidly cleared out, the outermost bins are unaffected, and planets from intermediate bins move inward to smaller a-values. As suggested by Figure 6.2, the rate at which bins clear out depends on the value of Q_*, but for any value of Q_*', the innermost bins clear first.

   If the initial a-values for real planets were uniformly distributed (and by "initial" we mean when tides began to dominate the evolution), we would expect the distribution of planets to be similar to Figure 6.4, with relatively few in a-bins with low densities and more in bins with high densities. For example, according to Figure 6.4, among planets that are 1 Gyr old, we might expect to observe about twice as many with a-values near 0.03 AU as we find with a-values near 0.025 AU.
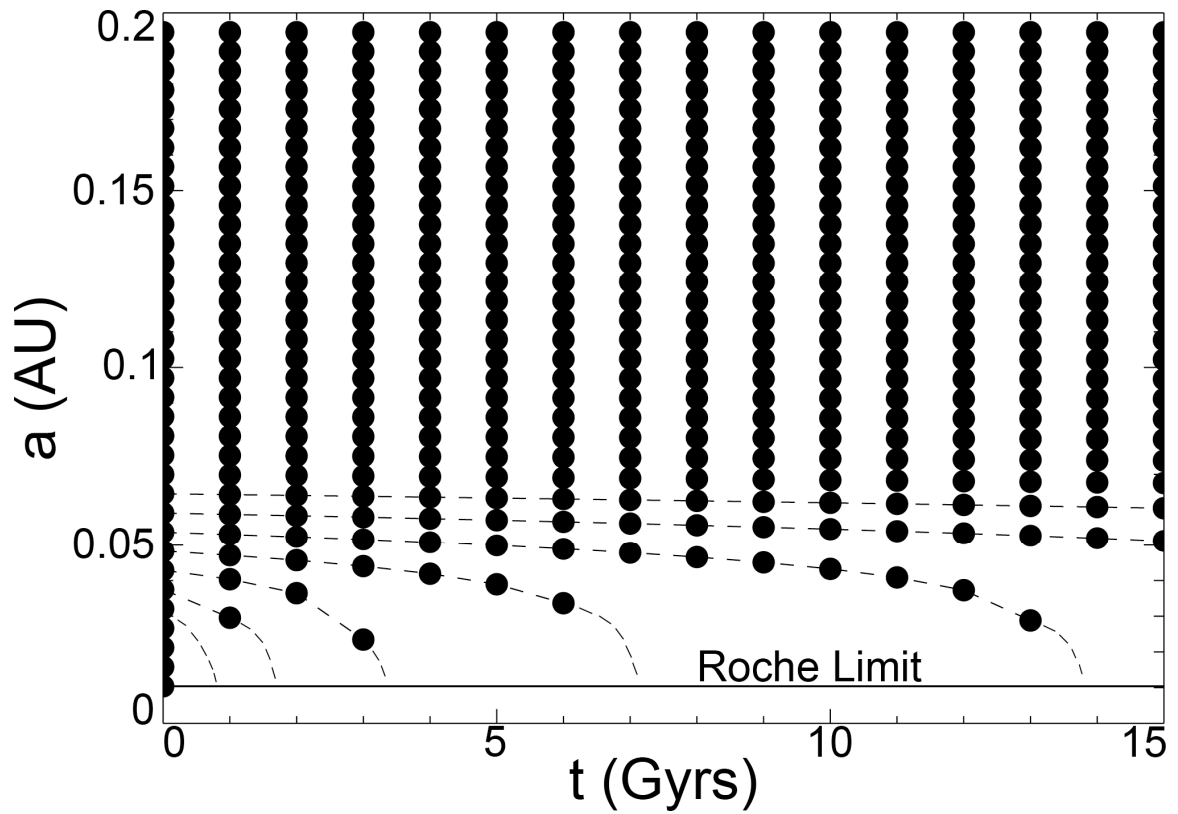
Figure 6.3: The tidal evolution for a hypothetical population of planets on circular orbits with a range of initial *a*-values uniformly distributed between the Roche limit at 0.01 AU and 0.2 AU. The dashed lines trace the tracks for a few representative examples, and the solid horizontal line shows the Roche limit.
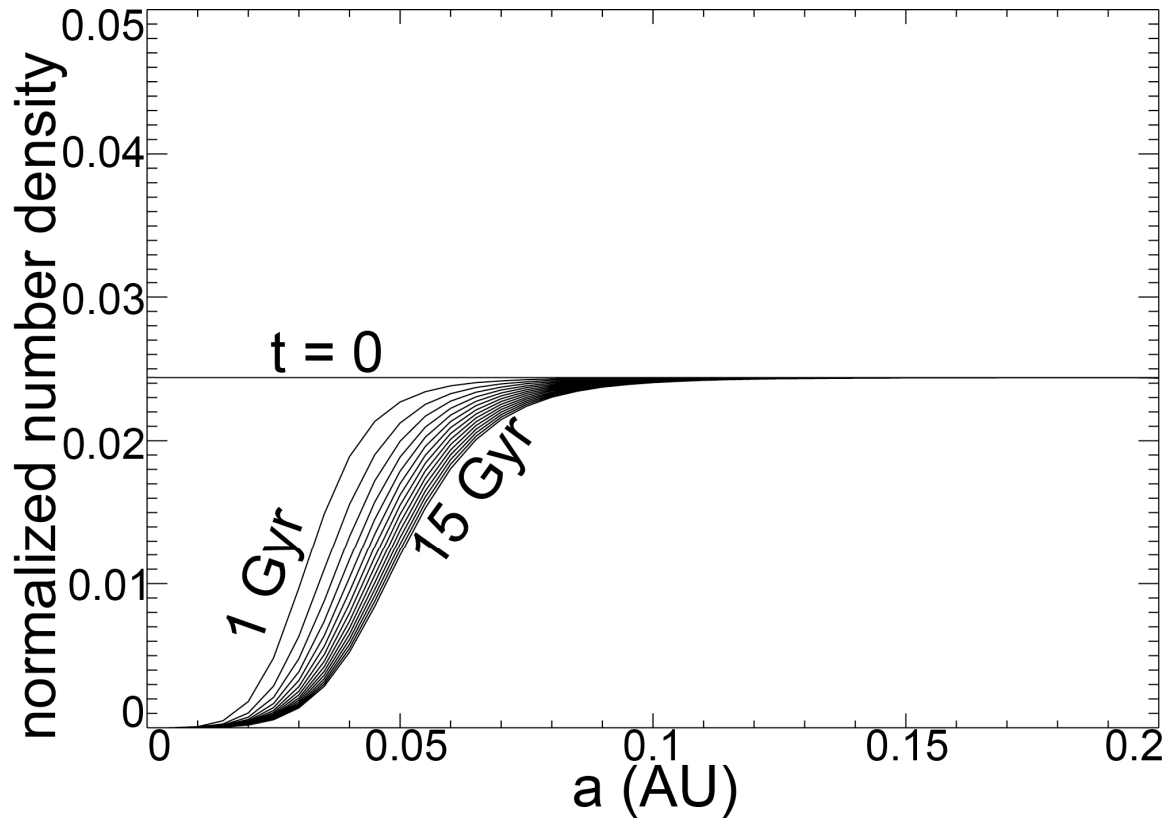
Figure 6.4: The normalized number density (defined in the text) of a population of planets, shown as a function of a, varies over time from an initial uniform distribution. Curves represent the distribution at intervals of 1 Gyr from t = 0 to t = 15 Gyr. For this figure $Q'_* = 10^6$.

In order to compare these models of the evolution of number density to the observed distribution, we recast Figure 6.4 as a plot of semi-major axis vs. stellar age, analogous to Figure 6.1. From Figure 6.4, we can extract the locus of points with any fixed number density on a plot of semi-major axis vs. age, yielding the solid curves in Figure 6.5. For example, consider a normalized number density of 0.015 in Figure 6.4. We see that after 1 Gyr, the histogram bin corresponding to a density of 0.015 is centered on 0.035 AU. After 2 Gyrs, the bin with that same density is centered on 0.04 AU. In order to map the 0.015 density contour in Figure 6.5, we draw a curve connecting the point at 1 Gyr and 0.035 AU to the point at 2 Gyrs and 0.04 AU (and also to all the intermediate and exterior points). This increase with age in the a-value corresponding to a fixed number density is reflected by the positive slope of the contours in Figure 6.5.

If the population represented by these contours were sampled observationally, depending on the total number of planets and the limits of completeness of the search, some bins might not be populated in the observational data. That is, we would not expect to have observed planets in the parts of the distribution below a particular limiting density. Thus the contour line for that density should represent a boundary, below which planets would not appear in the observed population. Note, however, that without knowing the actual number of planets or the completeness of the search to date, we cannot say which specific contour should give that boundary.

Figure 6.5: Contours represent the locus of points with a fixed value normalized number for the population shown in Figure 6.4 for a range of Q'_* values. From bottom to top, the contours shown are for 0.00015, 0.0015, and 0.015 in the same units as the y-axis in Figure 6.4.

However, we can test the plausibility of our model (that the low-*a* cut-off is due to tidal migration into the star) by determining whether any contour of the model distribution follows the cut-off in the observed distribution. Figure 6.5 includes the observed distribution and the apparent cut-off (from Figure 6.1) for comparison with the model contours. We see that, for all three values of Q'_*, the model contours do predict a paucity of planets with small *a*, and the contours do have slopes toward larger *a* with greater age. But none of the contours matches the relatively steep slope of the observed cut-off (dashed line in Figures 6.1 and 6.4).

6.3.2. Effects of the Age Distribution

The model above does not include an important selection effect: there are inherently fewer older stars than there are younger stars in the solar neighborhood (Takeda et al. 2007). Figure 6.6 shows a histogram of stellar ages for a large population of nearby F, G, and K stars, as reported by Takeda *et al.* (2007). The number of stars in a given age bin declines roughly linearly with age (although stellar ages do remain very uncertain [*e.g.* Saffe *et al.* 2005; Soderblom 2009]). We can also see this trend in Figure 6.1, especially at large *a*-values (where tides have little effect). For this version of our model we represent this reduction in the number of older stars with a straight-line fit (as shown in Figure 6.6).We use that function as the relative probability for a star to be a certain age.

We apply this reduction in the number of older stars to the population shown in Figure 6.4, reducing the number of planets (uniformly in all *a*-bins) in accord with their

increasing age. Figure 6.7 shows the results of modifying simulated population in this way.

The density contours corresponding to Figure 6.7 are shown on a plot of semi-major axis vs. age in Figure 6.8. Compared with Figure 6.5, the shapes of the contours at low a are steeper and, for great enough age, the contours become vertical, reflecting the reduction in all a-bins of the number of planets with age.

Comparing the slopes of the model contours to the low-a cut-off in the observed population, we find good fits for all values of Q'_*. For $Q'_* = 10^5$, 10^6, and 10^7, respectively, there is a reasonable fit for the density contours with values 0.00015, 0.0015 and 0.0045. In addition, the contours fit the reduction in numbers of old planets for larger a-values. Thus, incorporating the reduction in the number of older stars shows that observations are consistent with destruction of planets through tidal decay of their orbits.
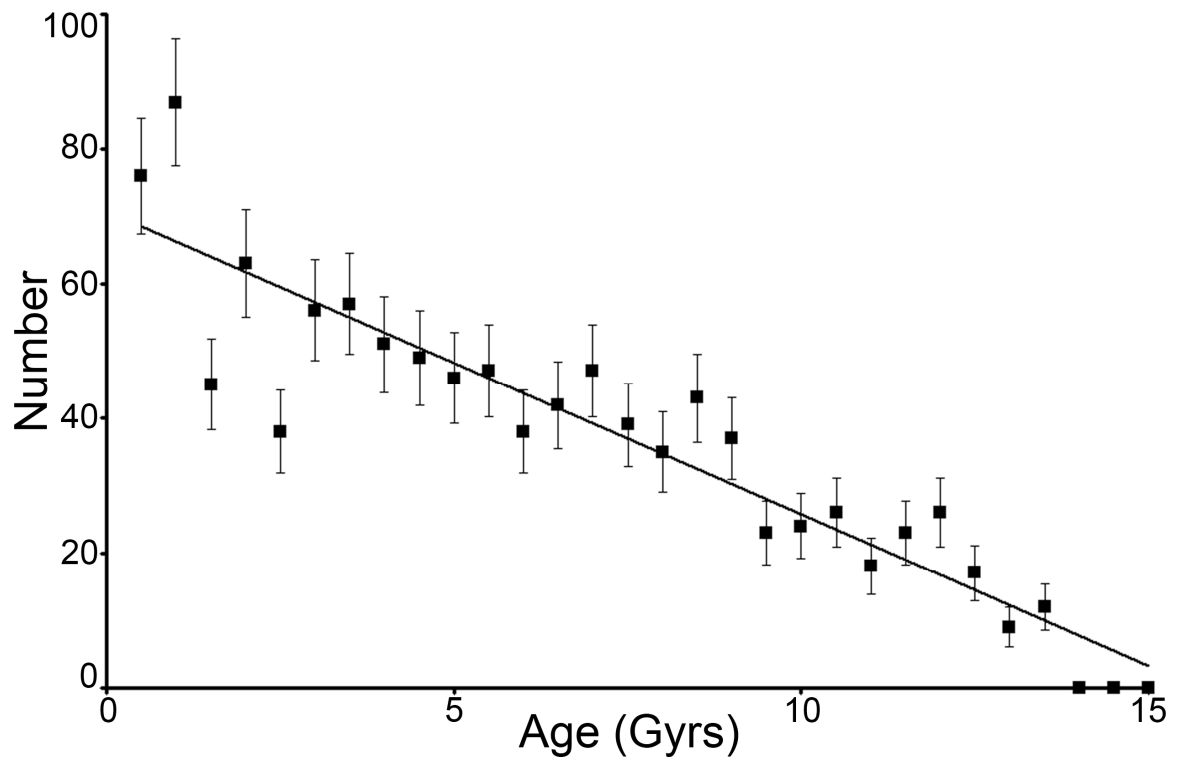
Figure 6.6: Histogram of stellar ages with a least-squares fit (Takeda *et al.* 2007). Error bars are based on Poisson statistics.
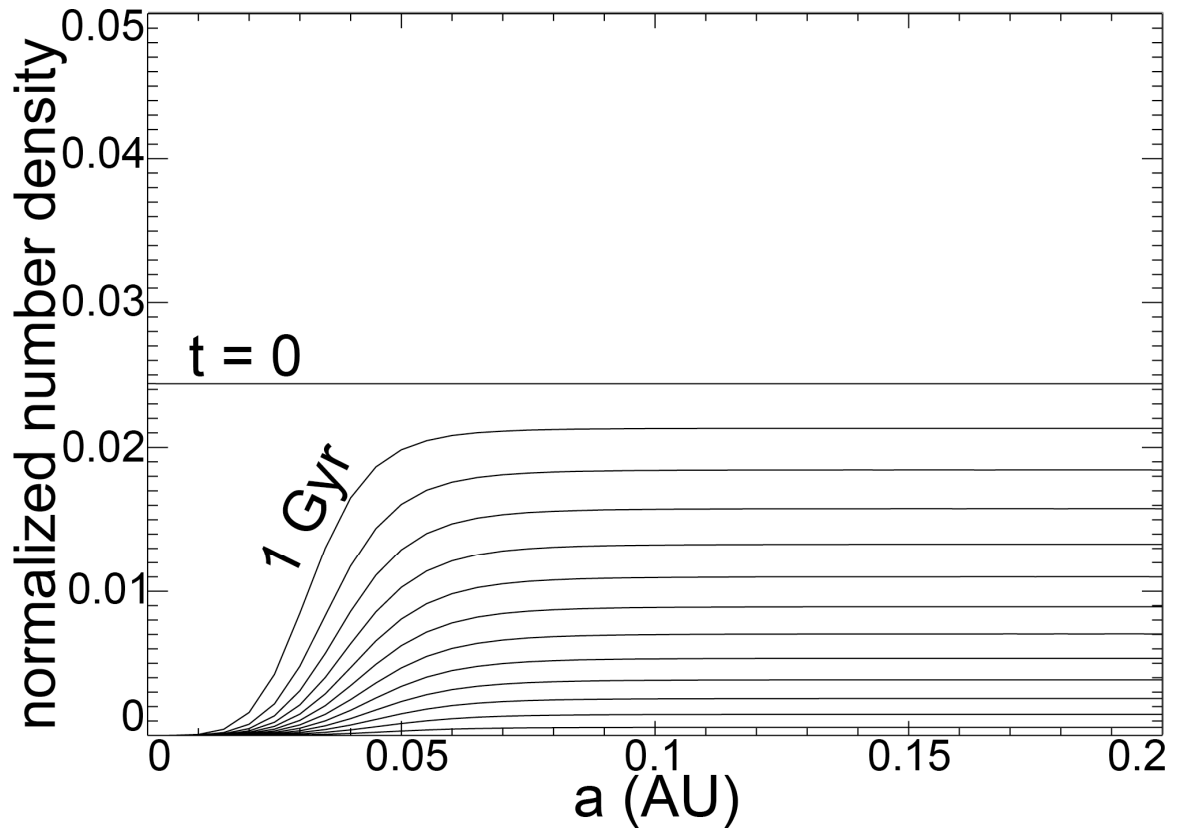
Figure 6.7: Same as Figure 6.4, except the number of planets is reduced with time by the same factor in all a-bins, according to the linear relationship in Figure 6.6. For this figure $Q'_* = 10^6$.
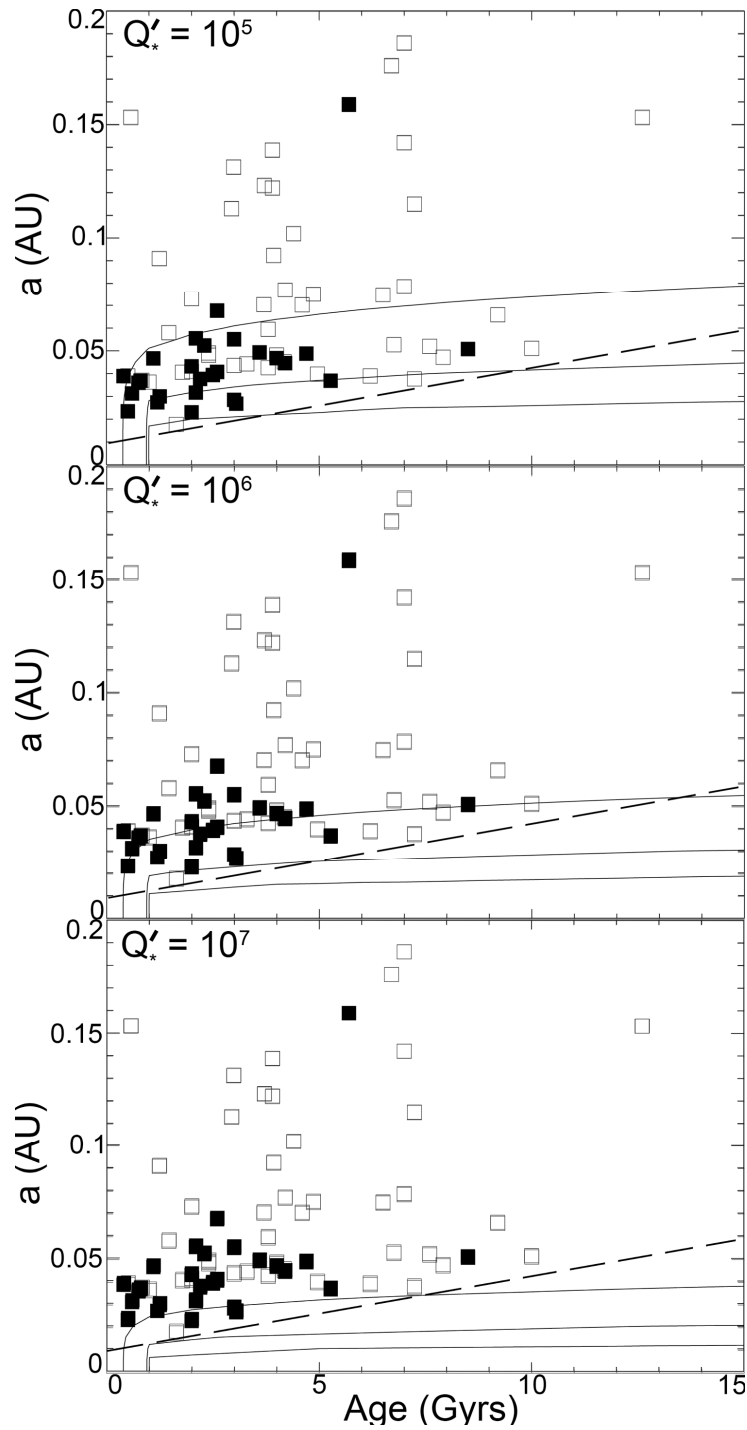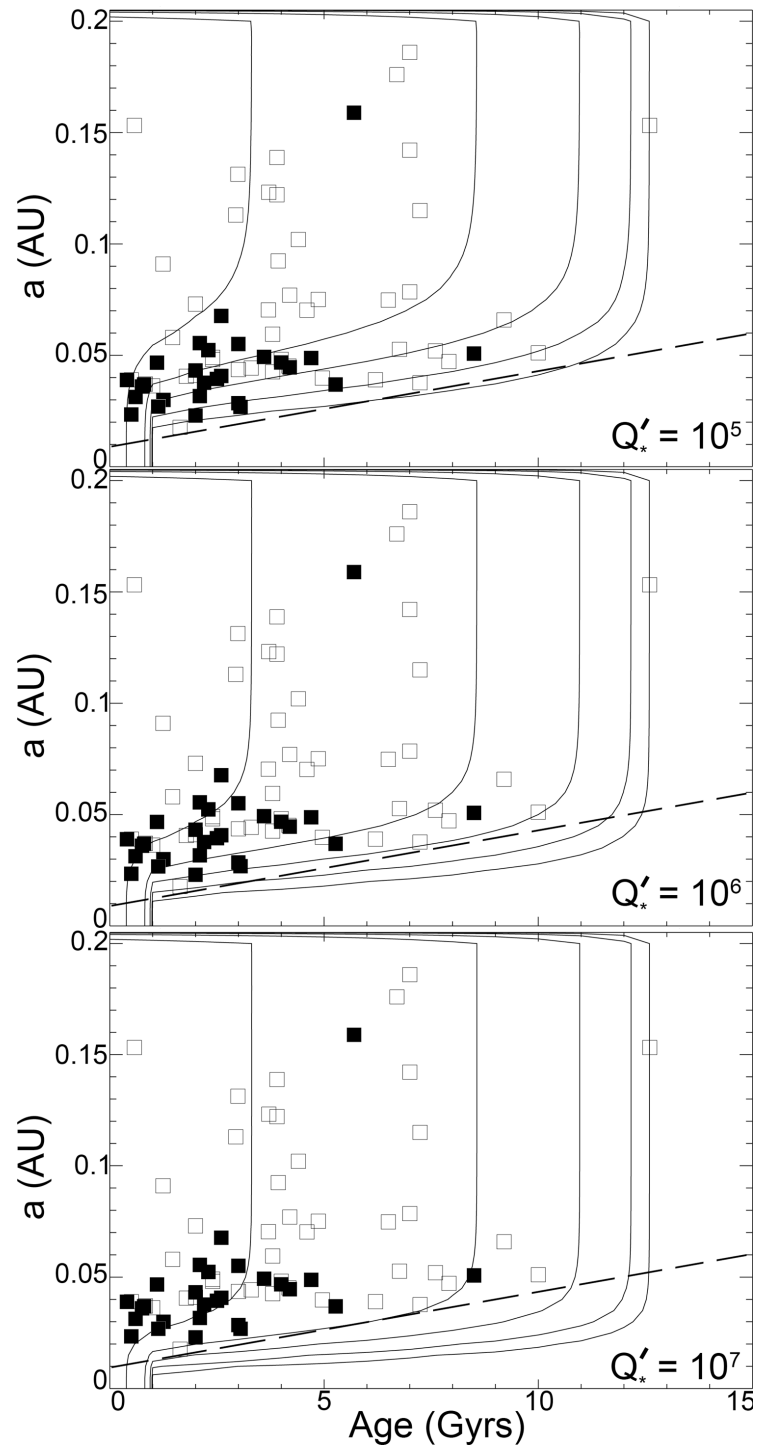
Figure 6.8: Contours represent the locus of points with a fixed value for the normalized number for the population shown in Figure 6.7 for a range of Q'_* values. From the bottom right to the top left, contours are shown for 0.00015, 0.00045, 0.0015, 0.0045, 0.0015, and 0.045 in the same units as the y-axis of Figure 6.7.

6.3.3. Effects of the Initial *a* Distribution

This analysis assumes that *a* begin with a uniform distribution. We also investigate the effects of choosing an alternative distribution. For example, consider an initial population of planets whose number density decreases with increasing *a*, as in the linear distribution at t = 0 in Figure 6.9. Such a distribution might reflect the effects of gas disk migration, for example. Figure 6.9 shows the evolution of such a population due to tidal variation of *a* and the loss with age (according to Figure 6.6). As time passes, the number density for the innermost bins drops rapidly, and the density in the bins farther out remains mostly unchanged, just as in previous calculations. If the distribution is weighted toward smaller *a* values, other assumptions about the initial distribution (*e.g.* that number density increases as a^2) give qualitatively similar results.

Density contours for semi-major axis vs. age are shown in Figure 6.10 for this case, analogous to Figures 6.5 and 6.8. Here contour lines show that the density drops for increasing *a* where *a* > 0.1 AU. At the lower-*a* cut-off, the contours lines follow the slope of the observed distribution (dashed line). In general, the model contours fit the observed distribution reasonably well. The agreement is especially good for $Q'_* = 10^7$, where the model yields a concentration of *a*-values around 0.05 AU, similar to that observed. These results suggest that we can account for the observed clustering of *a*-values and the low-*a* cut-off by invoking an initial distribution that favors closer planets, followed by tidal orbital decay. The concentration at 0.05 AU may not be a pile-up, but rather it could be the result of carving away part of the initial population. The orbits of many planets have decayed into their parent stars, and more will do so in the future.
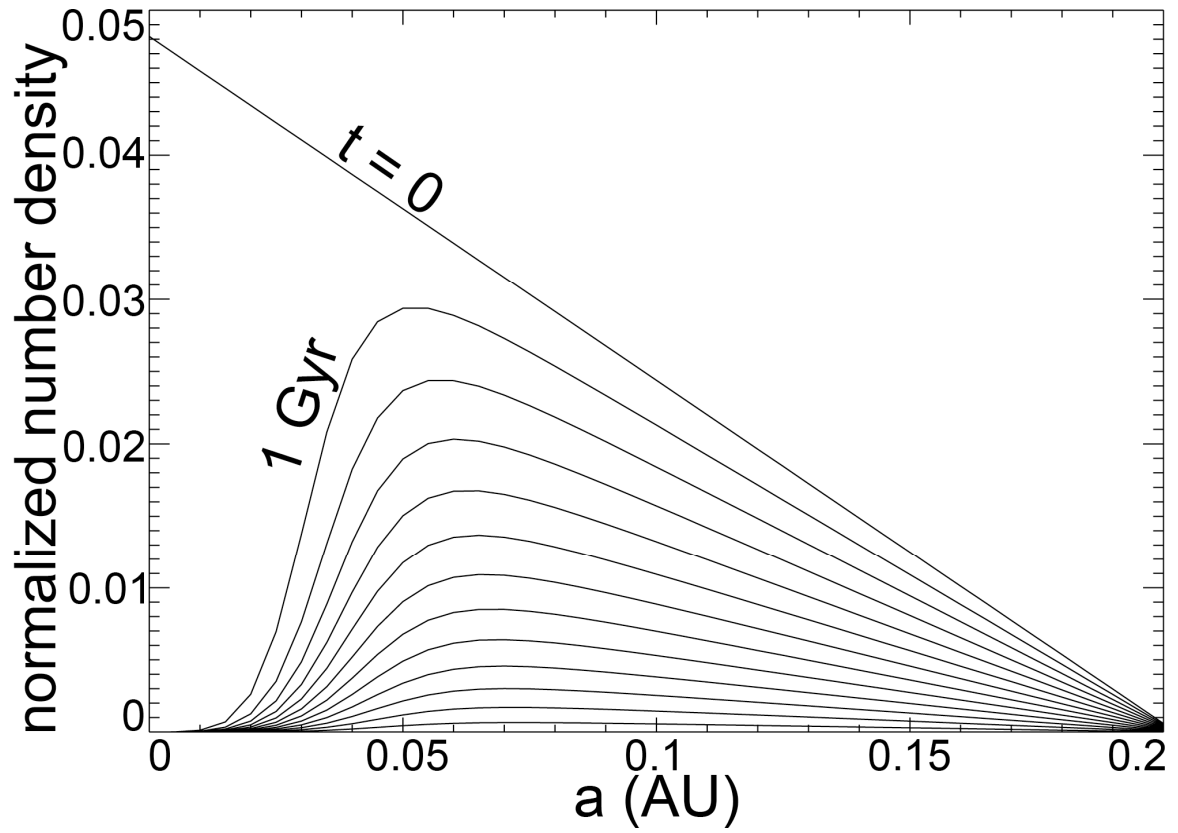
Figure 6.9: Same as Figure 6.4, except the number of planets is reduced with time by the same factor in all a-bins, according to the linear relationship in Figure 6.6. For this figure $Q'_* = 10^6$.
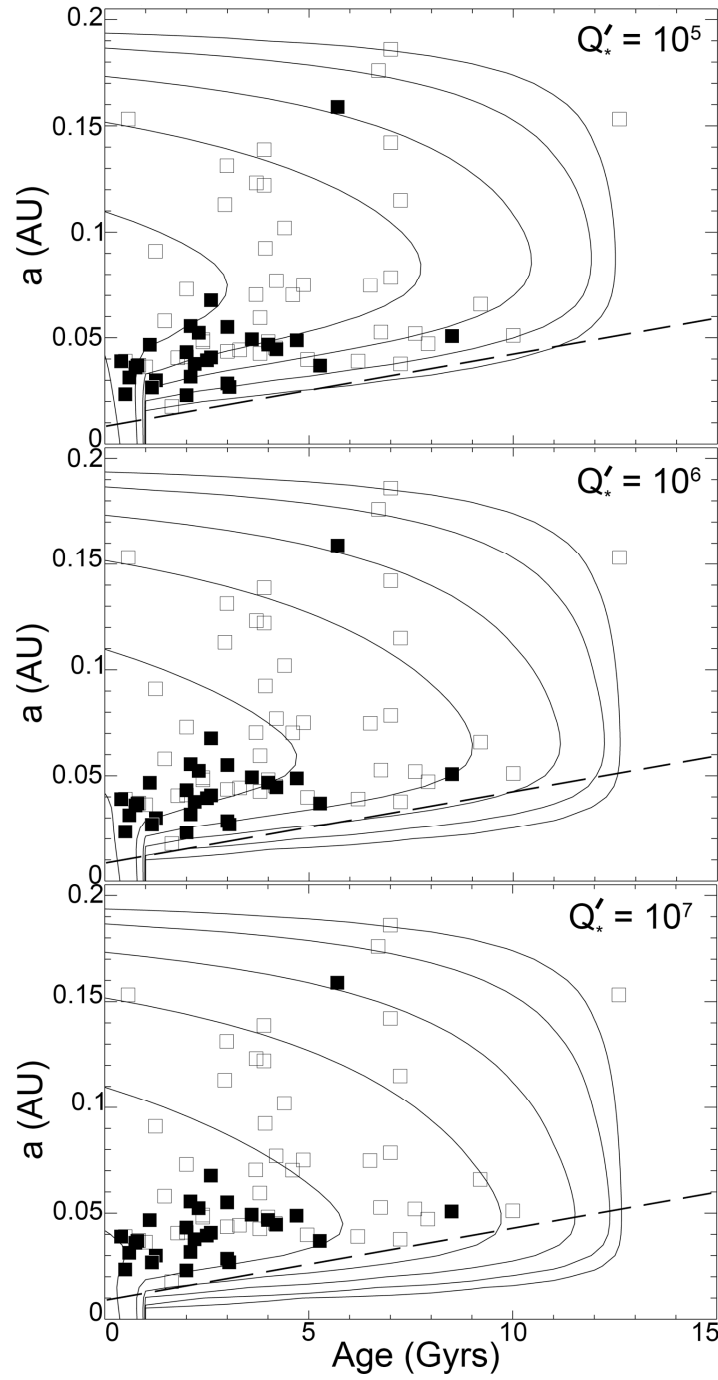
Figure 6.10: Contours represent the locus of points with a fixed value for the normalized number for the population shown in Figure 6.9 for a range of Q'_* values. Contours are shown for the same density values as in Figure 6.8.

6.4.   Discussion

6.4.1. Transiting Planets

The process of tidal evolution and destruction of planets discussed above has a profound effect on the observed distribution of a-values. It may also explain why transiting planets tend to be younger than non-transiting ones. Transit observations favor discovery of planets closer to their host star. The slope of the lower cut-off in a vs. age space (*e.g.* the dashed line in Figure 6.1, which we have shown can be explained by tidal evolution) means that the closest-in planets will tend to be youngest.

Transiting planets are also likely to be destroyed quickly by tides. Levrard *et al.* (2009) pointed out that the orbits of all known transiting exoplanets (except HAT-P-2 b) are likely to survive less than a few billion years. The preferential destruction of transiting planets relative to planets discovered in other ways should be kept in mind during future statistical studies.

Although the apparent trend in the ages of transiting planets is consistent with the expectations of tidal theory, the trend is subject to many uncertainties and observational selection effects. For example, if transiting planets are easier to find around younger stars, then the trend in their ages may not be due only to tidal destruction. Future work should consider the effects of these uncertainties.

6.4.2. Stellar Rotation Rates

Our results suggest that many planets have already been accreted by their host stars. One potentially observable effect would be an increase in stellar spin rate, as a planet's orbital angular momentum is transferred to the star. The change in rotation rate for a star is given by

$$\Delta\Omega_* = \frac{M_p\sqrt{GM_*a(1-e^2)}}{C_*M_*R_*^2} \tag{6.1}$$

where C_* is the stellar moment of inertia coefficient. For example, if a Jupiter-like planet in a circular orbit with initial $a = 0.05$ AU plunges into a Sun-like star, with a typical 30 day period and typical $C_* \sim 0.1$ (Massarotti 2008), the rotation period is reduced to only $\sim$ 5 days. Because main-sequence stars would otherwise tend to spin down as they age (Skumanich 1972; S. Barnes 2007), an anomalously high spin rate could be evidence for accretion of a tidally destroyed planet. Some anomalously rapid rotators have been found among red giants, and their rapid rotation rates have been taken as evidence for accretion of planets by the stars (Massorotti 2008). Perhaps candidates could also eventually be identified among main sequence stars.

6.4.3. Stellar Compositions

The accretion of planetary material might also change the host star's composition enough to be measurable. Gonzalez (1997) found that planet-hosting stars seemed to be enhanced in metallicity relative to their stellar neighbors. He proposed that this enhancement was due to pollution of the star by accretion of planetary material, which

would be consistent with our model. Fischer & Valenti (2005) found a similar trend but argued that metallicity enhancement of stars is primordial and not due to planetary accretion. In order to resolve this issue, it is important to consider metallicities of stars without planets (as well as those with) because they may have had planets in the past, which affected their metallicity. A particularly useful indicator of relatively recent accretion of planetary material may be ^{6}Li because Li is quickly destroyed by nucleosynthetic processes (Sandquist *et al.* 2002). In fact, correlating such spectral signatures with unusually fast rotation rates might provide evidence for past destruction and accretion of a planetary companion.

6.4.4. Stripped Planetary Cores

As a planet reaches the Roche limit, any gaseous atmosphere or envelope could be stripped off by tidal action, leaving only a rocky core (Trilling *et al.* 1998). Once this tidal stripping begins, it may happen quickly. Faber *et al.* (2005) showed that mass loss can be rapid for a planet in an eccentric orbit that crosses the Roche limit. But many planets reaching the Roche limit may be on circular orbits, and it would be useful to have models that apply in such cases.

As the planet losses mass, the orbital evolution slows, and the Roche limit for the planet shrinks. Thus the remaining planetary core may survive for a long time (Raymond *et al.* 2008a), so it is possible that a population of such bodies may be discovered as observations become more complete. In fact, the potentially rocky exoplanet CoRoT-7 b may represent the first discovery in this new class of planets.

6.4.5. Uncertainties and Assumptions

Although the results presented here have important implications, the details are subject to various uncertainties. The large uncertainties in stellar age and the limited size of the observational sample (so far) are important limitations for our analysis. Stellar ages are difficult to determine (*e.g.* Saffe *et al.* 2005; Soderblom 2009), so uncertainties are often large, in many cases as large as the derived age itself. However, the slope of the low-*a* cut-off noted in Figure 6.1 is robust against these uncertainties, as shown in Appendix A. As age estimates improve and more close-in exoplanets are found, our results should be revisited.

Our analysis also involves several assumptions that are reasonable, but subject to revision. For example, the tidal model described by Equations (3.1) and (3.2) assumes that the rotational period for the host star is much longer than the revolutionary period for the close-in planet. So far, rotational periods for almost all planet-hosting stars are of order 10 days or longer (Trilling 2000; Barnes 2001; S. Barnes 2007), consistent with our assumption. However, if the rotation period of the host star were to become equal to the orbital period as the planet migrates inward, the tidal evolution would cease, and the planet would not be destroyed. This situation could arise for a few transiting planets if tides spin up the stars sufficiently (Levrard *et al.* [2009]; see also Counselman [1973], Greenberg [1974], and Dobbs-Dixon et al. [2004]). However, loss of rotational angular momentum (*e.g.* through shedding of stellar wind or magnetic effects) should help to keep the star's rotation slow, so our assumption will hold in most cases.

We have also assumed that interactions among planets are negligible. In some cases, such interactions could affect the rate of tidal decay of orbits. The removal of a planet from a multiplanetary system through tides may also leave a discernible signature on the dynamical configuration of the remaining planets. These are important topics for on-going research.

6.5.   Conclusions

Tidal decay of close-in exoplanetary orbits can, and probably has, led to the destruction of many close-in exoplanets. Evidence for this destruction comes from the orbital distribution of observed close-in exoplanets: Older planets tend to be farther from their host stars than younger planets; transiting planets tend to be younger than non-transiting planets; the observed orbits show a cut-off in small a-values, which increases to larger a-values with increasing age. These trends can be explained by tidal evolution and destruction of close-in exoplanets. Tidal decay rates are quantitatively consistent with the observed distribution of planetary semi-major axes and ages for a wide range of tidal dissipation parameters.

While it is widely assumed that some mechanism must stop the inward migration of close-in exoplanets in order to explain the observed orbital distribution, our results show that it is not necessary. Our model also explains the short life expectancies of some of the closest-in planets (*e.g.* WASP-12 b, CoRoT-7 b, and OGLE-TR-56 b). They are simply the next in line to be tidally destroyed after the many that have already spiraled down into their stars. Transiting planets especially, because they must pass close to their

host stars to be observed in transit, will quickly be destroyed by tides, which explains why transiting planets tend to be relatively young.

Future observations may provide further evidence for tidal destruction of close-in exoplanets. Stars that have recently consumed a close-in planet may have unusual compositions and may rotate more quickly than expected. Tidal stripping of a gaseous planet's mass once the planet nears the Roche limit may strand the rocky cores of gaseous planets with orbits very close to their host stars, creating a distinctive class of planets that may be seen with improving surveys.

As stellar age estimates become more accurate, more close-in exoplanets are discovered, and our understanding of tidal effects improve, these results will need to be revisited. Nevertheless, our results suggest tidal destruction of close-in exoplanets is common, and many of the exoplanets we see today may soon be gone.

Name	min age (Gyrs)	mid age (Gyrs)	max age (Gyrs)	min (AU)	a	mid (AU)	a	max (AU)	a	age ref, a ref
51 Peg b	5.28	6.76	8.4	0.0497		0.0527		0.0557		39, 9
55 Cnc b	7.24	*9.53*	*11.82*	0.112		0.115		0.118		39, 26
55 Cnc e	7.24	*9.53*	*11.82*	0.0355		0.0377		0.0399		39, 26
BD-103166 b	0.53	4.18	*6.47*	0.0426		0.0452		0.0478		37, 9
CoRoT-7 b	0.7	1.1	2.2	*0.014*		0.017		*0.02*		12, 12
GJ 436 b	3	*5.29*	*7.58*	0.0276		0.0285		0.0293		18, 18
GJ 581 b	2	*4.29*	*6.58*	*0.038*		0.041		*0.044*		41, 5
GJ 581 c	2	*4.29*	*6.58*	*0.07*		0.073		*0.076*		41, 5
GJ 674 b	0.1	*0.5*	1	*0.036*		0.039		*0.042*		6, 6
HAT-P-1 b	*0.71*	3	*5.29*	0.0536		0.0551		0.0566		2, 2
HAT-P-2 b	1.2	2.6	3.4	0.0663		0.0677		0.0691		3, 3
HAT-P-3 b	0.1	0.4	6.9	0.0382		0.0389		0.0396		40, 40
HAT-P-4 b	3.6	4.2	6.8	0.0434		0.0446		0.0458		24, 24
HAT-P-5 b	0.8	2.6	4.4	0.04		0.0408		0.0415		4, 4
HAT-P-6 b	1.6	2.3	2.8	0.0515		0.0524		0.0532		32, 32
HAT-P-7 b	1.2	2.2	3.2	0.0372		0.0377		0.0382		33, 33
HD 102117 b	10.9	12.6	14.3	0.1444		0.1532		0.162		37, 9
HD 102195 b	0.6	*2.4*	4.2	*0.046*		0.0491		*0.052*		16, 16
HD 108147 b	2.3	4.4	6.6	0.0961		0.102		0.1079		37, 9
HD 117618 b	3.6	6.7	9.6	0.175		0.176		0.177		37, 9
HD 118203 b	3.8	4.6	5.4	0.0662		0.0703		0.0744		11, 9
HD 130322 b	0.77	1.24	6	0.0857		0.091		0.0963		37, 9
HD 13445 b	2.03	2.94	12.5	0.1065		0.113		0.1195		13, 9
HD 149026 b	1.2	2	2.8	0.0426		0.0432		0.0438		38, 45
HD 149143 b	6.4	7.6	8.8	*0.049*		0.052		*0.055*		11, 11
HD 162020 b	0.23	*4.865*	9.5	0.0708		0.0751		0.0794		37, 9
HD 168746 b	3.18	9.2	10.8	0.0621		0.0659		0.0697		37, 9
HD 17156 b	3.8	5.7	7	0.1545		0.1589		0.1643		14, 19
HD 179949 b	0.4	3.3	5.4	0.0417		0.0443		0.0469		37, 9
HD 185269 b	*1.91*	4.2	*6.49*	*0.074*		0.077		*0.08*		21, 21
HD 187123 b	2.26	3.8	10.6	0.0401		0.0426		0.0451		37, 9
HD 189733 b	0.6	*2.89*	*5.18*	*0.028*		0.0313		*0.035*		29, 43
HD 192263 b	0.55	0.57	7.6	0.1444		0.1532		0.162		37, 9
HD 195019 b	2.58	3.9	11.8	0.1308		0.1388		0.1468		37, 9
HD 209458 b	2	4	4.5	0.0459		0.0468		0.0477		29, 23
HD 217107 b	1.4	6.5	7.32	0.0705		0.0748		0.0791		37, 9
HD 2638 b	*0.71*	3	*5.29*	0.0411		0.0436		0.0461		31, 9
HD 27894 b	*1.61*	3.9	*6.19*	0.115		0.1221		0.1292		31, 9
HD 330075 b	*3.91*	6.2	*8.49*	*0.036*		0.039		*0.042*		34, 34
HD 38529 b	0.89	*2.99*	5.09	0.1237		0.1313		0.1389		37, 9
HD 41004 B b	1.48	1.64	9.5	0.0167		0.0177		0.0187		37, 9
HD 46375 b	1.68	4.96	7.7	0.0375		0.0398		0.0421		37, 9
HD 49674 b	0.55	*1.465*	2.38	0.0546		0.058		0.0614		37, 9
HD 63454 b	*0*	1	*3.29*	0.0342		0.0363		0.0384		31, 9

HD 6434 b	6.85	7	13.3	0.1339	0.1421	0.1503	37, 9
HD 68988 b	1.34	3.7	6.78	0.063	0.0704	0.0745	37, 9
HD 69830 b	4	*7*	10	*0.075*	0.0785	*0.082*	25, 25
HD 69830 c	4	*7*	10	*0.189*	0.186	*0.189*	25, 25
HD 73256 b	0.26	0.83	6.4	0.035	0.0371	0.0392	37, 9
HD 75289 b	1.29	4	5.8	0.0454	0.0482	0.051	37, 9
HD 76700 b	0.77	10	13.1	0.0481	0.0511	0.0541	37, 9
HD 83443 b	0.63	*1.785*	2.94	0.0383	0.0406	0.0429	37, 9
HD 88133 b	6.27	*7.915*	9.56	0.0445	0.0472	0.0499	37, 9
HD 99492 b	2.93	*3.71*	4.49	0.1161	0.1232	0.1303	37, 9
μ Ara d	1.45	*3.93*	6.41	0.0871	0.0924	0.0977	37, 9
OGLE-TR-111 b	1.1	*3.39*	*5.68*	0.0402	0.0467	0.0517	29, 30
OGLE-TR-132 b	0.5	*1.25*	2	0.0297	0.03	0.0302	17, 17
OGLE-TR-56 b	0.5	*2.79*	*5.08*	0.023	0.0234	0.0238	36, 36
τ Boo b	0.8	2.4	3.1	0.0453	0.0481	0.0509	37, 9
TrES-1	1.5	2.5	3.5	0.0394	0.0394	0.0394	29, 43
TrES-4	2.7	4.7	6.7	0.0466	0.0488	0.051	27, 27
υ And b	2.8	3.8	4.8	0.0561	0.0595	0.0629	15, 9
WASP-3 b	0.7	*2.1*	3.5	0.0307	0.0317	0.0322	35, 35
WASP-4 b	2	*4.29*	*6.58*	0.022	0.023	0.024	42, 42
WASP-5 b	1.7	*3.05*	4.4	0.0261	0.0268	0.0277	1, 1
WASP-10 b	0.6	0.8	1	0.0355	0.0369	0.0381	10, 10
WASP-14 b	0.5	0.75	1	0.035	0.036	0.037	22, 22
XO-1 b	*1.31*	3.6	*5.89*	*0.046*	0.0493	*0.053*	20, 20
XO-2 b	2.04	5.27	9.49	0.0367	0.0369	0.0371	7, 7
XO-4 b	0.6	2.1	3.5	0.0544	0.0555	0.0566	28, 28
XO-5 b	7.8	8.5	9.3	0.0503	0.0508	0.0511	8, 8

Table 6.1: Ages and *a*-values of close-in exoplanets used in our analysis. The minimum, middle and maximum values are indicated by "min", "mid" and "max" respectively. Italicized text indicates values that were determined as described in Appendix A. The references for ages and *a*-values are given in the rightmost column. References. (1) Anderson *et al.* (2008), (2) Bakos *et al.* (2007a), (3) Bakos *et al.* (2007b), (4) Bakos *et al.* (2007c), (5) Bonfils *et al.* (2005), (6) Bonfils *et al.* (2007), (7) Burke *et al.* (2007), (8) Burke *et al.* (2008), (9) Butler *et al.* (2006), (10) Christian *et al.* (2009), (11) Da Silva *et al.* (2006), (12) exoplanet.eu (as of 2009 Feb 10), (13) Fischer & Valenti (2005), (14) Fischer *et al.* (2007), (15) Fuhrmann *et al.* (1998), (16) Ge *et al.* (2006), (17) Gillon *et al.* (2007a), (18) Gillon *et al.* (2007b), (19) Gillon *et al.* (2008), (20) Holman *et al.* (2006), (21) Johnson *et al.* (2006), (22) Joshi *et al.* (2008), (23) Knutson *et al.* (2007), (24) Kovacs *et al.* (2007), (25) Lovis *et al.* (2006), (26) MacArthur *et al.* (2004), (27) Mandushev *et al.* (2007), (28) McCullough *et al.* (2008), (29) Melo *et al.* (2006), (30) Minniti *et al.* (2007), (31) Moutou *et al.* (2006), (32) Noyes *et al.* (2008), (33) Pal *et al.* (2008), (34) Pepe *et al.* (2004), (35) Pollaco *et al.* (2008), (36) Pont *et al.* (2007), (37) Saffe *et al.* (2006), (38) Sato *et al.* (2005), (39) Takeda *et al.* (2007), (40) Torres *et al.* (2007), (41) Udry *et al.* (2007), (42) Wilson *et al.* (2008), (43) Winn *et al.* (2007a), (44) Winn *et al.* (2007b), (45) Winn *et al.* (2008).

Chapter 7
Summary and Conclusions

In the field of extra-solar research, the almost daily discoveries of new planets continually pose new challenges to our understanding of planet formation. With many examples of planetary systems unlike our own, the study of extra-solar planets has helped us understand many planet formation processes whose influence is difficult to discern in our own solar system. The compositions, orbits, and physical properties of planets, satellites and minor bodies in our solar system reveal the system's origins in subtle ways. Only recently have observations begun to yield similarly sophisticated data for extra-solar systems, and they tell a story similar in many ways to the solar system's story, involving many of the same influences. However, the wide range of orbital and physical properties in extra-solar systems mean that the processes of planet formation and evolution can operate on a grander scale with dramatic consequences.

For our own solar system, the orbital architecture and the composition of the planets, satellites and minor bodies place important constraints on the system's early history. For example, the masses and compositions of Jupiter and Saturn suggest they accreted from the protoplanetary gas disk within a few Myrs of the Sun's formation, while the smaller masses and enrichment in heavy elements of Uranus and Neptune suggest they formed more slowly (*e.g.* Pollack et al. 1996). The orbits of giant planets also tell a story of their formative years. Recent models of the early dynamical evolution of our solar system suggest Jupiter and Saturn may have passed through a violent phase in which they gravitationally scattered Uranus and Neptune into their current orbits from

orbits much closer to the Sun (although still exterior to Saturn) (Morbidelli *et al.* 2007).

This evolutionary phase also seems to have left its signature on the orbital architecture of

the Kuiper belt (Levison & Morbidelli 2007). The breadth and depth of data about our

solar system through many years of ground-based and space-based observation have

allowed to construct a detailed, although still incomplete, history.

Although extra-solar systems are much farther away than planets in our solar

system, dramatic improvements to observational technology in recent years have allowed

us to piece together sophisticated theories of extra-solar systems formation. These

technologies have improved constraints on the distributions of orbital elements, the

masses, compositions and radii of planets, and allowed observers to disentangle the

complex signatures of multiple planets systems. With detections of more multiplanetary

systems, new dynamical interactions are discovered, old dynamical models are refined,

and astronomers are zeroing in on the initial conditions that gave rise to the planets we

see today. With better information about extra-solar planetary orbits, masses and

compositions, we have begun to piece together the complex histories of these systems.

One important piece of the puzzle, the orbital architecture of extra-solar systems,

seems to indicate a violent history. The wide distribution of both orbital eccentricities

and semi-major axes tell a story of gravitational interactions between accreting planets,

which eventually scatter the planets into elongated orbits (Rasio & Ford 1996;

Weidenschilling & Marzari 1996; Malhotra 2002; Barnes & Greenberg 2006a; Chatterjee

et al. 2008). Interactions between a nascent planet and its parent gas disk may drive rapid

migration of planets, which may be important for producing the wide range of orbital

semi-major axes. Migration in a gas disk can also leading to trapping in mean motion resonances (Lee & Peale 2002; Moorhead & Ford 2009), although gravitational scattering sometimes results in such resonances, too (Raymond *et al.* 2009). These processes may be especially important for the formation of close-in planets. In fact, the development of such models to explain the orbital properties of extra-solar systems was a key inspiration for the recent models for dynamical evolution of our own solar system. In this and many other ways, the study of extra-solar systems informs studies of this solar system, and vice versa.

However, despite a plethora of data, the transition between the final stages of planet formation and the initial planetary formation processes remains unclear. Fortunately, these initial processes set a planet's composition and internal structure, so the information provided by transit observations of close-in planets are crucial for untangling the dynamical and formation histories of planets. Agreement between observed radii and theoretical models with a range of assumptions permits the determination of internal structures and composition, and interest correlations have begun to emerge. For example, Burrows et al. (2007) pointed out that metal-rich planet-hosting stars have planets with more massive cores than metal-poor planet-hosting stars. If planets around metal-rich stars do indeed form from larger cores, it may provide strong evidence for the core-accretion model of planet formation (Pollack et al. 1996).

Unfortunately, the proximities of these close-in planets to their parent stars make them uniquely subject not only to intense stellar illumination but also tidal effects, and, as we've shown in this work, tides have played a profound role in shaping the orbits and

physical properties of close-in planets. However, the earliest models for tidal evolution of extra-solar planets seemed contradictory to the growing body of observational data. These models suggested tides should circularize the orbits of close-in planets only a few million years after they formed, even though many close-in planets had substantial eccentricities (Rasio *et al.* 1996). The cut-off in small *a* values might have suggested that tides had cleared out and destroyed the closet-in planets, but these same early models suggested that tidal evolution of semi-major axes was much too slow. Tidal heating had also been proposed to explain the surprising large radii of some transiting planets that seemed to require some internal source of heat, but, again, early models suggested tides were insufficient (Burrows *et al.* 2007).

A variety of models sprang up to account for these discrepancies. To explain the substantial eccentricities for many close-in planets, some authors proposed ad hoc tidal dissipation parameters (Matsumura *et al.* 2008), and others suggested that interactions with as yet undiscovered planets acted to delay eccentricity damping (*e.g.* Mardling 2007). To account for the gap in small *a* values, authors proposed finely tuned gravitational scattering mechanisms (Ford & Rasio 2006) or a clearing out of the protoplanetary gas disk very near a planet's host star so that a migrating planet would enter the gap and stop (Lin *et al.* 1996). The inflated radii of transiting planets were attributed to heating through tidal damping of exotic rotation states (Winn & Holman 2005).

However, as we've shown in this work, the contradictory conclusions reached by previous studies of tides simply result from inappropriate approximations. The non-zero

eccentricities of close-in planets can easily be accounted for if the coupled evolution of the semi-major axis is included. The cut-off in small a values is naturally explained by the acceleration of orbital decay and tidal destruction of planets as they near their host stars. Tidal heating of close-in planets was likewise more complex than previously realized, and the dramatic variation in tidal evolution rates was accompanied by commensurate variations in the heating rates.

By accounting for many of the conundrums posed by previous analyses, we have restored some confidence in our understanding of many planetary evolution processes. As has been assumed implicitly by many previous studies, the initial eccentricities for close-in planets did, indeed, resemble those of planets unaffected by tides, so whatever process set the latter probably also set the former. Also, many of the transiting planets with inflated radii to have undergone large tidal heating in the last few Gyrs, and recent work seems to confirm that this heating may explain the radii (Liu *et al.* 2008). Thus we may feel some measure of confidence about our estimates on the internal structures and compositions of many transiting planets.

While our research has answered many questions that have plagued the extra-solar planets community, it also suggests several other, potentially fruitful lines of inquiry. For example, what does it mean that the distribution of eccentricities for extra-solar planets was once uniform, across all semi-major axes? and how does that fit into models for the origins of close-in planets? The gravitational scattering model seems to suggest their eccentricities were clustered near unity (Ford & Rasio 2006), while the gas disk migration model seems to suggest their eccentricities were small (Lin *et al.* 1996).

Models of the thermal evolution of tidally evolving planets may also provide important constraints on the planets' origins. For example, the gravitational scattering suggests that tidal evolution brought close-in planets from highly eccentric orbits with a ~ few AU to close-in orbits with a ~ 0.1 AU. Such a large change in semi-major axis requires the dissipation of a lot of orbital energy (as much as 10^{37} J for Jupiter around the Sun) in less than a billion years (giving an average heating rate in excess of 10^{20} W). The dissipation of so much energy through tides raised on the host stars would probably spin up the stars significantly, while dissipation in the planets might heat the planets to the point of disruption. Coupled dynamical and thermal models of such processes might allow us to rule out certain origin scenarios.

During the tidal evolution, interactions with other planets, if present, would undoubtedly play a role. Some previous studies (Zhang & Hamilton 2006) suggest that those interactions may slow the tidal circularization process. Although inclusion of the evolution of semi-major axis explains the non-zero eccentricities for many close-in planets, the rates of circularization for some bodies (e.g. HD 41004 B b) are perhaps so rapid as to require the intercession of interactions with other planets to slow the evolution.

The evidence provided by the distribution of orbits of tidal destruction of planets begs the question "What happens to planets as they are destroyed?". We've assumed here that once a planet nears the Roche limit, it is rapidly disrupted by its star's tidal gravity, but how rapidly is it disrupted? Would it be possible to observe a planet in the process of tidal stripping? Previous studies in binary star systems suggest that, as a star is tidally stripped, conservation of orbital angular momentum causes the star's semi-major axis to

increase (Cameron & Iben 1986; Trilling *et al.* 1998). If the same holds true for a planet undergoing tidal stripping, the process may be more complicated than we've assumed here. In particular, how is the tidal stripping process modified by the presence of other, nearby planets? Does the tidal destruction and removal of a planet leave a discernible, dynamical signature on the remaining planetary system?

And we can turn back to our own solar system and consider similar questions for our own planets. Does the distribution of orbital eccentricities here as compared to extra-solar systems tell us anything new? Because large eccentricities seem to be so common among extra-solar planets, what prevented our own planets from acquiring large eccentricities? Given that extra-solar planets exhibit a range of eccentricities, is it plausible that our solar system just falls at the lower end of that distribution? The list of possible questions is endless.

In addition to elucidating important details regarding the origins and evolution of close-in planets, our work also highlights many of the important assumptions and limitations underlying tidal theory. Our analysis here shows that it involves many assumptions that are questionable, and understanding the subtle underpinnings of tidal theory is necessary before we can feel confident extending the theory to new regimes. Because the physical and orbital parameters of extra-solar systems span a wider range than planets and satellites in our own solar system, they may provide unique constraints on tidal evolution that have not been available before the discovery of extra-solar planets. In particular, recent formulations of tidal evolution that include corrections to the classical equations to very order in e should be re-considered in light of the results of

Error! Reference source not found. (Mardling & Lin 2002; Wisdom 2009). It's not clear that these impressively complex formulations provide any more accuracy than classical models that are simpler.

The wide array of extra-solar phenomena perhaps suggests a wide range of causes, but we've found that many of the observations can be explained with a simple, well-established model. Although many of the problems of extra-solar systems were new, we discovered that, in many cases, nothing new was required to solve them – we had the answers to the questions all along. As our understanding of the processes described here improved, these results should be revisited, but in spite of its limitations, the value of work lies in its simplicity. By providing straightforward answers to many previously unanswered questions, we have adhered to the important principle of Occam's razor, adding another vital brick to the growing edifice of human knowledge.

Appendix A

Monte Carlo Modeling of Extra-Solar Planetary Ages and *a*-values

The correlation of minimum *a*-values with age shown in Figure 6.1 is subject to considerable uncertainties regarding stellar ages. However inspection of Figure 6.1 suggests that the true ages of many of the planets would have to be considerably larger than shown in order to invalidate the correlation. In this appendix, we show that this correlation is robust through statistical modeling of the data despite the uncertainties. We perform Monte Carlo simulations of the data to show that there is always a positive correlation between minimum *a*-values and ages for the range of uncertainties, indicating that the cut-off in *a*-values highlighted in Figure 6.1 is not due to chance.

We calculated a correlation coefficient between minimum *a*-values and age for the data shown in Figure 6.1 by binning planetary ages in bins 1 Gyr wide. (Different bin sizes do not change our results.) Then, for each bin, we found the planet with the minimum *a*-value. For example, for the age bin extending from 0 to 1 Gyr, the minimum *a*-value is 0.023 AU (for the planet OGLE-TR-56 b). If there were no planets in an age bin, we assigned that bin the minimum *a*-value from the adjacent, younger bin. The age assigned to each bin is the upper boundary for the age bin, so the age assigned to the first bin is 1 Gyr, the age assigned to the second bin was 2 Gyr. (Again the choice of age for each bin doesn't affect our conclusions.) We then calculated the linear correlation coefficient for these 15 pairs of minimum *a*-values and ages. For the data illustrated in

Figure 6.1, that coefficient is 0.76, whose positive value is consistent with positive slope of the dashed line.

Next we tested the effect of the uncertainties in stellar ages and a-values on this correlation. We performed a series of Monte Carlo simulations by selecting new ages and a-values for each planet in our sample. For most planets in our sample, upper and lower limits for ages and a-values are available in the literature. For each of these planets, we chose a new age and a-value with a uniform probability to lie between the reported upper and lower limits and zero probability to lie outside that range.

However, for many of the planets in our sample, upper and lower limits on ages and a-values are not available in the literature. Some of planets only have lower bounds on ages, and others have only nominal ages and a-values with no reported uncertainties. To determine upper and lower limits on ages and a-values for these planets, we calculated the average uncertainty for planets with reported upper and lower bounds. For ages, we found the average uncertainty was 2.23 Gyrs, and for a-values, we found the average uncertainty was 0.0032 AU. For each of the planets with only a reported lower bound on the age, we chose a new age with a uniform probability to lie between the reported lower limit and the lower limit plus twice the average uncertainty. For the planets with only a nominal value, we chose an new value with a uniform probability to lie between the nominal age estimate minus the average uncertainty and plus the average uncertainty. For example, for the planet OGLE-TR-56 b, we have only a reported lower limit on the age of 0.5 Gyrs (Pont *et al.* 2007). For this planet, we allowed the new age to lie anywhere between 0.5 and 2.73 Gyrs. Table 6.1 shows the data we used. Values

shown in normal font are taken from the literature, while minimum ("min") and maximum ("max") values shown in bold, italicized font are upper and lower limits determined as described above. Middle values ("mid") shown in bold, italicized font are averages of the upper and lower limits reported in the literature.

For each new set of a-values and ages, we calculated the new correlation coefficient between the minimum a-value in an age bin and the age of that bin, as described previously. We chose a population of new ages and a-values 10,000 times to determine the range of correlation coefficients allowed by the uncertainties. A histogram of these correlation coefficients is shown as the solid line in Figure A.1. In spite of the large uncertainties, the correlation coefficient is always positive, with an average around 0.75. Therefore, we conclude that the low-a cut-off in Figure 6.1 is real and positively correlated with age, consistent with the predictions of tidal theory.
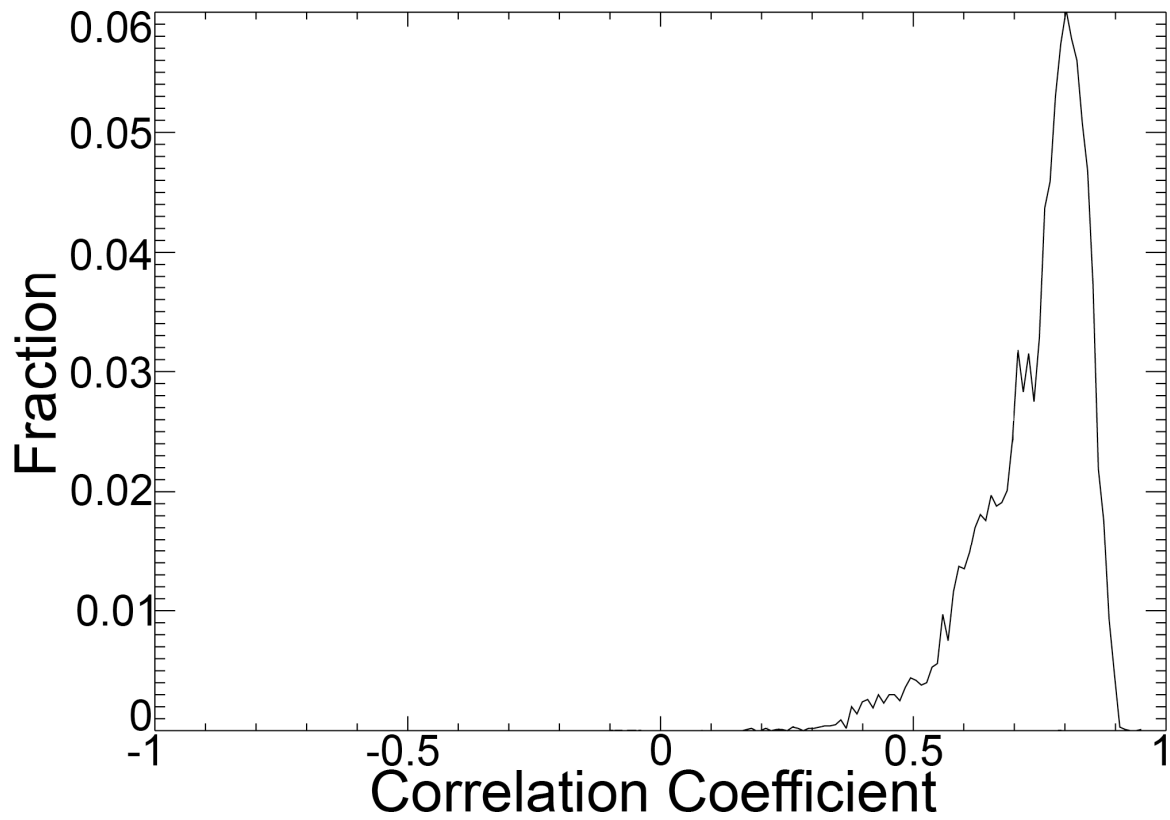
Figure A.1: Histogram of correlation coefficients for the correlation between the range of minimum a-values and ages. The y-axis represents the number of instances of a given value for the correlation coefficient divided by the total number of trials (10,000).

References

Adams, F., and G. Laughlin (2006). Effects of Secular Interactions in Extrasolar Planetary Systems. *Astrophysical Journal*, 649, 992.

Aksnes, K., and F. Franklin (2001). Secular Acceleration of Io Derived from Mutual Satellite Events. *Astronomical Journal*, 122, 2734.

Anderson, D. *et al.* (2008). WASP-5b: a dense, very hot Jupiter transiting a 12th-mag Southern-hemisphere star. *Monthly Notices of the Royal Astronomical Society*, 387, 4.

Bakos, G. *et al.* (2006). Refined Parameters of the Planet Orbiting HD 189733. *Astrophysical Journal,* 650, 1160.

Bakos, G. *et al.* (2007a). HAT-P-1b: A Large-Radius, Low-Density Exoplanet Transiting One Member of a Stellar Binary. *Astrophysical Journal*, 656, 552.

Bakos, G. *et al.* (2007b). HD 147506b: A Supermassive Planet in an Eccentric Orbit Transiting a Bright Star. *Astrophysical Journal*, 670, 826.

Bakos, G. *et al.* (2007c). HAT-P-5b: A Jupiter-like Hot Jupiter Transiting a Bright Star. *Astrophysical Journal*, 671, 173.

Barker, A., and G. Ogilvie. (2009). *Monthly Notices of the Royal Astronomical Society*, accepted.

Barnes, J. (2007). Effects of Orbital Eccentricity on Extrasolar Planet Transit Detectability and Light Curves. *Publications of the Astronomical Society of the Pacific,* 119, 986.

Barnes, R., and R. Greenberg. (2006a). Stability Limits in Extrasolar Planetary Systems. *Astrophysical Journal,* 638, 478.

Barnes, R. & R.Greenberg. (2006b). Behavior of Apsidal Orientations in Planetary Systems. *Astrophysical Journal Letters,* 652, L53.

Barnes, R. & R. Greenberg. (2007). Apsidal Behavior among Planetary Orbits: Testing the Planet-Planet Scattering Model. *Astrophysical Journal Letters,* 659, L53.

Barnes, R., Raymond, S., Jackson, B., and R. Greenberg. (2008b). Tides and the Evolution of Planetary Habitability. *Astrobiology*, 8, 557.

Barnes, S. (2001). An Assessment of the Rotation Rates of the Host Stars of Extrasolar Planets. *Astrophysical Journal,* 561, 1095.

Barnes, S. (2007). Ages for Illustrative Field Stars Using Gyrochronology: Viability, Limitations, and Errors. *Astrophysical Journal,* 669, 1167.

Baross, J., Lilley, M., and L. Gordon. (1982). Is the CH_4, H_2 and CO venting from submarine hydrothermal systems produced by thermophilic bacteria? *Nature* 298, 366.

Bodenheimer, P., Lin, D., and R. Mardling. (2001). On the Tidal Inflation of Short-Period Extrasolar Planets. *Astrophysical Journal,* 548, 466.

Bodenheimer, P., Laughlin, G., and D. Lin. (2003). On the Radii of Extrasolar Giant Planets. *Astrophysical Journal,* 592, 555.

Bonfils, X. *et al.* (2005). The HARPS search for southern extra-solar planets. VI. A Neptune-mass planet around the nearby M dwarf Gl 581. *Astronomy and Astrophysics Letters,* 443, L15.

Bonfils, X.*et al.* (2007). The HARPS search for southern extra-solar planets. X. A m sin i = 11 M_{Earth} planet around the nearby spotted M dwarf GJ 674. *Astronomy and Astrophysics,* 474, 293.

Borucki, W. and A. Summers. (1984). The photometric method of detecting other planetary systems. *Icarus*, 58, 121.

Boss, A. (2000). Possible Rapid Gas Giant Planet Formation in the Solar Nebula and Other Protoplanetary Disks . *Astrophysical Journal Letters,* 536, L101.

Bouchy, F. *et al.* (2005). ELODIE metallicity-biased search for transiting Hot Jupiters. II. A very hot Jupiter transiting the bright K star HD 189733 . *Astronomy and Astrophysics Letters,* 444, L15

Bramich, D. M. *et al.* (2005). A survey for planetary transits in the field of NGC 7789. *Monthly Notices of the Royal Astronomical Society,* 359, 1096.

Burke, C., Gaudi, B., DePoy, D., and R. Pogge. (2006). Survey for Transiting Extrasolar Planets in Stellar Systems. III. A Limit on the Fraction of Stars with Planets in the Open Cluster NGC 1245. *Astronomical Journal,* 132, 210.

Burke, C. *et al.* (2007). XO-2b: Transiting Hot Jupiter in a Metal-rich Common Proper Motion Binary. *Astrophysical Journal,* 671, 2115.

Burke, C. *et al.* (2008). XO-5b: A Transiting Jupiter-sized Planet with a 4 day Period. *Astrophysical Journal,* 686, 1331.

Burrows, A., Hubeny, I., Budaj, J., and W. Hubbard. (2007). Possible Solutions to the Radius Anomalies of Transiting Giant Planets. *Astrophysical Journal,* 661, 502.

Butler, R. P. *et al.* (2006). Catalog of Nearby Exoplanets. *Astrophysical Journal,* 646, 505.

Cameron, A. & I. Iben. (1986). On the behavior of double degenerate binaries associated with Type I supernovae. *Astrophysical Journal,* 305, 228.

Carone, L. & M. Patzöld. (2007). Constraints on the tidal dissipation factor of a main sequence star: The case of OGLE-TR-56b. *Planetary and Space Science*, 55, 643.

Chambers, J. (2006). Planet Formation with Migration. *Astrophysical Journal Letters,* 652, L133.

Charbonneau, D., Brown, T., Latham, D., and M. Mayor. (2000). Detection of Planetary Transits Across a Sun-like Star. *Astrophysical Journal Letters,* 529, L45.

Charbonneau, D. *et al.* (2006). Transit Photometry of the Core-dominated Planet HD 149026b. *Astrophysical Journal,* 636, 445.

Charbonneau, D. *et al.* (2007a). When Extrasolar Planets Transit Their Parent Stars. In B. Reipurth, D. Jewitt, and K. Keil (eds.) *Protostars and Planets V*, 701. (Tucson: Univ. Arizona Press).

Charbonneau, D. *et al.* (2007b). Precise Radius Estimates for the Exoplanets WASP-1b and WASP-2b. *Astrophysical Journal,* 658, 1322.

Chatterjee, S., Ford, E., Matsumura, S., and F. Rasio. (2008). Dynamical Outcomes of Planet-Planet Scattering. *Astrophysical Journal,* 686, 580.

Christian, D. *et al.* (2009). WASP-10b: a $3M_J$, gas-giant planet transiting a late-type K star. *Monthly Notices of the Royal Astronomical Society,* 392, 1585.

Chyba, C. (2000). Energy for microbial life on Europa. *Nature*, 403, 381-382.

Chyba, C., & C. Phillips. (2002). *Origins of Life and Evolution of the Biosphere*, v. 32, 1, 47.

Collier Cameron, A. *et al.* (2007). Efficient identification of exoplanetary transit candidates from SuperWASP light curves. *Monthly Notices of the Royal Astronomical Society,* 380, 1230.

Counselman, C. (1973). Outcomes of Tidal Evolution. *Astrophysical Journal,* 180, 307.

Cumming, A. *et al.* (2008). The Keck Planet Search: Detectability and the Minimum Mass and Orbital Period Distribution of Extrasolar Planets. *Publications of the Astronomical Society of the Pacific,* 120, 531.

D'Angelo, G., Lubow, S., and M. Bate. (2006). Evolution of Giant Planets in Eccentric Disks. *Astrophysical Journal,* 652, 1698.

Da Silva, R. *et al.* (2006). Elodie metallicity-biased search for transiting Hot Jupiters. I. Two Hot Jupiters orbiting the slightly evolved stars HD 118203 and HD 149143. *Astronomy and Astrophysics,* 446, 717.

Darwin, G. H. (1879). On the Bodily Tides of Viscous and Semi-Elastic Spheroids, and on the Ocean Tides upon a Yielding Nucleus. *Philosophical Transactions of the Royal Society,* London, 170, 1.

Davies, G. (1999). *Dynamic Earth*, Cambridge Univ. Press.

Deming, D., Seager, S., Richardson, L., and J. Harrington. (2005). Infrared radiation from an extrasolar planet. *Nature,* 434, 740.

Deming, D. *et al.* (2007). Spitzer Transit and Secondary Eclipse Photometry of GJ 436b. *Astrophysical Journal Letters,* 667, L199.

Dickey, J *et al.* (1994). Lunar Laser Ranging - a Continuing Legacy of the Apollo Program. *Science*, 265, 482.

Dobbs-Dixon, I., Lin, D., and R. Mardling. (2004). Spin-Orbit Evolution of Short-Period Planets. *Astrophysical Journal,* 610, 464.

O'Donovan, F. *et al.* (2006). TrES-2: The First Transiting Planet in the Kepler Field. *Astrophysical Journal Letters,* 651, L61.

Efroimsky, M., & V. Lainey. (2007). Physics of bodily tides in terrestrial planets and the appropriate scales of dynamical evolution. *Journal of Geophysical Research,* 112, E12.

Eggleton, P., Kiseleva, L., and P. Hut. (1998). The Equilibrium Tide Model for Tidal Friction. *Astrophysical Journal,* 499, 853.

Faber, J., Rasio, F., and B. Willems. (2005). Tidal interactions and disruptions of giant planets on highly eccentric orbits. *Icarus*, 175, 248.

Ferraz-Mello, S., Rodriguez, A., and H. Hussmann. (2008). Tidal friction in close-in satellites and exoplanets: The Darwin theory re-visited. *Celestial Mechanics and Dynamical Astronomy,* 101, 171.

Fischer, D. and J. Valenti. (2005). The Planet-Metallicity Correlation. *Astrophysical Journal,* 622, 1102.

Fischer, D. *et al.* (2007). Five Intermediate-Period Planets from the N2K Sample. *Astrophysical Journal,* 669, 1336.

Ford, E. and F. Rasio. (2006). On the Relation between Hot Jupiters and the Roche Limit. *Astrophysical Journal Letters,* 638, L45.

Ford, E., Havlikova, M., and F. Rasio. (2001). Dynamical Instabilities in Extrasolar Planetary Systems Containing Two Giant Planets. *Icarus*, 150, 303.

Fortney, J., Marley, M., and J. Barnes. (2007). Planetary Radii across Five Orders of Magnitude in Mass and Stellar Insolation: Application to Transits. *Astrophysical Journal,* 659, 1661.

Fuhrmann, K., Pfeiffer, M., and J. Bernkopf. (1998). F- and G-type stars with planetary companions: upsilon Andromedae, rho (1) Cancri, tau Bootis, 16 Cygni and rho Coronae Borealis. *Astronomy and Astrophysics,* 336, 942.

Ge, J. *et al.* (2006). The First Extrasolar Planet Discovered with a New-Generation High-Throughput Doppler Instrument. *Astrophysical Journal,* 648, 683.

Geissler, P., *et al.* (1999). Galileo Imaging of Atmospheric Emissions from Io. *Science*, 285, 870.

Gillon, M. *et al.* (2006). High accuracy transit photometry of the planet OGLE-TR-113b with a new deconvolution-based method. *Astronomy and Astrophysics,* 459, 249.

Gillon, M. *et al.* (2007a). Accurate Spitzer infrared radius measurement for the hot Neptune GJ 436b. *Astronomy and Astrophysics,* 471, 51.

Gillon, M. *et al.* (2007b). Detection of transits of the nearby hot Neptune GJ 436 b. *Astronomy and Astrophysics Letters,* 472, L13.

Gillon, M. *et al.* (2008). Improved parameters for the transiting planet HD 17156b: a high-density giant planet with a very eccentric orbit. *Astronomy and Astrophysics,* 485, 871.

Goldreich, P., and P. Nicholson. (1977). Turbulent viscosity and Jupiter's tidal Q. *Icarus*, 30, 301.

Goldreich, P. and S. Peale. (1966). Spin-orbit coupling in the solar system. *Astronomical Journal,* 71, 425.

Goldreich, P. and S. Soter. (1966). Q in the Solar System. *Icarus*, 5, 375.

Goldreich, P. (1963). On the eccentricity of satellite orbits in the solar system. *Monthly Notices of the Royal Astronomical Society,* 126, 257.

Gonzalez, G. (1997). The stellar metallicity-giant planet connection. *Monthly Notices of the Royal Astronomical Society,* 285, 403.

Gorda, S. and M. Svechnikov. (1998). Determination of empirical mass-luminosity and mass-radius relations for main-sequence stars that are the components of eclipsing binary systems. *Astronomy Reports*, 42, 793.

Greenberg, R. (1974). Outcomes of tidal evolution for orbits with arbitrary inclination. *Icarus*, 23, 51.

Greenberg, R. (1982). Orbital evolution of the Galilean satellites. in D. Morrison (ed.) *Satellites of Jupiter*, 65 (Tucson: Univ. of AZ Press).

Greenberg, R. (1989). Planetary accretion in M. Belton, R. West, and J. Rahe (eds.) *Time-Variable Phenomena in the Jovian System*, 100 (Washington, DC: NASA).

Greenberg, R., Geissler, P., Hoppa, G., and R. Tufts. (2002). Tidal-Tectonic Processes and Their Implications for the Character of Europa's Icy Crust. *Reviews of Geophysics*, 40, 1.

Greenberg, R. (2005). *Europa, The Ocean Moon: Search for an Alien Biosphere.* Springer Praxis Books.

Guillot, T. (2005). The Interiors of Giant Planets: Models and Outstanding Questions. *Annual Reviews of Earth and Planetary Science,* 33, 493.

Hawley, S., Gizis, J., and I. Reid. (1996). Local Three-dimensional Simulations of an Accretion Disk Hydromagnetic Dynamo. *Astronomical Journal,* 112, 2799.

Henry, G., Marcy, G., Butler, R., and S. Vogt. (2000). A Transiting ``51 Peg-like'' Planet. *Astrophysical Journal,* 531, 415.

Hillenbrand, L. *et al.* (1998). Circumstellar Disks in the Orion Nebula Cluster. *Astronomical Journal,* 116, 1816.

Holman, M. *et al.* (2006). The Transit Light Curve Project. I. Four Consecutive Transits of the Exoplanet XO-1b. *Astrophysical Journal,* 652, 1715.

Hubbard, W. (1984). *Planetary Interiors*, (New York: Van Nostrand Reinhold Co).

Hubbard, W. *et al.* (2007). Effects of mass loss for highly-irradiated giant planets. *Astrophysical Journal Letters,* 658, L59.

Hurford, T. (2005). *Tides and Tidal Stresses: Applications to Europa*. PhD Dissertation. Univ. of AZ.

Hut, P. (1981). Tidal evolution in close binary systems. *Astronomy and Astrophysics,* 99, 126.

Ida, S., and D. Lin. (2004). Toward a Deterministic Model of Planetary Formation. I. A Desert in the Mass and Semimajor Axis Distributions of Extrasolar Planets. *Astrophysical Journal,* 604, 388.

Ibgui, L., and A. Burrows (2009). Coupled Evolution with Tides of the Radius and Orbit of Transiting Giant Planets: General Results. *Astrophysical Journal,* submitted.

Jackson, B., Greenberg, R., and R. Barnes. (2008a). Tidal Evolution of Extra-Solar Planets. *Astrophyical Journal,* 678, 1396.

Jackson, B., Greenberg, R., and R., Barnes. (2008b) Tidal Heating of Extra-Solar Planets. *Astrophysical Journal,* 681, 1631.

Jackson, B., Barnes, R., and R., Greenberg. (2008c). Tidal heating of terrestrial extrasolar planets and implications for their habitability. *Monthly Notices of the Royal Astronomical Society,* 391, 237.

Jackson, B., Barnes, R., and R. Greenberg. (2009). Observational Evidence for Tidal Destruction of Exoplanets. *Astrophysical Journal*, in press.

Jeffreys, H. (1961). The effect of tidal friction on eccentricity and inclination. *Monthly Notices of the Royal Astronomical Society,* 122, 339.

Johnson, J. *et al.* (2006). An Eccentric Hot Jupiter Orbiting the Subgiant HD 185269. *Astrophysical Journal,* 652, 1724.

Johnson, J. *et al.* (2004). Radiation effects on the surfaces of the Galilean satellites. In: Bagenal, F., Dowling, T.E., McKinnon, W. B. (eds.), *Jupiter: The Planets, Satellites, and Magnetosphere,* 485. Cambridge Univ. Press, Cambridge, UK.

Joshi, Y. *et al.* (2009). WASP-14b: 7.3 M_J transiting planet in an eccentric orbit. *Monthly Notices of the Royal Astronomical Society,* 392, 1532.

Kalas, P. *et al.* (2009). Fomalhaut b: Direct Detection of a Jupiter-mass Object Orbiting Fomalhaut. *Science*, 322, 1345.

Kaltenegger, L., Traub, W., and K. Jucks. (2007). Spectral Evolution of an Earth-like Planet. *Astrophysical Journal,* 658, 598.

Kaspar, M. (1959). *Kepler*, Abelard-Schuman, London and New York.

Kasting, J., Whitmire, D., and R. Reynolds. (1993). Habitable Zones around Main Sequence Stars. *Icarus*, 101, 108.

Kaula, W. (1968). *An Introduction to Planetary Physics*, Wiley, N.Y.

Knutson, H. *et al.* (2007). A map of the day-night contrast of the extrasolar planet HD 189733b. *Astrophysical Journal,* 655, 564.

Konopliv, A., & C. Yoder. (1996). Venusian k_2 tidal Love number from Magellan and PVO tracking data. *Geophysical Research Letters,* 23, 1857.

Koppel, T. (2007). *Ebb and Flow: Tides and Life on Our Once and Future Planet,* The Dundurn Group, Toronto.

Kovacs, G. *et al.* (2007). HAT-P-4b: A Metal-rich Low-Density Transiting Hot Jupiter. *Astrophysical Journal,* 670, 41.

Lambeck, K. (1977). Tidal Dissipation in the Oceans: Astronomical, Geophysical and Oceanographic Consequences. *Transactions of the Philosophical Society of London A,* 287, 545-594.

Lammer, H. *et al.* (2008). Coronal Mass Ejection (CME) Activity of Low Mass M Stars as An Important Factor for The Habitability of Terrestrial Exoplanets. II. CME-Induced Ion Pick Up of Earth-like Exoplanets in Close-In Habitable Zones. *Astrobiology*, 7, 185.

Laughlin, G. *et al.* (2005a). A Comparison of Observationally Determined Radii with Theoretical Radius Predictions for Short-Period Transiting Extrasolar Planets. *Astrophysical Journal,* 621, 1072.

Laughlin, G. *et al.* (2005b). The GJ 876 Planetary System: A Progress Report. *Astrophysical Journal,* 622, 1182.

Laughlin, G. *et al.* (2005c). On the Eccentricity of HD 209458b. *Astrophysical Journal Letters,* 629, L121.

Lee, M., & S. Peale (2002). Dynamics and Origin of the 2:1 Orbital Resonances of the GJ 876 Planets. *Astrophysical Journal*, 567, 596.

Levison, H., & A. Morbidelli. (2007). Models of the collisional damping scenario for ice-giant planets and Kuiper belt formation. *Icarus*, 188, 522.

Levrard, B., Winnisdoerffer, C., and G. Chabrier. (2009). Falling Transiting Extrasolar Giant Planets. *Astrophysical Journal,* 692, 9.

Lin, D., Bodenheimer, P., and D. Richardson. (1996). Orbital migration of the planetary companion of 51 Pegasi to its present location. *Nature*, 380, 606.

Lin, D., and J. Papaloizou. (1985). On the dynamical origin of the solar system. in *Protostars and Planets II,* 981. (Univ. of AZ: Tucson).

Lissauer, J. (2007). Planets Formed in Habitable Zones of M Dwarf Stars Probably Are Deficient in Volatiles. *Astrophysical Journal Letters,* 660, L149.

Lissauer, J. (1993). Planet formation. *Annual Review of Astronomy and Astrophysics,* 31, 129.

Liu, X., Burrows, A., and L. Ibgui. (2008). Theoretical Radii of Extrasolar Giant Planets: the Cases of TrES-4, XO-3b, and HAT-P-1b. *Astrophysical Journal,* 687, 1191.

Love, A. (1911). *Some Problems in Geodynamics,* Cambridge Univ. Press, Cambridge, UK.

Lovis, C. *et al.* (2006). An extrasolar planetary system with three Neptune-mass planets. *Nature*, 441, 305.

Lucy, L., and M. Sweeney. (1971). *Astronomical Journal,* 76, 544.

Lunine, J. (2005). *Astrobiology: A Multidisciplinary Approach*, Pearson, San Francisco.

Macdonald, G. (1964). Tidal Friction. *Review of Geophysics*, 2, 467.

Malhotra, R. (2002). A Dynamical Mechanism for Establishing Apsidal Resonance. *Astrophysical Journal Letters,* 575, L33.

Mandushev, G. *et al.* (2007). TrES-4: A Transiting Hot Jupiter of Very Low Density. *Astrophysical Journal,* 667, 195.

Maness, H. *et al.* (2007). The M Dwarf GJ 436 and its Neptune-Mass Planet. *Publications of the Astronomical Society of the Pacific,* 119, 90.

Marcy, G. *et al.* (2001). A Pair of Resonant Planets Orbiting GJ 876. *Astrophysical Journal,* 556, 296.

Mardling, R. and D. Lin. (2002). Calculating the Tidal, Spin, and Dynamical Evolution of Extrasolar Planetary Systems. *Astrophysical Journal,* 573, 829.

Marding, R., and D. Lin. (2004). On the Survival of Short-Period Terrestrial Planets. *Astrophysical Journal,* 614, 955.

Mardling, R. (2007). Long-term tidal evolution of short-period planets with companions. *Monthly Notices of the Royal Astronomical Society,* 382, 1768.

Marzari, F. and S. Weidenschilling. (2002). Eccentric Extrasolar Planets: The Jumping Jupiter Model. *Icarus*, 156, 570.

Massarotti, A. (2008). Stellar Rotation and Planet Ingestion in Giants. *Astronomical Journal,* 135, 2287.

Mathieu, R. (1994). Pre-Main-Sequence Binary Stars. *Annual Reviews of Astronomy and Astrophysics,* 32, 465.

Matsumura, S., Takeda, G., & F. Rasio (2008). On the Origins of Eccentric Close-In Planets. *Astrophysical Journal*, 686, 29.

Mayor, M. *et al.* (2004). The CORALIE survey for southern extra-solar planets. XII. Orbital solutions for 16 extra-solar planets discovered with CORALIE. *Astronomy and Astrophysics,* 415, 391.

Mayor, M. *et al.* (2009a). The HARPS search for southern extra-solar planets. XIII. A planetary system with 3 super-Earths (4.2, 6.9, and 9.2 M_{Earth}). *Astronomy and Astrophysics,* submitted.

Mayor, M. *et al.* (2009b). The HARPS search for southern extra-solar planets XVIII. An Earth-mass planet in the GJ 581 planetary system. *Astronomy and Astrophysics,* submitted.

Mayor, M. and D. Queloz. (1995). A Jupiter-Mass Companion to a Solar-Type Star. *Nature*, 378, 355.

McArthur, B. *et al.* (2004). Detection of a Neptune-Mass Planet in the ρ^1 Cancri System Using the Hobby-Eberly Telescope. *Astrophysical Journal Letters,* 614, L81.

McCullough, P. *et al.* (2006). A Transiting Planet of a Sun-like Star. *Astrophysical Journal,* 648, 1228.

McCullough, P. *et al.* (2008). XO-4b: An Extrasolar Planet Transiting an F5V Star *Astrophysical Journal*, submitted.

McEwen, A. *et al.* (1992). New Voyager 1 Hot Spot Identifications and the Heat Flow of Io. *Bulletin of the American Astronomical Society,* 24, 935.

McEwen, A. *et al.* (2004). The lithosphere and surface of Io. In: Bagenal, F., Dowling, T.E., McKinnon, W. B. (Eds.), Jupiter: The Planets, Satellites, and Magnetosphere. Cambridge Univ. Press, Cambridge, UK, pp. 307-328.

Melo, C *et al.* (2006). On the age of stars harboring transiting planets. *Astronomy and Astrophysics,* 460, 251.

Melosh, J., and A. Vickery. (1989). Impact erosion of the primordial atmosphere of Mars. *Nature*, 338, 487.

Miller-Ricci, E. *et al.* (2008). MOST Space-based Photometry of the Transiting Exoplanet System HD 209458: Transit Timing to Search for Additional Planets. *Astrophysical Journal*, 682, 586.

Minniti, D. *et al.* (2007). Millimagnitude Photometry for Transiting Extrasolar Planetary Candidates. III. Accurate Radius and Period for OGLE-TR-111-b . *Astrophysical Journal,* 660, 858.

Moorhead, A., & E. Ford. (2009). submitted to *Astrophysical Journal,* arXiv0904.3336.

Morbidelli, A. *et al.* (2007). Dynamics of the Giant Planets of the Solar System in the Gaseous Protoplanetary Disk and Their Relationship to the Current Orbital Architecture. *Astronomical Journal*, 134, 1790.

Moutou, C. *et al.* (2004). Accurate radius and mass of the transiting exoplanet OGLE-TR-132b. *Astronomy and Astrophysics Letters,* 424, L31.

Moutou, C. *et al.* (2006). ELODIE metallicity-biased search for transiting Hot Jupiters. III. A hot Jupiter orbiting the star HD 185269. *Astronomy and Astrophysics,* 458, 327.

Murray, C., & Dermott, S. (1999). *Solar System Dynamics*, Cambridge Univ. Press.

Nagasawa, M., Ida, S., and T. Bessho. (2008). Formation of Hot Planets by a Combination of Planet Scattering, Tidal Circularization, and the Kozai Mechanism. *Astrophysical Journal,* 678, 498.

Noyes, R. *et al.* (2008). HAT-P-6b: A Hot Jupiter Transiting a Bright F Star. *Astrophysical Journal,* 673, 79.

O'Brien, D., Geissler, P., and R. Greenberg. (2002). A Melt-through Model for Chaos Formation on Europa. *Icarus*, 156, 152.

O'Neill, C., and A. Lenardic. (2007). Geological consequences of super-sized Earths. *Geophysical Research Letters,* 34.

O'Donovan, F., *et al.* (2007). TrES-3: A Nearby, Massive, Transiting Hot Jupiter in a 31 Hour Orbit. *Astrophysical Journal,* 663, 37.

Ogilvie, G., and D. Lin. (2004). Tidal Dissipation in Rotating Giant Planets. *Astrophysical Journal,* 610, 477.

Ogilvie, G., & D. Lin. (2007). Tidal Dissipation in Rotating Solar-Type Stars. *Astrophysical Journal,* 661, 1180.

Ogilvie, G. (2009). Tidal dissipation in rotating fluid bodies: a simplified model. *Monthly Notices of the Royal Astronomical Society*, in press.

Pal, A. *et al.* (2008). HAT-P-7b: An Extremely Hot Massive Planet Transiting a Bright Star in the Kepler Field. *Astrophysical Journa,* 680, 1450.

Papaloizou, J. (2007). Protoplanet magnetosphere interactions. *Astronomy and Astrophysics,* 463, 775.

Papuc, A., and G. Davies. (2008). The internal activity and thermal evolution of Earth-like planets. *Icarus*, 195, 447.

Peale, S. (1977). in J. Burns (ed.) *Planetary Satellites*, 87 (Tucson: Univ. Arizona Press).

Peale, S., and P. Cassen. (1978). Contribution of tidal dissipation to lunar thermal history. *Icarus*, 36, 245.

Peale, S., and M. Lee. (2002). A Primordial Origin of the Laplace Relation Among the Galilean Satellites. *Science*, 298, 593.

Peale, S., Cassen, P., and R. Reynolds. (1979). Melting of Io by tidal dissipation. *Science*, 203, 892.

Pepe, F. *et al.* (2004). The HARPS search for southern extra-solar planets. I. HD 330075 b: A new ``hot Jupiter''. *Astronomy and Astrophysics,* 423, 385.

Pepper, J & B. Gaudi. (2005). Searching for Transiting Planets in Stellar Systems. *Astrophysical Journal,* 631, 581.

Pollack, J. *et al.* (1996). Formation of the Giant Planets by Concurrent Accretion of Solids and Gas. *Icarus*, 124, 62.

Pollacco, D. *et al.* (2008). WASP-3b: a strongly irradiated transiting gas-giant planet. *Monthly Notices of the Royal Astronomical Society,* 385, 1576.

Pont, F. *et al.* (2007). Hubble Space Telescope time-series photometry of the planetary transit of HD 189733: no moon, no rings, starspots. *Astronomy and Astrophysics,* 465, 1069

Press, W. B. *et al.* (1996). *Numerical Recipes in C: The Art of Scientific Computing,* (New York: Press Syndicate of the University of Cambridge).

Rasio, F. *et al.* (1996). Tidal Decay of Close Planetary Orbits. *Astrophysical Journal,* 470, 1187.

Rasio, F., and E. Ford. (1996). Dynamical instabilities and the formation of extrasolar planetary systems. *Science*, 274, 954.

Raymond, S., Barnes, R., and A. Mandell. (2008a). Observable consequences of planet formation models in systems with close-in terrestrial planets. *Monthly Notices of the Royal Astronomical Society,* 384, 663.

Raymond, S., Barnes, R., Armitage, P., and N. Gorelick. (2008b) A Dynamical Perspective on Additional Planets in 55 Cancri. *Astrophysical Journal,* 687, 107.

Raymond, S., Scalo, J., and V. Meadows. (2007). A Decreased Probability of Habitable Planet Formation around Low-Mass Stars. *Astrophysical Journal,* 669, 606.

Raymond, S., *et al.* (2008). Mean Motion Resonances from Planet-Planet Scattering. *Astrophysical Journal*, 687, 107.

Regenauer-Lieb, K., Yuen, D., and J. Branlund. (2001). The Initiation of Subduction: Criticality by Addition of Water? *Science*, 294, 578.

Reynolds, R. T. *et al.* (1983). On the habitability of Europa. *Icarus*, 56, 246.

Rivera, E. *et al.* (2005). A ~7.5 M_{Earth} Planet Orbiting the Nearby Star, GJ 876. *Astrophysical Journal,* 634, 625.

Saffe, C. *et al.* (2005). On the ages of exoplanet host stars.*Astronomy and Astrophysics,* 443, 609.

Sandquist, E. *et al.* (2002). A Critical Examination of Li Pollution and Giant-Planet Consumption by a Host Star. *Astrophysical Journal,* 572, 1012.

Sato, B. *et al.* (2005). The N2K Consortium. II. A Transiting Hot Saturn around HD 149026 with a Large Dense Core. *Astrophysical Journal,* 633, 465.

Selsis, F. *et al.* (2007). Habitable planets around the star Gliese 581? *Astronomy and Astrophysics,* 476, 1373.

Showman, A., Cooper, C., Fortney, J., and M. Marley. (2008). Atmospheric Circulation of Hot Jupiters: Three-dimensional Circulation Models of HD 209458b and HD 189733b with Simplified Forcing. *Astrophysical Journal,* 682, 559.

Skumanich, A. (1972). Time Scales for CA II Emission Decay, Rotational Braking, and Lithium Depletion. *Astrophysical Journal,* 171, 565.

Soderblom, D. (2009). How Old Is That Star? *Science*, 323, 45.

Sotin, C., Grasset, O., and A. Mocquet. (2007). Mass radius curve for extrasolar Earth-like planets and ocean planets. *Icarus*, 191, 337.

Sozzetti, A. *et al.* (2007). Improving Stellar and Planetary Parameters of Transiting Planet Systems: The Case of TrES-2. *Astrophysical Journal,* 664, 1190.

Takeda, G. *et al.* (2007). Structure and Evolution of Nearby Stars with Planets. II. Physical Properties of ~1000 Cool Stars from the SPOCS Catalog. *Astrophysical Journal Supplement,* 168, 297.

Tarter, J. *et al.* (2007). A Reappraisal of The Habitability of Planets around M Dwarf Stars. *Astrobiology*, 7, 30.

Terquem, C., Papaloizou, J., and D. Lin. (1998). On the Tidal Interaction of a Solar-Type Star with an Orbiting Companion: Excitation of g-Mode Oscillation and Orbital Evolution. *Astrophysical Journal,* 502, 788.

Tinker, J., Pinsonneault, M., & D. Terndrup (2002). Angular Momentum Evolution of Stars in the Orion Nebula Cluster. *Astrophysical Journal,* 564, 877.

Torres, G. *et al.* (2007). HAT-P-3b: A Heavy-Element-rich Planet Transiting a K Dwarf Star. *Astrophysical Journal,* 666, 121.

Trilling, D. *et al.* (1998). Orbital Evolution and Migration of Giant Planets: Modeling Extrasolar Planets . *Astrophysical Journal,* 500, 428.

Trilling, D. (2000). Tidal Constraints on the Masses of Extrasolar Planets *Astrophysical Journal Letters,* 537, L61.

Udry, S. *et al.* (2002). The CORALIE survey for southern extra-solar planets. VIII. The very low-mass companions of HD 141937, HD 162020, HD 168443 and HD 202206: Brown dwarfs or ``superplanets''?. *Astronomy and Astrophysics,* 390, 267.

Udry, S. *et al.* (2007). The HARPS search for southern extra-solar planets. XI. Super-Earths (5 and 8 M{Earth}) in a 3-planet system. *Astronomy and Astrophysics Letters,* 469, L43.

Valencia, D., Sasselov, D., and R. O'Connell. (2007a). Radius and Structure Models of the First Super-Earth Planet. *Astrophysical Journal,* 656, 545.

Valencia, D., Sasselov, D., and R. O'Connell. (2007b). Inevitability of Plate Tectonics on Super-Earths.*Astrophysical Journal Letters,* 670, L45.

Valenti, J. and D. Fischer. (2005). Spectroscopic Properties of Cool Stars (SPOCS). I. 1040 F, G, and K Dwarfs from Keck, Lick, and AAT Planet Search Programs. *Astrophysical Journal Supplement,* 159, 141.

Vance, S., *et al.* (2007). Hydrothermal Systems in Small Ocean Planet. *Astrobiology,* 7, 987.

Verbunt, F. and C. Zwaan. (1981). Magnetic braking in low-mass X-ray binaries. *Astronomy and Astrophysics Letters,* 100, L7.

Vogt, S. *et al.* (2005). Five New Multicomponent Planetary Systems. *Astrophysical Journal,* 632, 638.

Walker, J., Hays, P., and J. Kasting. (1981). A negative feedback mechanism for the long-term stabilization of the earth's surface temperature. *Journal of Geophysical Research,* 86, 9776.

Ward, W. (1997). Protoplanet Migration by Nebula Tides. *Icarus,* 126, 261.

Weidenschilling, S. and F. Marzari. (1996). Gravitational scattering as a possible origin for giant planets at small stellar distances. *Nature*, 384, 619.

West, A. *et al.* (2008). Constraining the Age-Activity Relation for Cool Stars: the Sloan Digital Sky Survey Data Release 5 Low-Mass Star Spectroscopic Sample. *Astronomical Journal,* 135, 785.

Williams, D. and D. Pollard. (2002). Earth-like worlds on eccentric orbits: excursions beyond the habitable zone. *International Journal of Astrobiology,* 1, 61.

Williams, D., Kasting, J., and R. Wade. (1997). Habitable moons around extrasolar giant planets. *Nature* 385, 234.

Wilson, D. *et al.* (2008). WASP-4b: A 12th Magnitude Transiting Hot Jupiter in the Southern Hemisphere. *Astrophysical Journal,* 675, 113.

Winn, J. and M. Holman. (2005). Obliquity Tides on Hot Jupiters. *Astrophysical Journal Letters,* 628, L159.

Winn, J. *et al.* (2007a). The Transit Light Curve Project. V. System Parameters and Stellar Rotation Period of HD 189733. *Astronomical Journal,* 133, 11.

Winn, J. *et al.* (2007b). The Transit Light Curve Project. III. Tres Transits of TrES-1. *Astrophysical Journal,* 657, 1098.

Winn, J. *et al.* (2008). The Transit Light Curve Project. IX. Evidence for a Smaller Radius of the Exoplanet XO-3b. *Astrophysical Journal,* 683, 1076.

Wright, J. *et al.* (2007). Four New Exoplanets and Hints of Additional Substellar Companions to Exoplanet Host Stars. *Astrophysical Journal,* 657, 533.

Yoder, C. and S. Peale. (1981). The tides of Io. *Icarus*, 47, 1.

Zahn, J. (1977). Tidal friction in close binary stars. *Astronomy and Astrophysics,* 57, 383.

Zahn, J. (1989). Tidal evolution of close binary stars. I - Revisiting the theory of the equilibrium tide. *Astronomy and Astrophysics,* 220, 112.

Zhang, K. and D. Hamilton. (2006). Orbital Evolution in Extrasolar Planetary Systems. *Bulletin of the American Astronomical Society,* 38,   482.

Zucker, S. *et al.* (2004). Multi-order TODCOR: Application to observations taken with the CORALIE echelle spectrograph. II. A planet in the system HD 41004. *Astronomy and Astrophysics,* 426, 695.